Golden Engineering
EMPOWERING YOUR ANTENNA INNOVATIONS

Antennas and Beyond!

2026

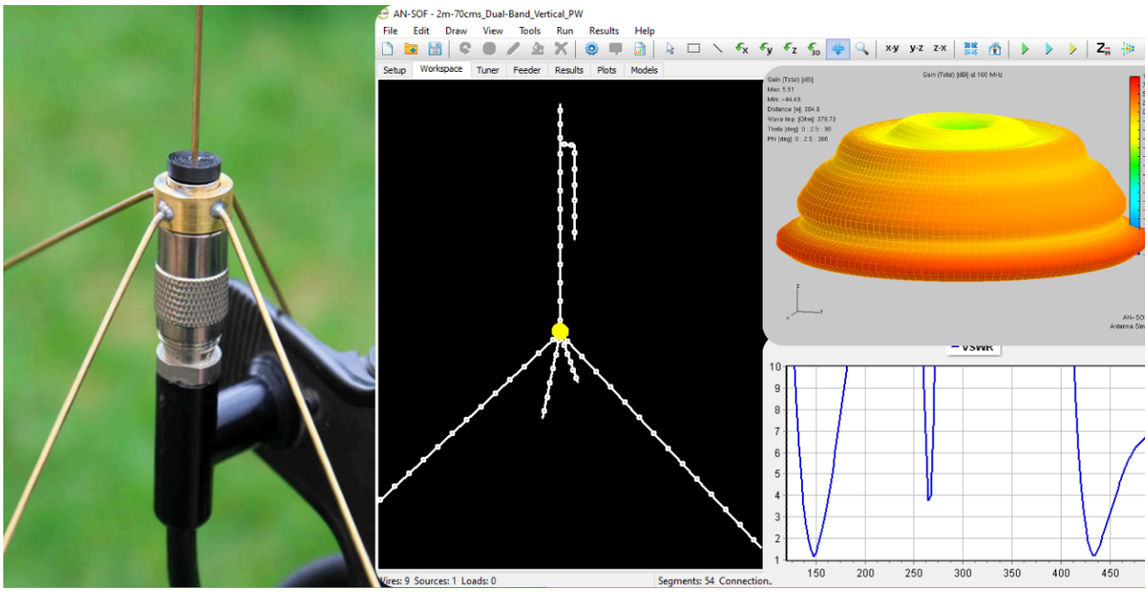

Technical Compendium: Antennas and Beyond!

This collection distills a year of simulation benchmarks and technical workflows into one guide. Whether you are in **The Antenna Lab**, **The Ham's Corner**, or on the **Advanced RF Edge**, these insights will help you achieve pro-grade precision at a minimum cost.

Tony Golden

Table of Contents

Linear Antenna Theory: Historical Approximations and Numerical Validation

Share this Article

Discover the vital role of historical theoretical results alongside advanced numerical calculations in accurately approximating current distribution on linear antennas.

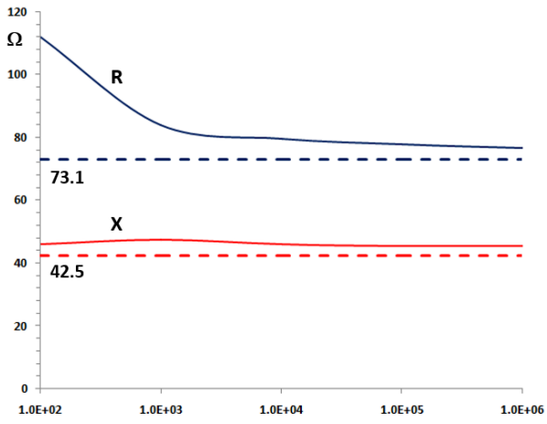

MoM simulation results for the input impedance of a center-driven half-wave dipole as a function of its length to radius ratio.
Gap size = 0.5% of dipole length

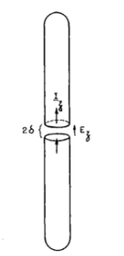

Fig. 12.3. Cylindrical antenna with a gap; the assumed field and current are indicated.

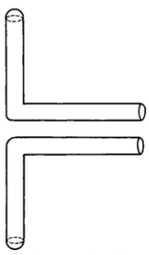

Fig. 12.4. Two-wire drive.

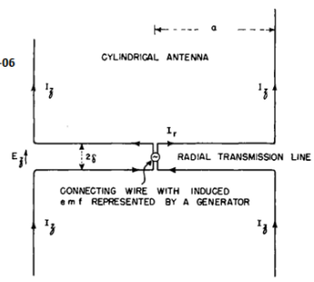

Fig. 12.6. Transmitting system with radial transmission line.

This article provides a comprehensive review of the theoretical approximations to the current distribution on **linear antennas** that were analytically derived during the first half of the 20th century. While the advancements in computing and numerical calculation methods have enabled higher precision, the historical theoretical results continue to serve as vital references for **validating calculation methods** implemented in algorithms. By examining these approximations, researchers can ensure the accuracy and reliability of modern numerical techniques used in antenna analysis and design.

Historical Theoretical Results: Approximations to Current Distribution

In 1956, **Ronold W. P. King** published his monumental work titled *"The Theory of Linear Antennas,"* which laid the foundation for understanding linear antennas and became a benchmark for future research. This section explores the significant contributions of

King's work, specifically focusing on the first four approximations to the current distribution on cylindrical antennas derived through an iterative method.

- **0th-Order Approximation > Perfect Sinusoid for Infinitely Thin Antennas**: The 0th-order approximation considers infinitely thin antennas (wire radius = 0) with a delta-gap source (zero gap width between the antenna terminals at the source position). This approximation involves a perfect sinusoidal current distribution.
- **1st-Order Approximation > Accounting for Finite Radius Effect**: The 1st-order approximation incorporates the finite radius effect (wire radius > 0) into the current distribution calculation. In this case, it is necessary to incorporate an additional term to the perfect sinusoidal function in order to obtain the 1st-order current distribution.
- **2nd-Order Approximation > Controversies Surrounding Finite Gap at the Source**: The 2nd-order approximation takes into account the finite gap at the source position, which has historically sparked controversies and debates.
- **3rd-Order Approximation > Considering Feedline Effect**: The 3rd-order approximation considers the feedline effect, which accounts for the boundary conditions at the feeding point resulting from the connection of a transmission line to feed the antenna.

Current Distribution Along a Half-Wave Dipole

To illustrate the aforementioned approximations, this section focuses on the current distribution in amplitude along a center-fed half-wave dipole. **Figure 1** provides a graphical representation of the normalized current, $i(s)$, as a function of position in wavelengths, s/λ. It should be noted that the actual current distribution exhibits a sign change in its derivative, $\partial i/\partial s$ (the electric charge), at the dipole center due to the excitation source.

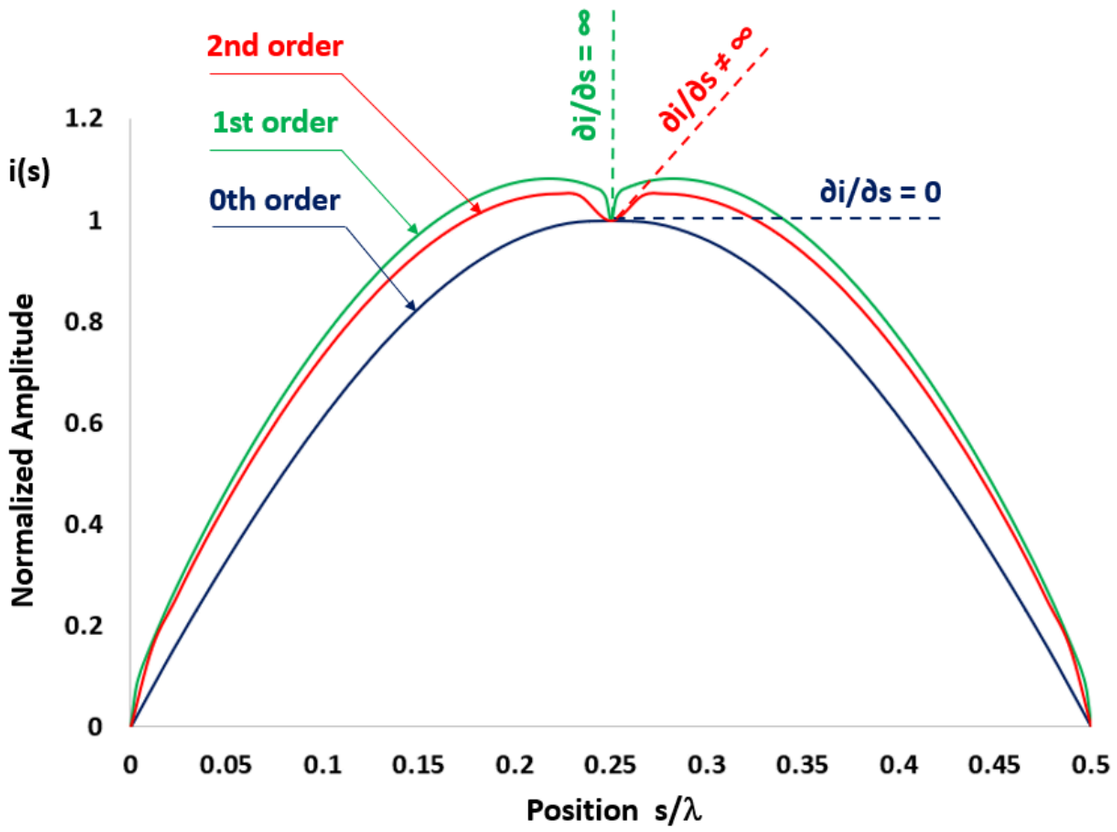

Fig. 1: Normalized amplitude current distribution along a center-fed half-wave dipole. The figure illustrates the 0th, 1st, and 2nd order approximations, highlighting the discontinuity of the current derivative at the feed point.

- **0th-Order Approximation > Perfect Sine Function with Zero Derivative: Figure 1** demonstrates that the 0th-order approximation, representing a wire radius of 0, yields a perfect sine function. Consequently, the derivative at the source position is zero, $\partial i/\partial s = 0$. However, King's analytical solution results in a finite input impedance of $73.1 + j42.5\ \Omega$, which has been widely accepted and corroborated by other methods.
- **1st-Order Approximation > Finite Wire Radius and Divergent Input Impedance:** The 1st-order approximation considers a finite wire radius and exhibits an infinite derivative, $\partial i/\partial s \to \infty$, at the source position. This singularity arises from the zero gap at the antenna terminals and has generated extensive debates throughout the history of linear antennas. As a consequence, the input impedance diverges.
- **2nd-Order Approximation > Finite Source Gap and Converging Input Impedance:** Incorporating a finite source gap, the 2nd-order approximation yields a finite derivative at the source position. As a result, the input impedance converges to a finite value, dependent on the dipole wire thickness and the separation between its feeding terminals.
- **3rd-Order Approximation > Consideration of Transmission Line Feed:** Although not visually distinguishable from the 2nd order on a graph, the 3rd-order approximation accounts for the characteristic impedance of the transmission line at the feed point. This effect, though small, can be accurately calculated using the **Method of Moments** with an **exact Kernel**.

Validating Numerical Methods: Impedance Convergence

Validating numerical methods is a critical step in ensuring their accuracy, achieved by examining the limiting cases predicted by theory. As demonstrated, the 0th-order input impedance (wire radius = 0) of a center-fed half-wave dipole is determined to be $73.1 + j42.5\ \Omega$. Consequently, this value should serve as a **horizontal asymptote** for the input impedance when the dipole length-to-radius ratio tends to infinity.

Figure 2 presents simulation results obtained using **AN-SOF**, which utilizes the **Method of Moments with an exact Kernel**. The figures from King's book illustrate the antenna terminals in detail, where a radial transmission line was considered to account for 3rd-order effects. **Notably, the calculated input impedance indeed converges to the theoretical value as predicted.**

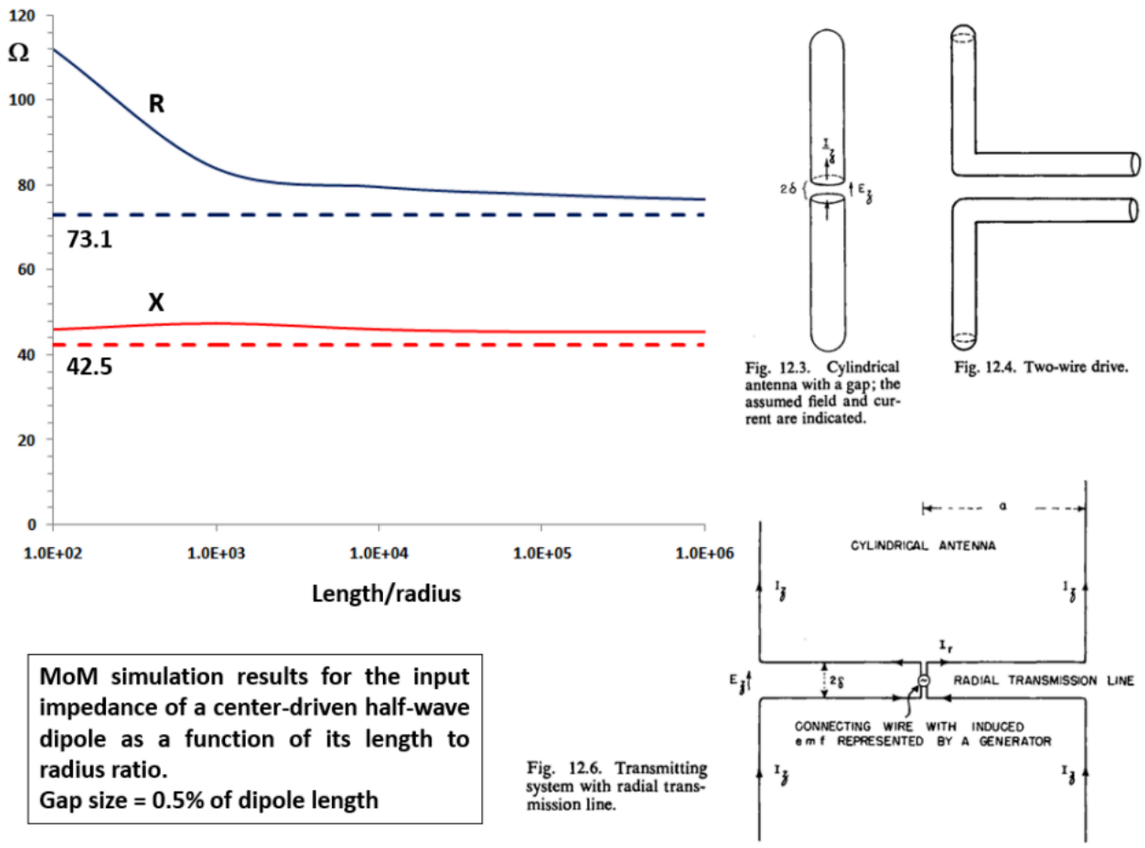

***Fig. 2**: Simulation results using the Method of Moments with an exact kernel, depicting the input impedance of a center-fed half-wave dipole as a function of its length-to-radius ratio. The figure also includes a comparison with the theoretical asymptotes. The cylindrical antenna illustrations are taken from King's book.*

For a more comprehensive investigation into the impedance convergence of cylindrical antennas, **a detailed study on the validation of AN-SOF can be accessed through this link**.

Conclusions

This article has reviewed the historical approximations of current distribution on linear antennas as presented in Ronold W. P. King's book. The four approximations, namely the 0th, 1st, 2nd, and 3rd-order approximations, have been thoroughly examined. These approximations progressively refine the theoretical model of a

cylindrical antenna by considering factors such as the finite wire radius, the finite gap at the feed point, and the incorporation of the connected transmission line.

Moreover, the article has highlighted the importance of **numerical validation** in establishing the reliability of modern methods. The validation process involved comparing the numerical results to the limiting cases predicted by theory. Through the **AN-SOF** simulation, which utilizes the **Method of Moments with an exact kernel**, the calculated input impedance successfully demonstrated convergence to the theoretical values.

Further Reading

- For further reading, we highly recommend the book *"The Theory of Linear Antennas"* by Ronold W. P. King, Harvard University Press, 1956. This seminal work provides a comprehensive understanding of linear antennas and serves as a benchmark for research in the field.
- In the paper *"Currents, Charges, and Near Fields of Cylindrical Antennas"* by R.W.P. King and Tai Tsun Wu, Radio Science Journal of Research NBS/USNC-URSI, Vol. 69D, No. 3, pp. 429-446, March 1965, the authors compare the sinusoidal current distribution with measured data and identify the need for an additional term in the model.
- To delve deeper into the source gap problem, we refer to *"The Influence of the Width of The Gap Upon The Theory of Antennas"* by L. Infeld, Quarterly of Applied Mathematics, Vol. V, No. 2, pp. 113-132, July 1947. This study provides valuable insights into the effects of gap width on antenna theory.

See Also:

- **Modeling a Center-Fed Cylindrical Antenna with AN-SOF**
- **Validating Dipole Antenna Simulations: A Comparative Study with King-Middleton**
- **Energy Conservation and Gain Convergence in Cylindrical Dipoles: A Numerical Validation Study**

Technical Keywords: Linear Antenna Theory, Current Distribution, Cylindrical Antenna, Source Gap Problem, Method of Moments (MoM), Sinusoidal Approximation, King-Middleton Theory, Numerical Validation, Delta-gap Excitation, Historical Electromagnetics.

About the Author

Tony Golden

RF ENGINEER & PHYSICS PH.D. With 25+ years in Computational Electromagnetics, I'm a passionate researcher focused on antenna modeling and design. As Founder of Golden Engineering LLC, I develop accessible, high-performance simulation tools that help RF

engineers optimize their designs, educators teach complex concepts, and hobbyists bring antenna projects to life.

Have a question?

💬 **Ask me** | ✉️ **Email me** | 🌐 **Follow me**

Antennas and Beyond!

Get Exclusive Updates

Share this Article

Energy Conservation and Gain Convergence in Cylindrical Dipoles: A Numerical Validation Study

Verify the numerical precision of the AN-SOF engine through this detailed validation study of cylindrical dipoles. By testing the principle of energy conservation, comparing input resistance against far-field radiation resistance, we demonstrate a near-perfect correlation with errors below 0.035%. This article also explores gain convergence, establishing that 10 segments per wavelength are sufficient to achieve high-precision results for linear antenna modeling.

The Principle of Energy Conservation

In the field of computational electromagnetics, the reliability of a numerical solver is fundamentally tied to its adherence to the laws of physics. One of the most stringent tests for any **Method of Moments (MoM)** engine is the verification of **the energy conservation principle**. In a **lossless** antenna system, an ideal environment with no ohmic or dielectric dissipation, the power supplied at the feed point (P_{in}) must be identical to the power radiated into the far-field (P_r).

This physical requirement allows for a unique validation check. By independently calculating the **Input Resistance** (R_{in}) from the voltage and current at the source and the **Radiation Resistance** (R_r) from the integration of the radiated power in the far-field, we can quantify the numerical precision of the solver. In an ideal PEC (Perfect Electric Conductor) model, any deviation between these two values is a direct measure of numerical artifacting rather than physical loss.

Simulation Model and Parameters

To conduct this validation, a center-fed cylindrical dipole was configured with the following parameters:

- **Physical Length:** $L = 0.5$ m.
- **Wire Radius:** $a = 5$ mm.
- **Source Gap:** $g = L/200$ (2.5 mm).

- **Frequency Range:** $200\ \mathrm{MHz}$ to $600\ \mathrm{MHz}$.
- **Environment:** Free space (lossless).

This frequency sweep is chosen to observe the antenna's behavior across multiple electrical lengths. At $300\ \mathrm{MHz}$, the wavelength (λ) is approximately 1 meter, making the $0.5\mathrm{m}$ dipole a half-wave radiator. At $600\ \mathrm{MHz}$, the dipole reaches a full-wavelength ($L = \lambda$), where it enters a high-impedance anti-resonant state.

Comparative Analysis of the Dipole Input and Radiation Resistances

Figure 1 shows the input and radiation resistance as functions of frequency. The radiation resistance is derived by integrating the Poynting vector in the far-field to determine total radiated power and dividing the result by the square of the RMS current at the dipole center. In AN-SOF, the radiated power is available via the **Power Budget** window in the **Results** menu, while the input current can be retrieved through the **List Currents** command.

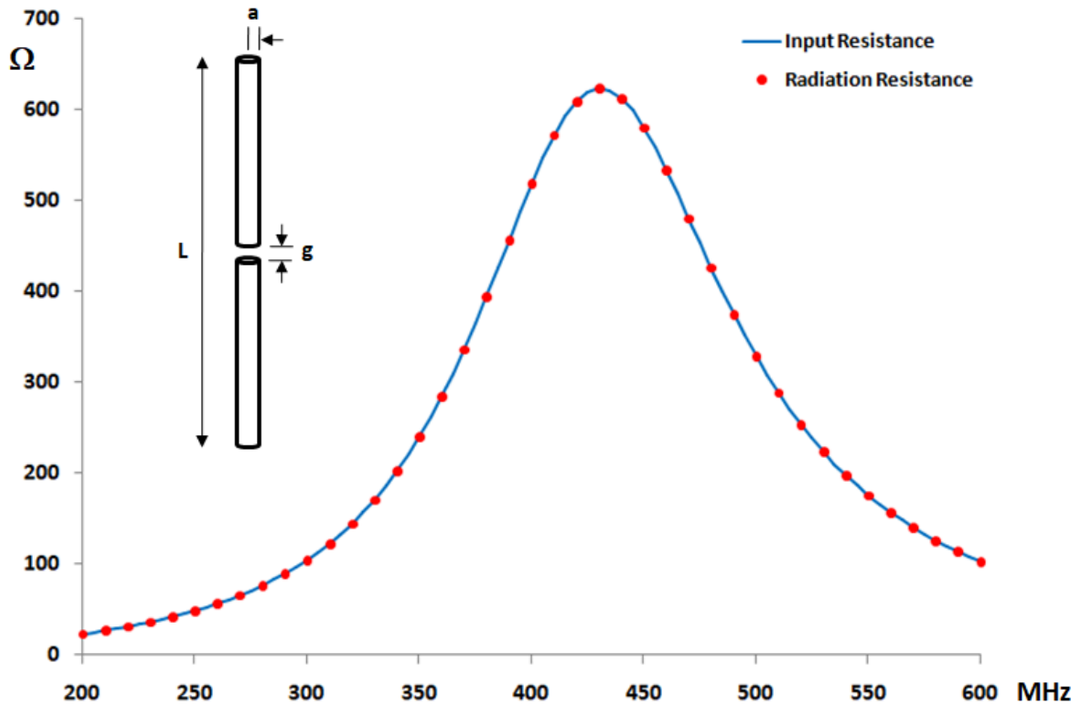

Fig. 1: Input and radiation resistances of a lossless, center-fed cylindrical antenna in free space as a function of frequency, with $L = 0.5\ \mathrm{m}$, $a = 5\ \mathrm{mm}$, *and* $g = L/200$.

The results demonstrate a remarkable level of agreement. As seen in **Figure 2**, which tracks the percentage difference between these two quantities, the error remains consistently below **0.035%** across the entire frequency range. This near-zero discrepancy confirms that the AN-SOF engine performs far-field power integration and near-field source calculations as a unified, energy-consistent system.

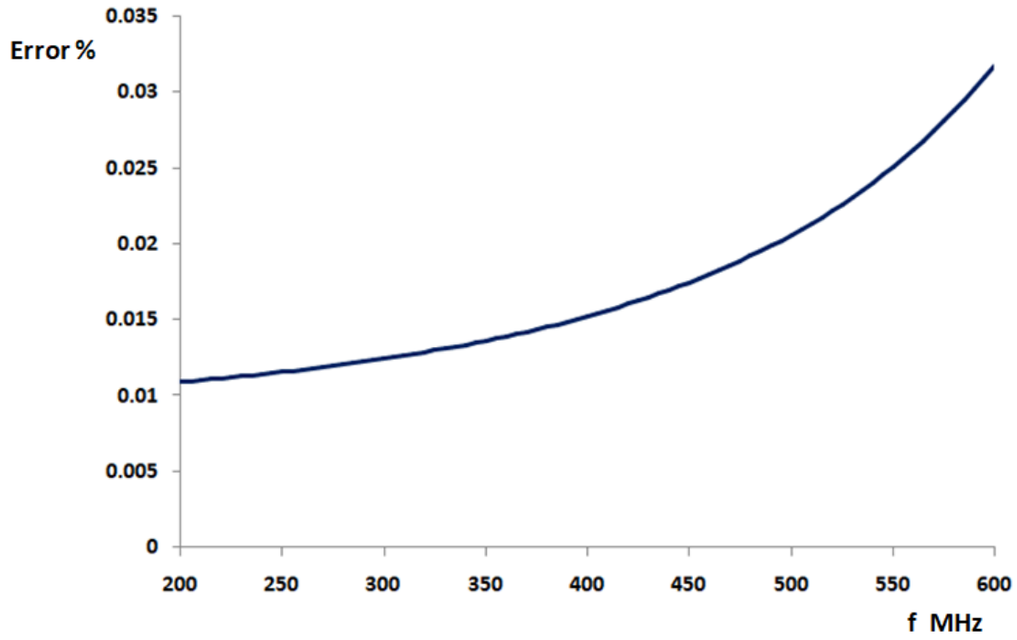

Fig. 2: Percentage difference between the input and radiation resistances shown in Fig. 1 as a function of frequency for a lossless, center-fed cylindrical antenna.

Gain Convergence and Discretization Guidelines

A second critical aspect of numerical validation is **convergence**. In MoM simulations, the accuracy of the results depends on the density of the wire segmentation. We investigated the convergence of the calculated peak gain (G) for a half-wave dipole as the number of segments $(2N)$ increases, where N represents the number of segments per dipole arm.

Figure 3 (left) shows that the gain values converge monotonically starting with as few as $2N = 3$ segments. To establish a practical baseline for engineers and designers, **Figure 3 (right)** highlights the error relative to the final asymptotic gain value. The data confirms that utilizing 5 segments per half-wavelength, equivalent to **10 segments per wavelength**, results in a gain error of less than **0.5%**. This validates the common "10 segments per λ" rule of thumb as a standard for linear antenna modeling to achieve accurate far-field metrics such as antenna gain.

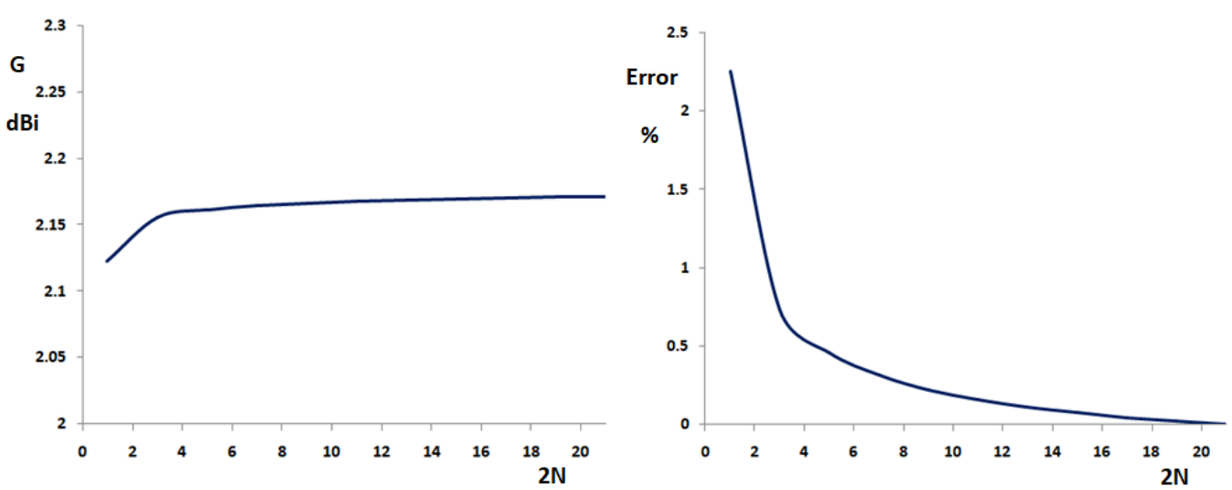

***Fig. 3**: (Left) Gain in dBi of a center-fed half-wave dipole as a function of the total number of segments, and (right) percentage error between the gain and its asymptotic value.*

Conclusion

The validation study of the center-fed cylindrical dipole demonstrates the exceptional numerical stability and precision of the AN-SOF solver. By achieving an energy conservation error of less than 0.035%, the software proves it can accurately handle the complex relationship between feed-point impedance and far-field radiation.

Furthermore, the convergence analysis provides a definitive benchmark for practitioners. The monotonic convergence of gain and the low error associated with standard segmentation densities ensure that users can obtain high-fidelity results with efficient computational overhead. Ultimately, these results provide the necessary confidence that AN-SOF's treatment of linear antennas is grounded in strict physical conservation laws, making it a reliable tool for both resonant and harmonic antenna design.

See Also:

- **Modeling a Center-Fed Cylindrical Antenna with AN-SOF**
- **Validating Dipole Antenna Simulations: A Comparative Study with King-Middleton**
- **Linear Antenna Theory: Historical Approximations and Numerical Validation**

Technical Keywords: Cylindrical Dipole, Radiation Resistance, Input Resistance, Energy Conservation, Numerical Convergence, Gain Precision, Center-fed Antenna, AN-SOF Validation, Method of Moments, Segmentation Density.

About the Author

Tony Golden

RF ENGINEER & PHYSICS PH.D. With 25+ years in Computational Electromagnetics, I'm a passionate researcher focused on antenna modeling and design. As Founder of Golden Engineering LLC, I develop accessible, high-performance simulation tools that help RF engineers optimize their designs, educators teach complex concepts, and hobbyists bring antenna projects to life.

Have a question?

💬 **Ask me** | ✉️ **Email me** | 🌐 **Follow me**

AN-SOF in Action: Modeling and Understanding the Performance of Fractal Antennas

Share this Article

Dive into the fascinating world of fractal antennas! This article explores their revolutionary design principles using AN-SOF simulation software. Discover how self-similar patterns unlock wider bandwidths, smaller sizes, and superior efficiency compared to traditional antennas.

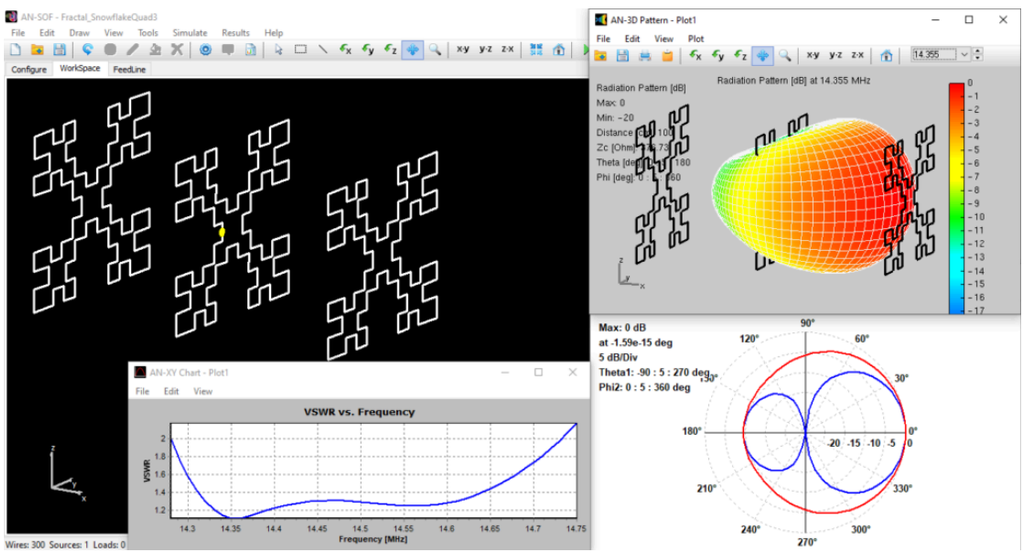

Key Takeaways

- **Compact Wideband Design:** Fractal antennas like the snowflake quad achieve wide bandwidths in a surprisingly small size compared to traditional antennas.
- **Array for Enhanced Performance:** The article explores a 3-element array based on the snowflake fractal, potentially improving bandwidth compared to simpler designs.
- **AN-SOF Simulation Advantage:** AN-SOF software allows for simulating and optimizing the performance of complex fractal antenna structures.

Fractal Antennas: A Game-Changer in Antenna Design

The realm of antennas has seen a fascinating union between mathematics and engineering with the introduction of **fractal antennas** (**Fig. 1**). Fractals, once confined

to the world of computer-generated imagery, have become a unifying principle in science, even linked to **chaos theory**.

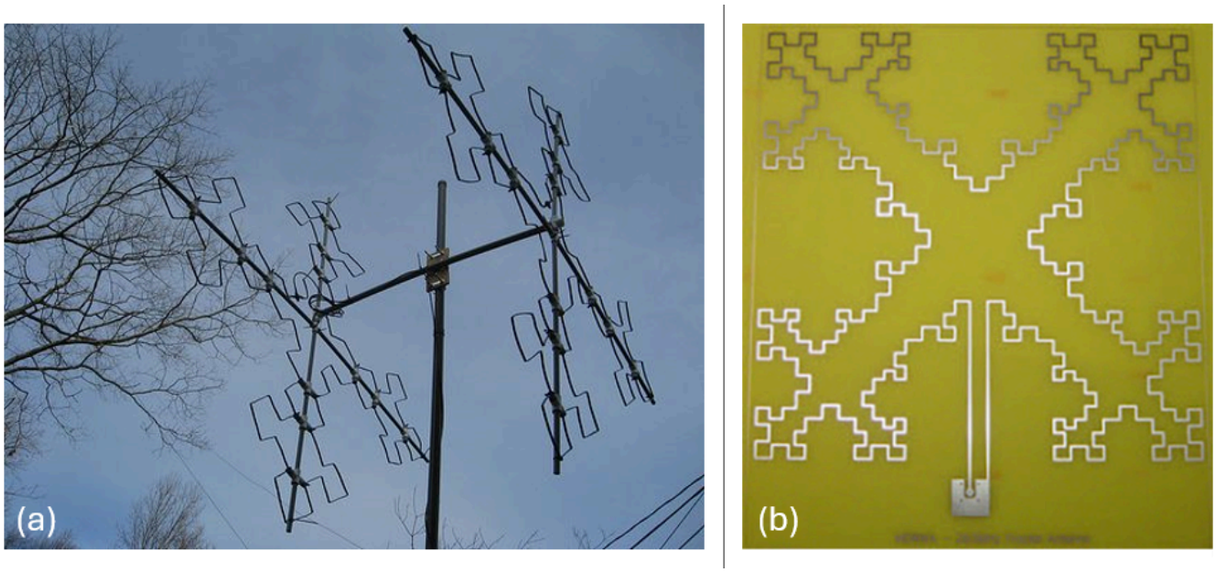

Fig. 1: *Fractal Antenna Diversity. (a) Fractal antennas transcend PCBs. Here's a full-size, mast-mounted example (Image: UMITS). (b) A microstrip fractal quad antenna fabricated on a dielectric substrate (Image: CC BY-SA license).*

In the domain of antennas, fractals translate into powerful designs that boast **high radiation efficiency**, **wider bandwidths**, and **minimized side lobes**. A fractal antenna is essentially a radiating element that capitalizes on **self-similar patterns** to increase the **effective perimeter** of radiating material. This approach allows fractal antennas to be significantly smaller (50-75%) compared to traditional counterparts, while offering advantages in terms of reliability and **cost-effectiveness**.

The beauty of fractal designs lies in their versatility. They can be implemented across various existing antenna types, including dipoles, monopoles, patches, conformals, biconicals, discones, spirals, helicals, and even compact variants. This translates to benefits like multi-band operation, wide bandwidths, and a **low-profile form factor**. These characteristics make them ideal for applications with limited space and complex circuitry, and their robust nature has led to widespread adoption in military applications.

Unlike traditional antennas that require specific design features for each operating frequency, fractal antennas excel in their ability to operate effectively across **multiple frequencies simultaneously**. This stems from their underlying concept – a recursively generated geometry with **fractional dimensions**. Fractals possess intriguing properties, such as having a **finite area** yet an **infinite perimeter**.

Practical Applications and Promising Potential

The future of wireless communication holds immense promise for fractal antennas. They offer the potential for robust and efficient communication systems with a **reduced number of antenna elements**. This makes them suitable for both **individual antennas** and **antenna arrays**.

Experimental Validation

Experiments conducted with fractal antenna designs, such as the **Koch curve** and **Sierpinski triangle** (**Fig. 2**), have yielded impressive results. These trials have demonstrated improved performance, wider transmission bands, and the potential **to eliminate the need for matching circuits**.

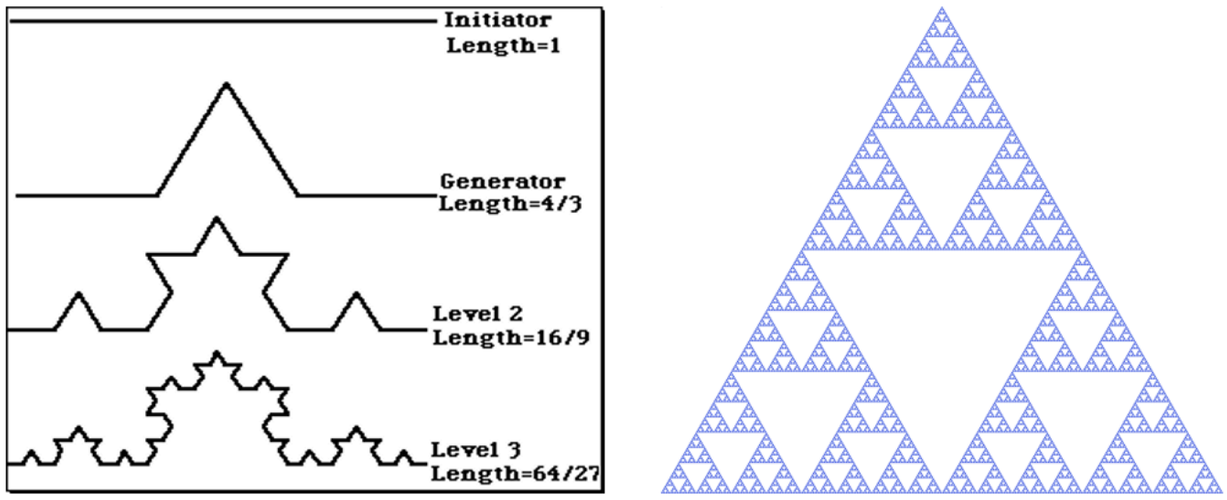

Fig. 2: Koch curve (left) and Sierpinski triangle (right) (Images: CC BY-SA license).

A Deeper Dive

In the article **"The Fractal Antenna"** by Angel Vilaseca, HB9SLV, fractalization of the Quad antenna is explained (VHF Communications, Vol. 33, pp. 213-226, 2001-Q4). Vilaseca's article dives into the design sequence of the Quad antenna transforming through the first three stages (MI1, MI2, and MI3) of the **Minkowski square fractalization** (**Fig. 3**). It also presents experimental results by Nathan Cohen, N1IR, for **an array of two MI2 elements designed for the 10m band**.

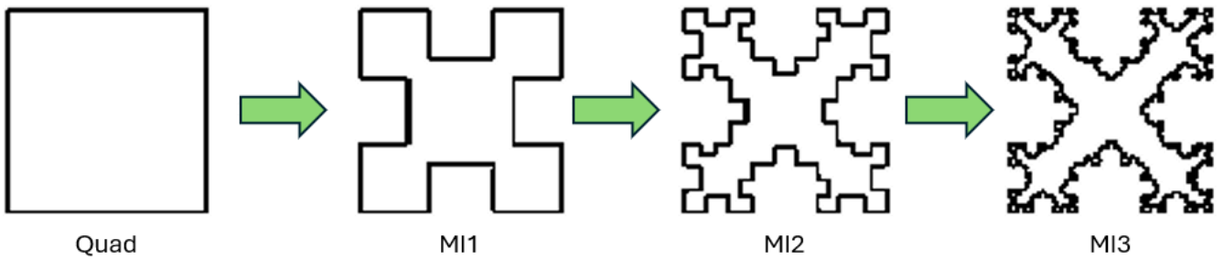

Fig. 3: Stages of Minkowski Square Fractalization.

In the next section, we'll delve into AN-SOF modeling using a specific example – an MI2 fractal quad loop.

Modeling the MI2 Fractal Loop with AN-SOF

The **MI2 Fractal Loop antenna** is a pioneering design by Dr. Nathan Cohen, documented in his research paper co-authored with R.G. Hohlfeld titled *"Fractal Loops and the Small Loop Approximation"* (Communications Quarterly, Vol. 6, pp. 77-81, 1996). This design offers a compelling example of how fractal geometry translates into practical antenna benefits.

According to Cohen's report, the MI2 Fractal Loop boasts an **input resistance of 26 Ohms** and a **gain of 2 dBi** at its first resonant frequency in the **20m band**. This design achieves a desirable resonant resistance within a reduced physical size.

AN-SOF Simulation Results

Our AN-SOF simulation results for the MI2 Fractal Loop antenna are consistent with the published data. The first resonance occurs between **15.33 and 15.34 MHz**, with an input resistance of **28 Ohms**, closely aligned with the reported value. The simulated antenna gain is **1.90 dBi**, demonstrating good agreement with Cohen's findings.

The **2:1 VSWR bandwidth**, a crucial parameter indicating efficient power transfer, is **1.04%** in our simulation. The model itself has a compact size of **2.8 x 2.662 meters**, showcasing the space-saving potential of fractal designs. However, it's important to note that the **total wire length** of the MI2 antenna is **27.56 meters**, which corresponds to **1.38 times its design wavelength** (λ = 20 meters).

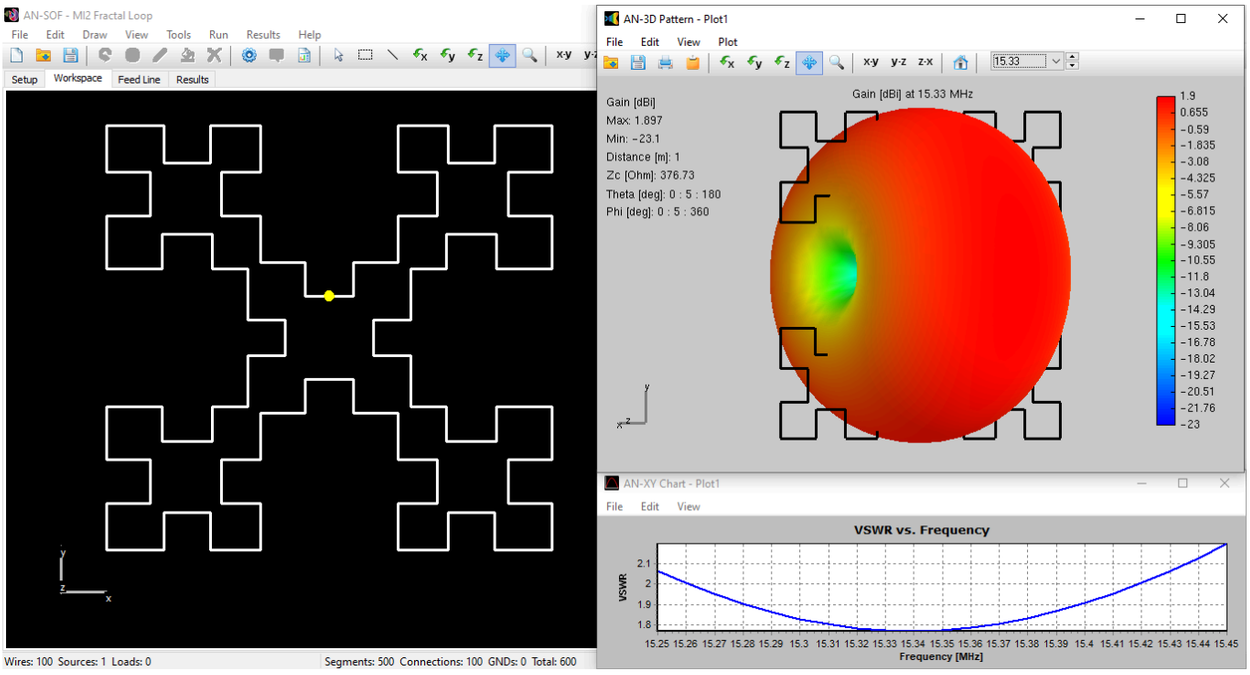

Fig. 4: Simulated Radiation Pattern and VSWR of MI2 Fractal Loop Antenna.

Download Model

Figure 4 presents a comprehensive view of the MI2 model within the AN-SOF workspace (left). The image also showcases the 3D radiation pattern obtained from the simulation, which resembles the **donut-shaped** pattern characteristic of a **short dipole antenna**. Finally, the VSWR curve on the right visually depicts the bandwidth where the VSWR remains below 2, ranging from 15.26 to 15.42 MHz.

Next Steps

This analysis of the MI2 Fractal Loop antenna using AN-SOF serves as a springboard for further exploration. In the next section, we'll simulate a 3-element array of MI2 loops, aiming to achieve potentially **increased bandwidth** compared to Dr. Cohen's original 2-element design.

Expanding the Potential: 3-Element Array of Snowflake Quads

The MI2 fractal loop antenna is also known as the **snowflake quad**. This section explores a concept that expands on Dr. Cohen's work: a 3-element array derived from this snowflake fractal design.

The AN-SOF model and simulation results in **Fig. 5** are particularly noteworthy. Our simulations demonstrate that a 3-element array can nearly **double the reported bandwidth** of a 2-element MI2 Fractal Loop antenna. This improvement stems from the array configuration, which utilizes a strategically placed **reflector**, **driven element**, and **director** to optimize performance.

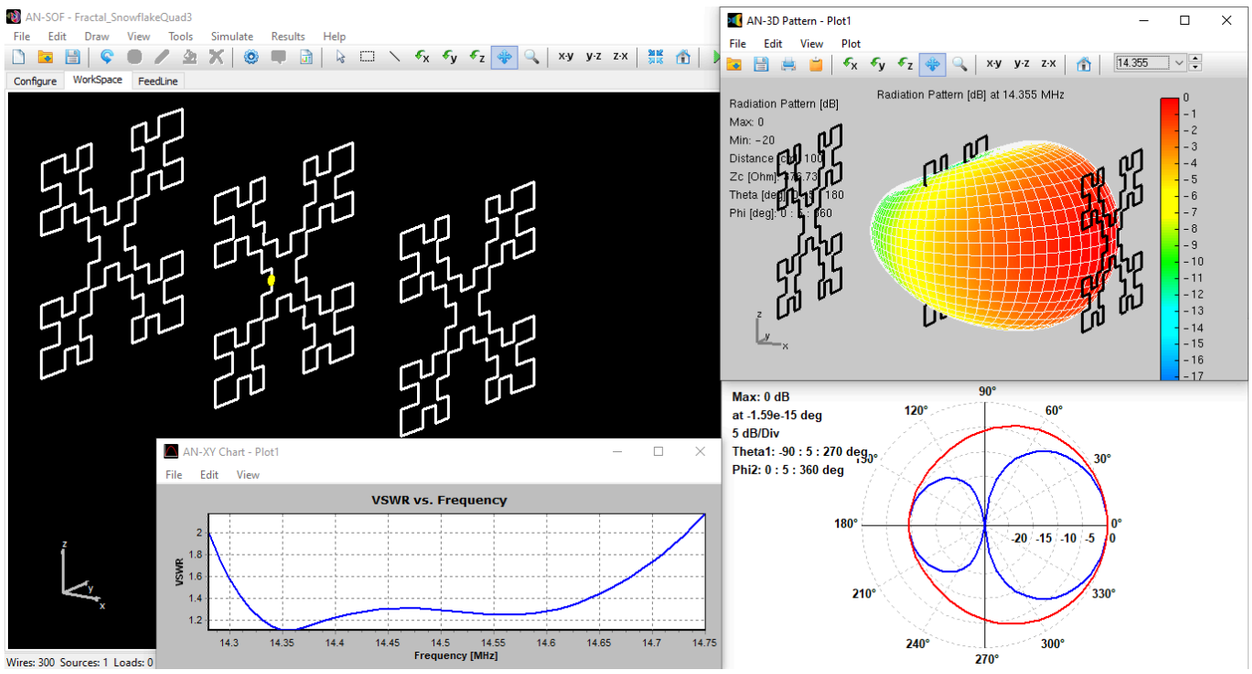

Fig. 5: 3-Element MI2 Fractal Loop Array (20m band).

Download Model

Compelling Performance in the 20m Band

Here's a breakdown of the simulated performance for the 3-element array operating in the 20m band (around 14 MHz):

- **Compact Quad Size:** Each quad element measures approximately 290 x 290 cm, representing a mere 0.14 x 0.14 wavelength footprint.
- **Optimized Element Spacing:** The elements within the array are spaced at roughly 280 cm for optimal signal interaction.
- **Wide Bandwidth:** The simulated results indicate a substantial bandwidth of 450 kHz (VSWR < 2), centered around 14.5 MHz. This translates to a notable improvement over 2-element designs.
- **Balanced Gain and Front-to-Back Ratio:** The array exhibits a gain of 6 dBi, while maintaining a front-to-back ratio of 10 dB.
- **Beamwidth and Polarization:** The simulated beamwidth of the array is approximately 80°, making it suitable for various communication applications. The antenna maintains vertical polarization for consistent signal orientation.

Practical Advantages and Considerations

While the 3-element array might not achieve the same level of gain as a larger 3-element Yagi-Uda antenna, it offers a compelling trade-off. The fractal design

delivers a remarkably wide bandwidth within a very compact size. Additionally, it eliminates the need for a matching circuit, as its impedance is simulated to be **50 Ohms at resonance**, allowing for direct connection to a 50 Ohm coaxial cable. This translates to a simpler and potentially lower-cost antenna system.

Figure 5 provides a comprehensive view of this design. On the left, the 3-element array is shown within the AN-SOF workspace. The right side displays the radiation pattern, and the bottom left corner presents the VSWR curve, which visually represents the bandwidth where the VSWR remains below 2.

Scaling the Snowflake Quad for Different Bands

To design a snowflake quad antenna for a band other than the 20m example, we simply need to rescale the antenna dimensions. For instance, to operate in the 10m band (around 30 MHz), you would divide the model dimensions by 2.

AN-SOF makes rescaling straightforward using the **Scale Wires** command (**Fig. 6**). Here's how to do it:

1. Click the "Selection Box" button on the AN-SOF toolbar and draw a box that encompasses the entire antenna.
2. Navigate to the main menu: **Edit > Scale Wires**.
3. Set the scale factor to 0.5 to halve the antenna dimensions.

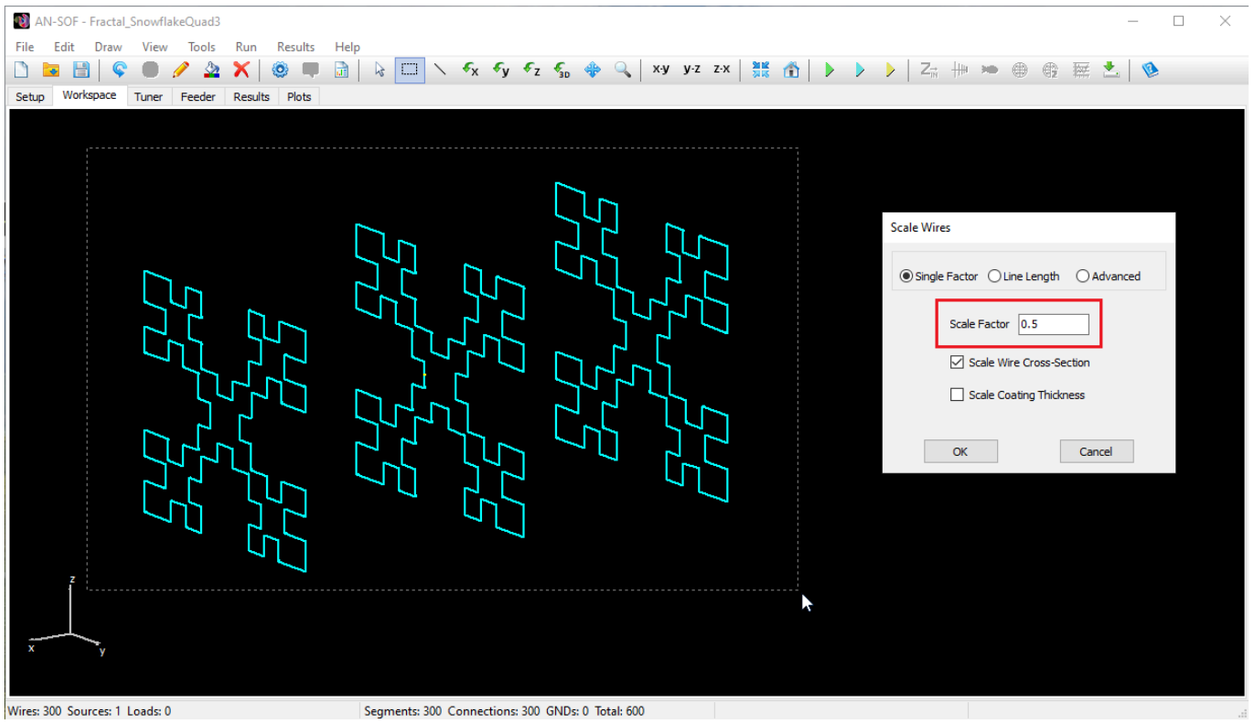

Fig. 6: Rescaling the 3-Element MI2 Fractal Loop Array in AN-SOF.

Optionally, you can also scale the **wire cross-section radius**. However, it's important to note that if you don't scale the wire thickness, the resonance frequency in the 10m band won't be precisely double the 20m band's resonance. This is because the wire thickness affects the antenna's input impedance.

Looking Ahead

The 3-element snowflake quad array exemplifies the potential of fractal antennas to deliver exceptional performance within compact and practical designs. In the next section, we'll conclude by summarizing the key takeaways and exploring exciting future directions for fractal antenna research.

Concluding Remarks

This final section serves to summarize the key takeaways from our exploration of fractal antennas and address some frequently asked questions.

1. Fractal Concept: Unveiling the Beauty of Complexity

At their core, fractals are self-similar patterns that exhibit intricate detail at every scale. Imagine a coastline – as you zoom in, you discover smaller and smaller coves and inlets that resemble the overall shape of the entire coastline. This concept of infinite complexity within a bounded structure is a hallmark of fractals.

While chaos theory delves into seemingly random systems exhibiting underlying order, the connection to fractals is more philosophical. Fractals, with their intricate self-similarity, can sometimes represent the unpredictable behavior observed in chaotic systems. However, not all fractals are inherently chaotic.

2. Antenna Application: When Geometry Gets Smart

The magic of fractal antennas lies in their ability to leverage these self-similar patterns **to increase the electrical length** of an antenna within **a compact physical size**. This translates to several advantages:

- **Wider Bandwidths:** Fractal designs can achieve a broader range of operational frequencies compared to traditional antennas of similar size.
- **Enhanced Efficiency:** The increased electrical length improves radiation efficiency, leading to stronger signal transmission and reception.
- **Reduced Size:** Fractal antennas can be significantly smaller than their traditional counterparts, making them ideal for applications with limited space constraints.

3. Practical Examples: Fractals in Action

The **MI2 Fractal Loop antenna** exemplifies the potential of fractal designs. It offers a desirable resonant resistance within a **compact form factor**. Additionally, the **3-element snowflake quad array** demonstrates how fractal geometries can be used to create arrays with impressive bandwidth and front-to-back ratios.

Beyond these examples, fractal design principles can be applied to various antenna types, including dipoles, monopoles, and patches. This versatility opens doors for innovation across a wide range of antenna applications.

In Conclusion

Fractal antennas represent a fascinating and revolutionary approach to antenna design. Their ability to achieve superior performance within compact sizes makes them ideal for a wide range of applications, from mobile communication to military technology. As research in this field continues to evolve, we can expect to see even more innovative and efficient fractal antenna designs emerge in the years to come.

See Also:

- **The MI2 Fractal Loop: Achieving Resonant Efficiency in Compact Apertures**
- **New Tools in AN-SOF: Selecting and Editing Wires in Bulk**
- **Overcoming 7 Limitations in Antenna Design: Introducing AN-SOF's Conformal Method of Moments**

About the Author

Tony Golden

RF ENGINEER & PHYSICS PH.D. With 25+ years in Computational Electromagnetics, I'm a passionate researcher focused on antenna modeling and design. As Founder of Golden Engineering LLC, I develop accessible, high-performance simulation tools that help RF engineers optimize their designs, educators teach complex concepts, and hobbyists bring antenna projects to life.

Have a question?

💬 **Ask me** | ✉️ **Email me** | 🌐 **Follow me**

Antennas and Beyond!

Get Exclusive Updates

Share this Article

Modeling Common-Mode Currents in Coaxial Cables: A Hybrid Approach

Share this Article

This article presents a hybrid modeling approach for coaxial transmission line antenna feeders, focusing on the impact of common-mode currents on the antenna radiation pattern. By explicitly modeling the outer shield of coaxial cables, we can accurately predict and mitigate RF interference, enhancing antenna system performance for RF engineers and enthusiasts.

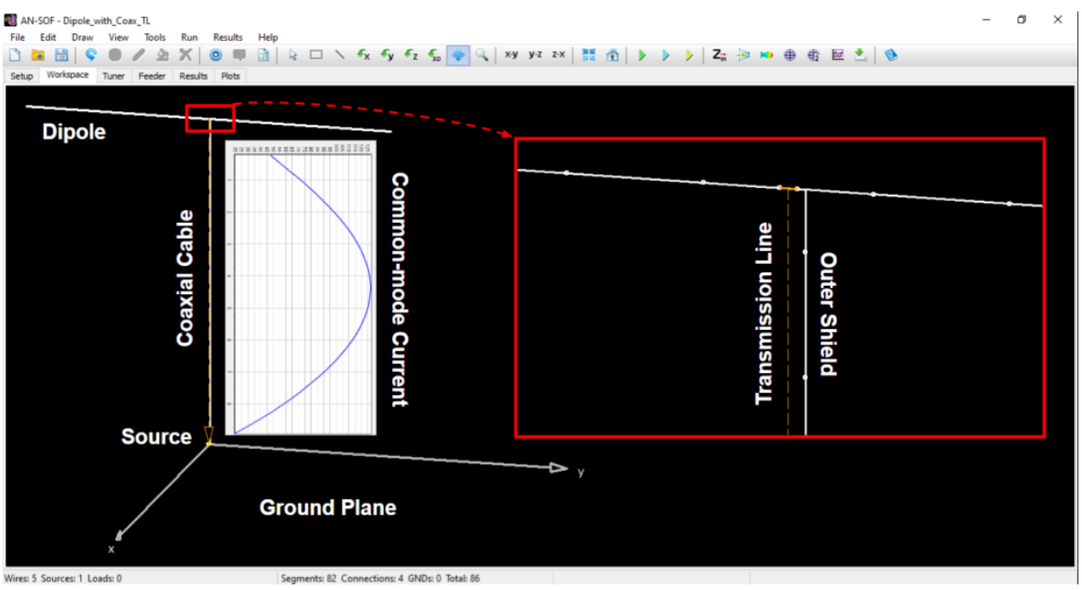

Introduction

In the realm of antenna engineering, the impact of **common-mode currents on coaxial cable feeders** is a crucial factor to consider. These currents can cause **unintended radiation**, potentially leading to RF interference in nearby equipment and reducing the overall performance of the antenna system. Understanding and mitigating these effects are essential for achieving optimal antenna performance, especially in applications involving precise and sensitive RF measurements.

Hybrid Modeling of Coaxial Transmission Line

To accurately model the behavior of coaxial cables used in antenna systems, this study presents a **hybrid approach**. The antenna model discussed here comprises **a**

resonant dipole nearly half a wavelength long, positioned horizontally at a height of half a wavelength above a **lossy ground plane**. It is centrally fed through a 50 Ohm transmission line, representing a coaxial cable connected to a voltage source near ground level.

As sources must always be connected to wire segments, a very short wire (just 0.3% of the wavelength) having **one segment** supporting the source has been added near the ground plane. The frequency is set to 14 MHz in the simulation just as an example, since the purpose is to describe the model conceptually.

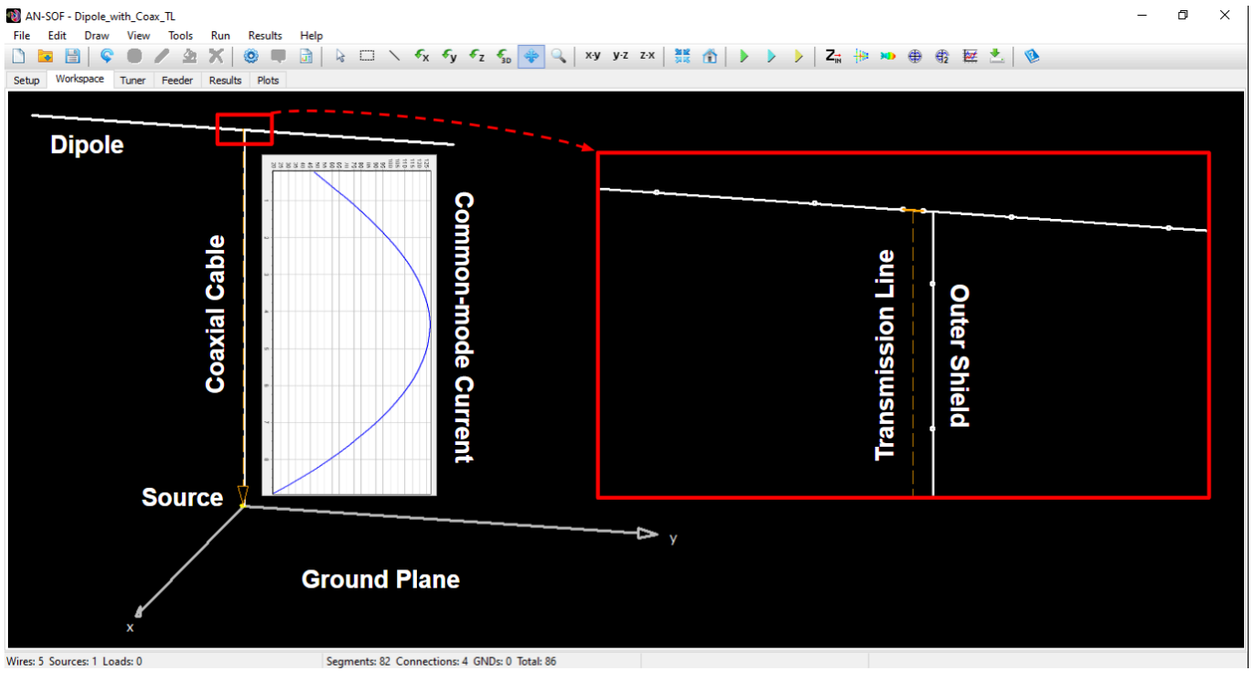

Fig. 1: Horizontal dipole model with coaxial feeder in AN-SOF's workspace above an average ground plane, showing the common-mode current along the coax shield.

Download Model

While the initial model includes the source, transmission line, and dipole, **an additional vertical wire has been integrated to represent the outer surface of the coaxial cable shield**. This addition exemplifies a hybrid model of the coaxial transmission line: the interior of the line is implicitly modeled, as it does not radiate, while the exterior of the shield is explicitly represented by a metallic wire with a diameter matching that of the cable shield. This approach allows for the accurate representation of **the radiation effect of the common-mode current** flowing on the exterior of the coaxial cable shield, which may cause RF interference in the vicinity of the antenna.

By applying an input power of 100 W and plotting the common-mode current in the vertical wire, the current's peak value of 127 mA is observed in the middle of the wire, following a nearly sinusoidal pattern, as expected for a half-wave wire. Figure 1 shows the antenna model in AN-SOF's workspace on the left, where the current distribution along the coax shield is plotted. The inset on the right provides a zoomed-in view of the horizontal dipole center, showcasing the transmission line model and the wire representing the coax shield, both connected to the dipole center. The maximum current at the dipole center is 1.12 A for an input power of 100 W at the source. Therefore, the common-mode current is on the order of 10% of the current on the dipole.

The detailed procedure to model the coaxial cable in AN-SOF can be found at this link: **Modeling Coaxial Cables**.

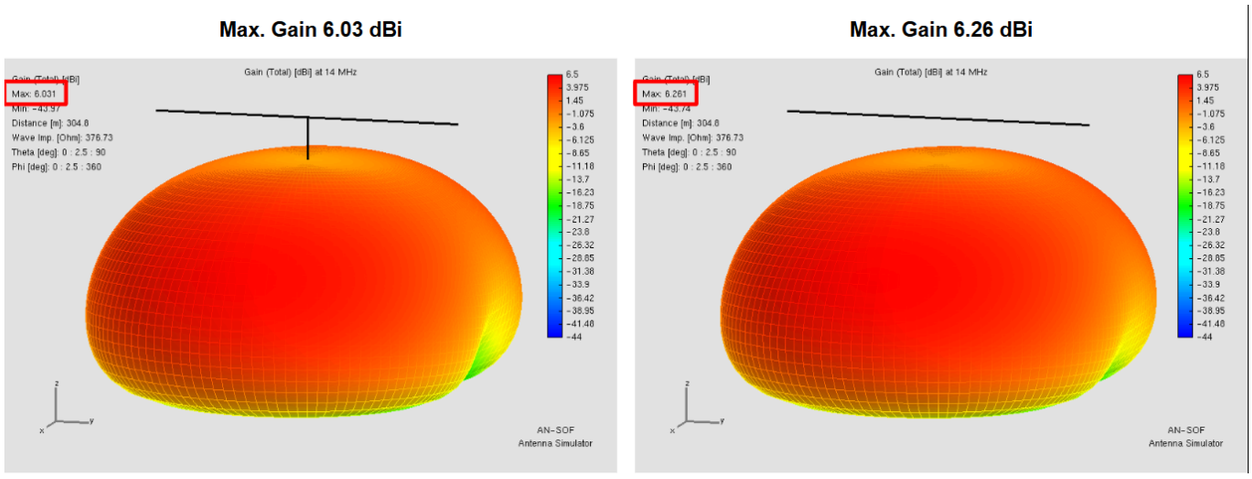

Fig. 2: Gain pattern of the horizontal dipole with (left) and without (right) the vertical wire modeling the coax shield.

If we plot the 3D radiation pattern of the antenna modeled with and without the coax shield, a slight effect can be observed, as shown in Figure 2, where the gain in dBi is represented with the coax shield on the left and without the coax shield on the right. Removing the coax shield effect in the feeder increases the gain from 6.03 to 6.26 dBi.

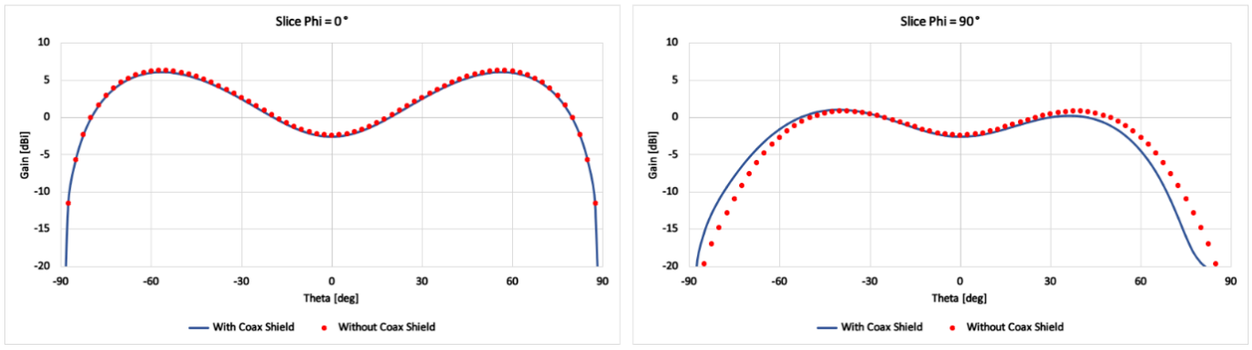

Fig. 3: Vertical slices of the gain pattern of the horizontal dipole with coaxial feeder for azimuth angles Phi = 0° (left) and Phi = 90° (right), with (solid blue curves) and without (dotted red curves) the coax shield.

The distortion in the radiation pattern is more clearly appreciated in Figure 3, where a slice for Phi = 0° is shown on the left and for Phi = 90° on the right. The blue solid curves represent the gain with the coax shield, and the red dotted curves represent the gain without the coax shield. The coax shield effect is more clearly appreciated in the slice parallel to the dipole (Phi = 90°).

We invite readers to further explore the impact of the coax shield by analyzing its effect on the feedpoint impedance at the source position.

Conclusion

The presented **hybrid modeling approach for coaxial transmission lines** provides a comprehensive way to account for the external radiation effects caused by **common-mode currents**. By explicitly modeling the outer surface of the coaxial cable shield, this method enables accurate predictions of potential RF interference,

ensuring better performance and reliability of antenna systems. This approach is particularly valuable for RF engineers, ham radio amateurs, and students focused on achieving precision in antenna design and simulation.

See Also:

- **Transmission Line Feeding for Antennas: The Four-Square Array**
- **The Lazy-H Antenna: A 10-Meter Band Design Guide**

About the Author

Tony Golden

RF ENGINEER & PHYSICS PH.D. With 25+ years in Computational Electromagnetics, I'm a passionate researcher focused on antenna modeling and design. As Founder of Golden Engineering LLC, I develop accessible, high-performance simulation tools that help RF engineers optimize their designs, educators teach complex concepts, and hobbyists bring antenna projects to life.

Have a question?

💬 **Ask me** | ✉️ **Email me** | 🌐 **Follow me**

Precision Modeling of Small Loop Antennas: Validating the Conformal Method of Moments (CMoM)

Share this Article

Validate the precision of the Conformal Method of Moments (CMoM) through this rigorous study of small loop antennas. By comparing simulated circular and square loops against classical asymptotic theory, we demonstrate how AN-SOF accurately models radiation resistance and directivity in the low-frequency limit, where antenna size is a tiny fraction of a wavelength. This article provides essential insights into shape-independence and numerical stability for electrically small radiator design.

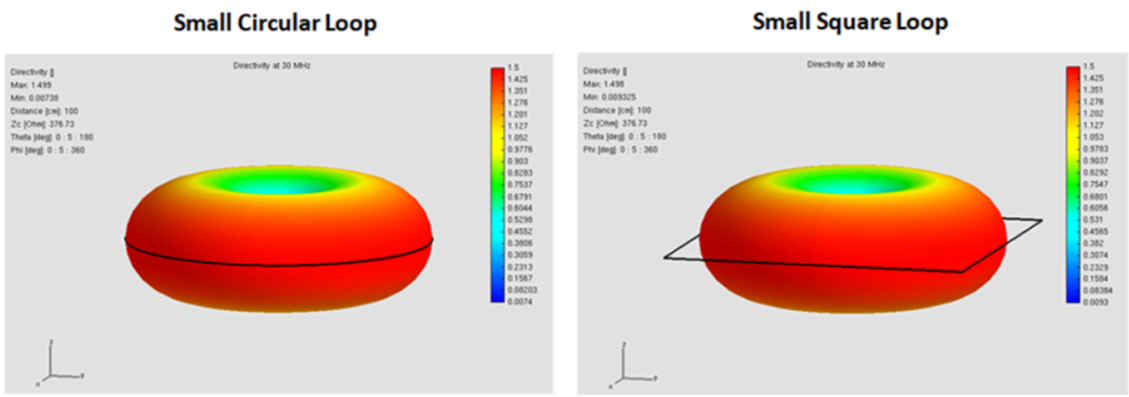

Introduction to Small Loop Electromagnetics

Small loop antennas, defined as those where the total circumference is significantly smaller than the operating wavelength (λ), represent a fundamental class of radiators in radio frequency design. These antennas are characterized by a primarily **inductive** input impedance and **a radiation resistance that is notoriously low**, making them a challenge for both physical implementation and numerical simulation.

A critical theoretical prediction for these structures is that when the loop size tends toward zero, its radiation resistance, R_r, becomes independent of its geometric shape (e.g., circular vs. square) and depends solely on its physical area, A,

measured in square wavelengths. This relationship is governed by the following asymptotic expression:

$$R_r = 31200 \left(\frac{A}{\lambda^2} \right)^2 \qquad (1)$$

This equation assumes a **uniform current distribution** along the loop circumference, a condition typically met only when the loop is electrically "tiny". Validating this behavior requires a simulation engine capable of handling extreme discretization challenges and **curved geometries with high precision**.

Advantages of the Conformal Method of Moments (CMoM)

The simulation results presented in this study were obtained using the **Conformal Method of Moments (CMoM)** implemented in the AN-SOF engine. Traditional Method of Moments (MoM) codes often rely on "staircase" approximations for curved structures, which can introduce artificial numerical noise, especially when calculating the very low radiation resistances typical of small loops.

The CMoM implementation provides two distinct advantages for this analysis:

1. **Geometric Fidelity:** It allows for the exact modeling of curved antenna contours, eliminating the errors associated with linear segment approximations.
2. **Low-Frequency Stability:** It remains numerically stable at extremely low frequencies, or equivalently, in scenarios where the antenna dimensions are a minute fraction of the wavelength.

Simulation Setup and Parameter Comparison

To demonstrate these capabilities, we compared two distinct geometries with an identical area of $0.01\ \mathrm{m}^2$:

- **Square Loop:** $0.1\ \mathrm{m} \times 0.1\ \mathrm{m}$.
- **Circular Loop:** Radius of $0.05642\ \mathrm{m}$.

The loops were simulated across a frequency range of $20\ \mathrm{MHz}$ to $200\ \mathrm{MHz}$. At $100\ \mathrm{MHz}$ ($\lambda \approx 3\ \mathrm{m}$), the normalized loop area is approximately $0.0011\lambda^2$, placing these structures firmly in the "small loop" category.

Input Resistance and Theoretical Departure

Figure 1 illustrates the computed input resistance for both the circular and square loops alongside the theoretical prediction from Equation (1).

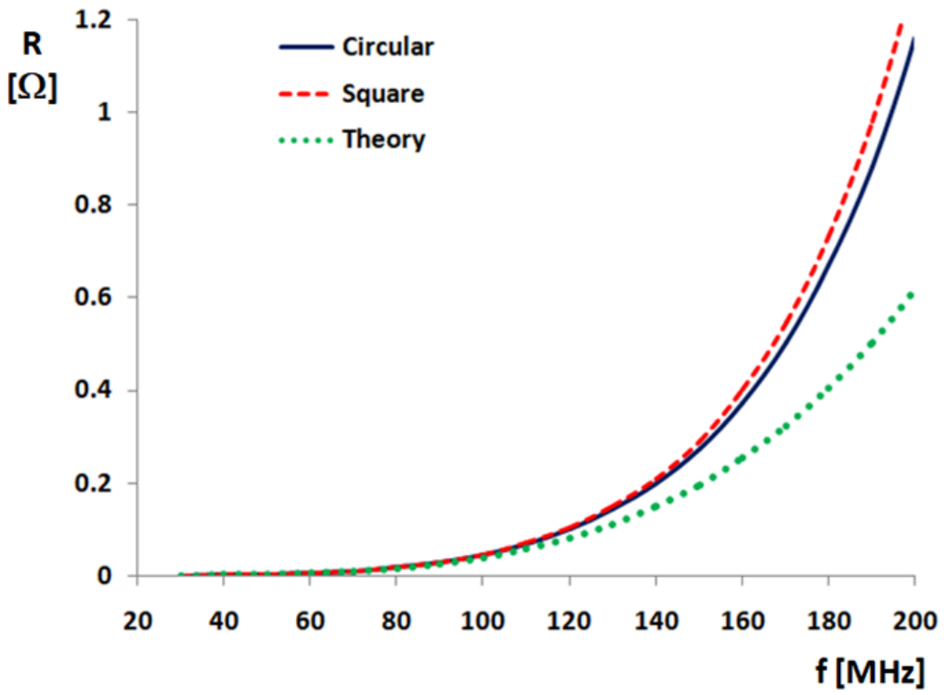

***Fig. 1**: Input resistance of small circular and square loops, calculated using AN-SOF, compared to the theoretical radiation resistance curve. Both loops have an area of* $0.01\ \mathrm{m}^2$.

At lower frequencies (below $100\ \mathrm{MHz}$), the simulation results for both shapes align perfectly with the theoretical curve, confirming that **the radiation resistance is indeed independent of shape in the small-limit case**. However, as the frequency increases toward $200\ \mathrm{MHz}$, the theoretical prediction begins to depart from the simulation results. This divergence occurs because the assumption of a perfectly uniform current distribution and the validity of the simple asymptotic formula begin to fail as the loop circumference becomes a more significant fraction of the wavelength.

Directivity and Radiation Patterns

Another hallmark of small loop theory is that the peak directivity should be independent of both loop size and frequency, reaching a constant value of $1.5\ (3/2)$. This is identical to the directivity of a **Hertzian dipole**.

The AN-SOF simulation confirms this behavior across the sweep. **Figure 2** shows the peak directivity remaining near the horizontal asymptote of 1.5, with only slight variations occurring as the loops approach $200\ \mathrm{MHz}$. The resulting radiation pattern is “donut-shaped,” with the nulls aligned along the axis of the loop, as shown in **Fig. 3**.

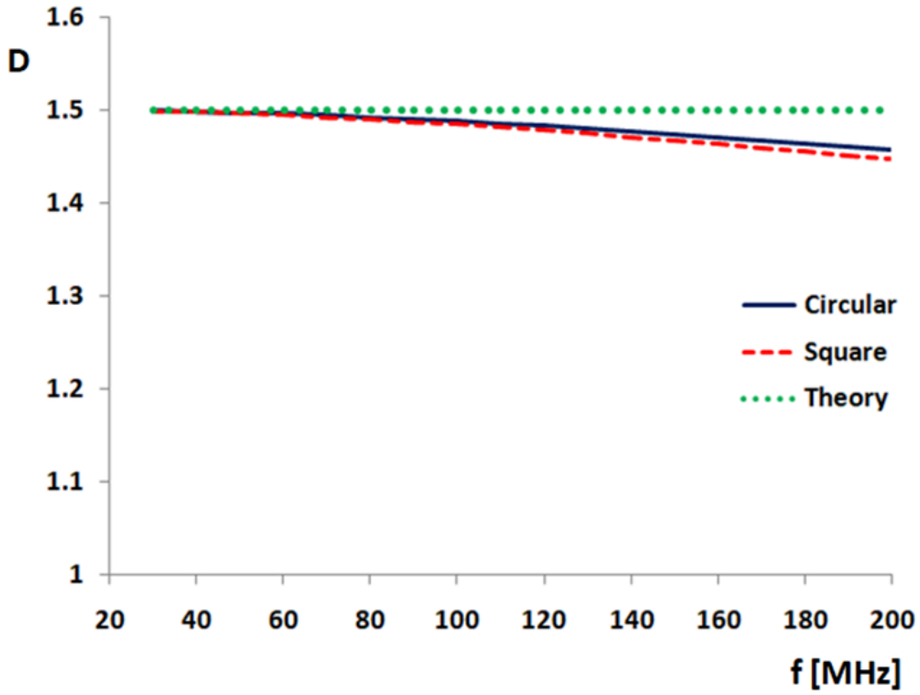

***Fig. 2**: Directivity of small circular and square loops, calculated using AN-SOF, plotted as a function of frequency. The loops have an equal area of $0.01\ \mathrm{m}^2$. The horizontal asymptote at 1.5 represents the theoretical directivity value.*

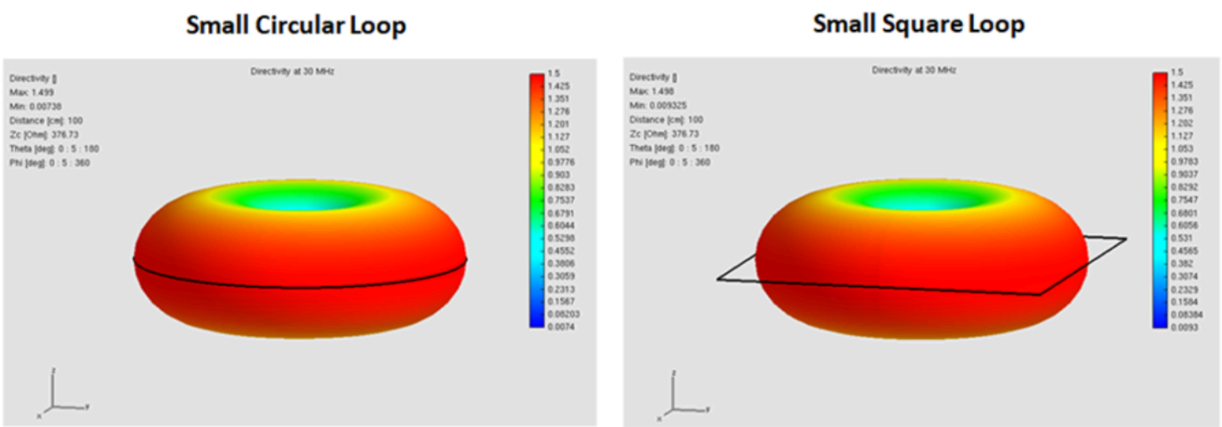

Fig. 3: Radiation patterns of small circular (left) and square (right) loops, both having an equal area of $0.01\ \mathrm{m}^2$, simulated using AN-SOF at $30\ \mathrm{MHz}$.

The mathematical expression for this **directivity pattern** is:

$$D = \frac{3}{2}\sin^2\theta \qquad (2)$$

where θ is the angle measured from the loop axis.

In **Fig. 4**, a vertical slice of the radiation pattern at $30\ \mathrm{MHz}$ shows an almost perfect match between the circular loop simulation and the theoretical sine-squared distribution of Equation (2). The square loop results at this frequency are so closely aligned that they are indistinguishable to the naked eye, further validating the shape-independence of the far-field pattern in the small-loop limit.

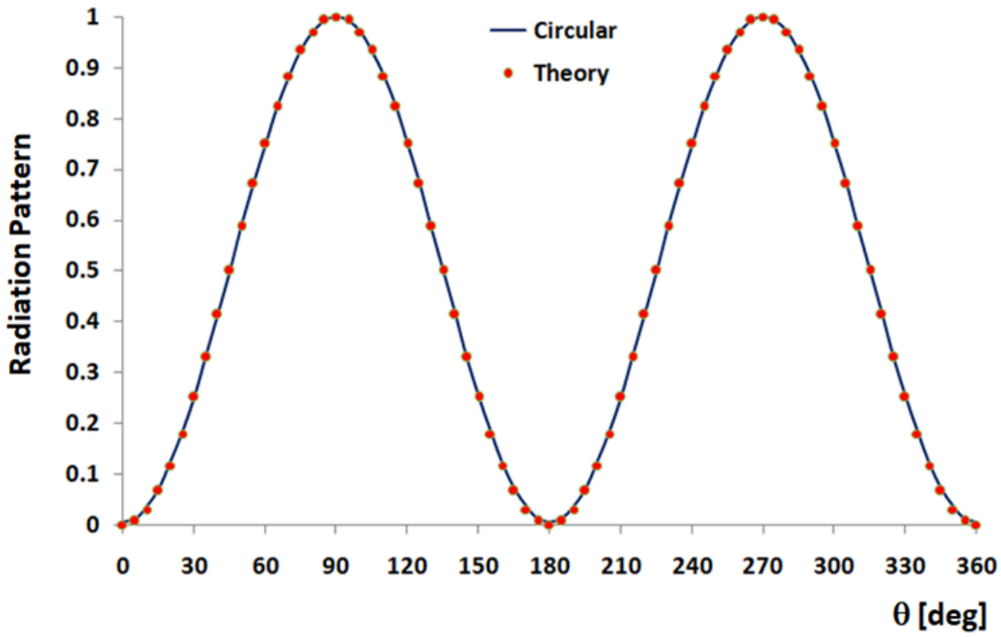

***Fig. 4**: Vertical radiation pattern slice for a small circular loop antenna with an area of $0.01\ \mathrm{m}^2$. The solid line represents the AN-SOF simulation result at $30\ \mathrm{MHz}$, and the dots correspond to the theoretical approximation.*

Conclusion

The analysis of small circular and square loops serves as a powerful validation of the AN-SOF engine and its CMoM implementation. By accurately capturing the convergence of radiation resistance for different geometries at low frequencies, the simulation confirms the fundamental "area-only" dependence predicted by theory.

Furthermore, the stability of the 1.5 directivity value and the precision of the donut-shaped radiation patterns demonstrate that AN-SOF can handle the high-dynamic-range requirements of modeling electrically tiny antennas without falling victim to numerical instability. This benchmark provides antenna designers with the confidence that CMoM is a robust tool for designing not only large-scale arrays but also the compact, high-Q radiators utilized in specialized low-frequency and sensing applications.

See Also:

- **Modeling a Circular Loop Antenna in AN-SOF: A Step-by-Step Guide**
- **Precision Simulations with AN-SOF for Magnetic Loop Antennas**
- **Learning Antennas Through Simulation: 4.1 Loop Antennas**

Technical Keywords: Small Loop Antenna, Radiation Resistance, Peak Directivity, Conformal Method of Moments (CMoM), AN-SOF Simulation, Low-Frequency Electromagnetics, Hertzian Dipole Pattern, Asymptotic Theory.

About the Author

Tony Golden

RF ENGINEER & PHYSICS PH.D. With 25+ years in Computational Electromagnetics, I'm a passionate researcher focused on antenna modeling and design. As Founder of Golden Engineering LLC, I develop accessible, high-performance simulation tools that help RF engineers optimize their designs, educators teach complex concepts, and hobbyists bring antenna projects to life.

Have a question?

💬 **Ask me** | ✉️ **Email me** | 🌐 **Follow me**

Antennas and Beyond!

Get Exclusive Updates

Share this Article

Precision Simulations with AN-SOF for Magnetic Loop Antennas

Share this Article

Explore dual-loop magnetic antenna design and simulation with AN-SOF. Model performance at five frequencies, showcasing radiation patterns, current distributions, and tuning values. Automated bulk simulations streamline the process.

Magnetic loop antennas are widely used in amateur radio. A common design involves a **dual-loop configuration** where a larger loop, equipped with a **tuning capacitor**, is magnetically coupled to a smaller, internal loop. The coaxial cable feeding the antenna connects to the smaller loop. This antenna is simple to construct using readily available coaxial cable. Importantly, the interaction between the loops is inductive, not physical.

The accompanying figure shows a simulation of a magnetic loop antenna. The larger loop, made from **RG-8 cable**, has a diameter of **70 cm**, while the smaller loop, made from **RG-6 cable**, has a diameter of **15 cm**. The loops are separated by **2 cm** at the base. The required tuning capacitor values for resonance at **3.5, 7, 14, 21, and 29 MHz** are indicated.

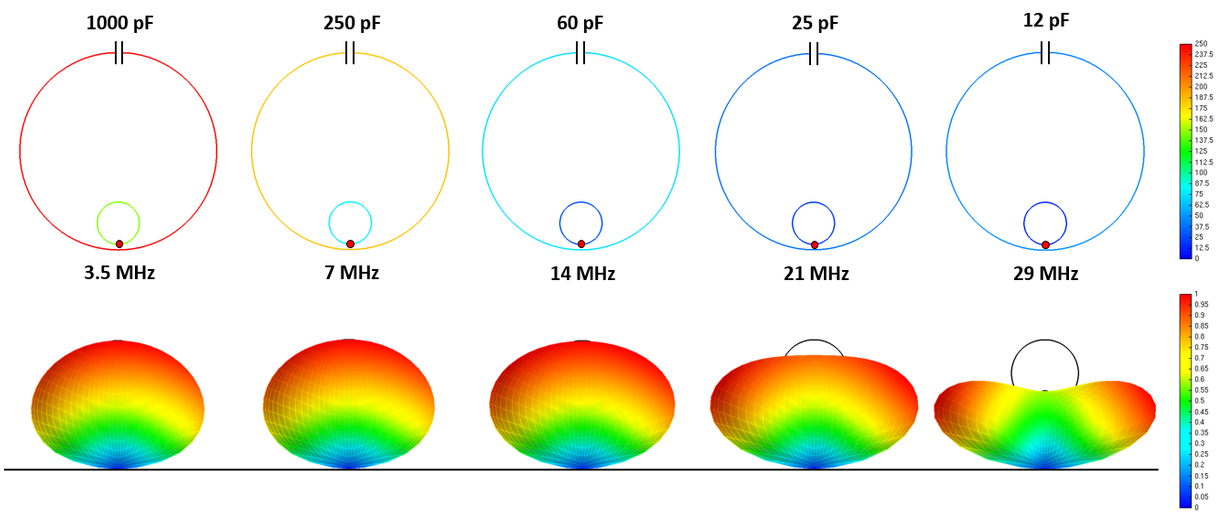

A series of images showcasing radiation patterns, current distributions, and tuning capacitor values for the magnetic loop antenna across 3.5, 7, 14, 21, and 29 MHz. Simulated using AN-SOF Antenna Simulator.

Download Model

Placed one meter above a ground plane, the antenna's radiation pattern deviates from the typical toroidal shape expected of a small loop in free space. The color scale on the loops represents current distribution at each resonant frequency.

The **AN-SOF Antenna Simulator** enables accurate simulations of this antenna design using the **Conformal Method of Moments** with **curved segments** to precisely model loop shapes. AN-SOF's **exact Kernel** accurately handles the close proximity of the loops at the antenna's base.

The simulator streamlines the calculation process by automating resonance calculations for the five specified frequencies. To access this feature, go to the AN-SOF main menu and select "**Run Bulk Simulation**" under the "Run" category. This allows you to easily run calculations on the five provided .nec files, which can be downloaded by pressing the "Download Model" button above. Importantly, this feature is available in the **trial version of AN-SOF**.

See Also:

- **Modeling a Circular Loop Antenna in AN-SOF: A Step-by-Step Guide**
- **Exploring the Spiral Loop Antenna: A Compact Solution for 80m DXing**

About the Author

Tony Golden

RF ENGINEER & PHYSICS PH.D. With 25+ years in Computational Electromagnetics, I'm a passionate researcher focused on antenna modeling and design. As Founder of Golden Engineering LLC, I develop accessible, high-performance simulation tools that help RF engineers optimize their designs, educators teach complex concepts, and hobbyists bring antenna projects to life.

Have a question?

💬 **Ask me** | ✉️ **Email me** | 🌐 **Follow me**

Exploring the Spiral Loop Antenna: A Compact Solution for 80m DXing

Share this Article

Uncover the compact marvel of the Spiral Loop Antenna, offering a unique solution for 80m DXing enthusiasts seeking efficient performance in limited space.

Key Takeaways

- **Space-Saving Alternative:** Spiral loops offer a compact solution, addressing the space constraints of traditional dipoles.
- **Tackling Efficiency Challenges:** Despite efficiency hurdles, spiral loops provide easy tuning and a respectable bandwidth.
- **AN-SOF's Precision:** AN-SOF enables accurate spiral loop modeling, empowering hams to innovate designs for diverse conditions.

A **half-wave dipole** for the **80 meters** band (3.75 MHz) would require a length of **40 meters**, making it difficult to install at home due to space constraints and potential neighbor complaints.

In contrast, a **spiral loop** offers a compact size and relative ease of tuning. Essentially an **inductor** with a **variable capacitor** connected at the feed point to achieve **resonance**, it provides an attractive alternative. However, **its radiation resistance is extremely small**, typically on the order of milliohms, resulting in low efficiency.

Unfortunately, any small loss can significantly impact the antenna's efficiency, including losses in the capacitor, wires, interconnections, solder joints, surrounding objects, and ground plane. Despite these challenges, the antenna can be tuned to achieve a wide bandwidth, albeit with reduced efficiency. Maximum radiation occurs vertically when the antenna is installed perpendicular to the ground plane, although some suggest horizontal installation to mitigate potential high voltages across the tuning capacitor.

The AN-SOF model depicted in the figure below consists of a **50 cm** frame on each side, corresponding to **0.00625 of the wavelength** (λ = 80 m), with **7 turns** of wire. Simulating closely spaced and bent wire segments, as depicted, is crucial for accurate representation.

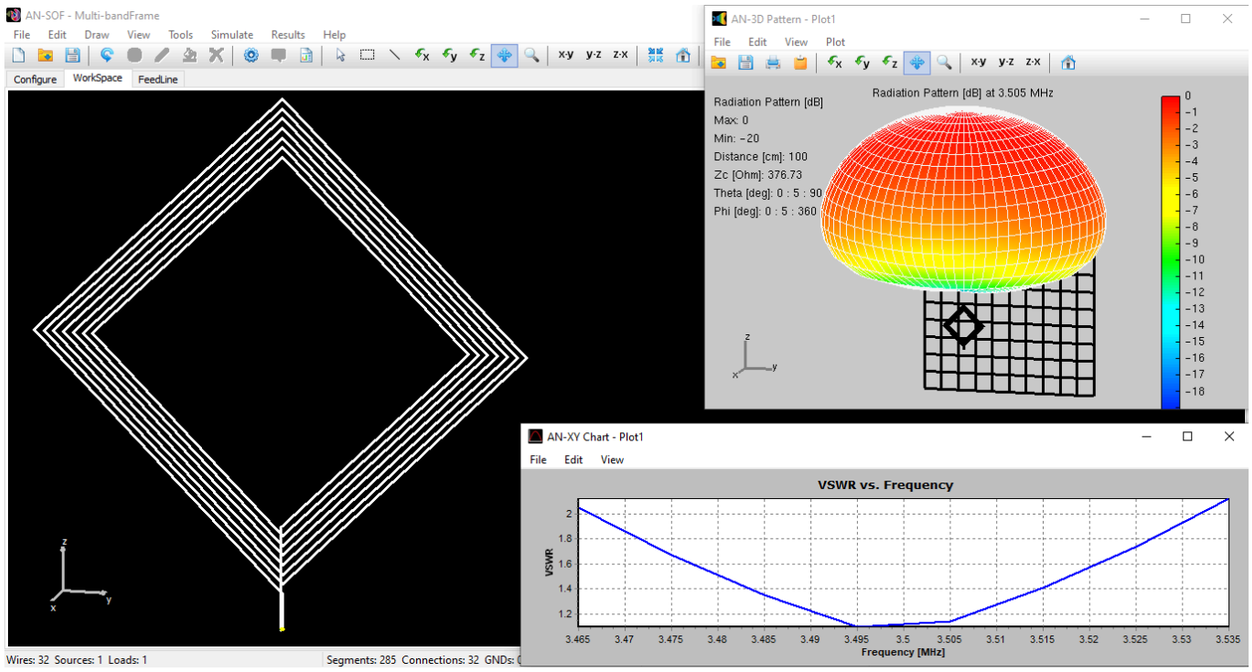

AN-SOF model of a spiral loop antenna with surrounding objects and ground losses.

Download Model

The following input resistance results demonstrate the impact of incorporating losses in the ground plane and adding surrounding objects, such as a wall:

- Perfect ground: **4 milliohms**
- “Cities industrial poor” ground: **1.3 Ohms**
- “Cities industrial poor” ground + wall: **49 Ohms**

The figure above depicts the 3D radiation pattern of the spiral loop antenna in the presence of a wall and a ground plane with “Cities industrial poor” characteristics (conductivity σ = 0.0001 S/m and relative permittivity ε_r = 3). The lower vertex of the antenna frame is elevated 1.5 m above the ground. The wall, measuring 3 m x 3 m, is positioned 3 m away from the antenna and is modeled by a 10 x 10 wire grid. In this scenario, **the radiation pattern points upward**, although it is **omnidirectional in the horizontal plane**. Additionally, the figure shows the VSWR as a function of frequency, with a bandwidth for VSWR = 2 of about 70 KHz, representing 2% of the center frequency of 3.5 MHz.

This design can be easily adapted into a **multi-band antenna** by shorting turns of wire, similar to adjusting a variable inductor, enabling operation on the 40, 30, and 20 meter bands.

In conclusion, AN-SOF’s capability to accurately model antennas with **closely spaced and bent wires** proves invaluable in analyzing complex designs like the spiral loop antenna. By simulating intricate geometries and accounting for factors such as surrounding objects and ground losses, AN-SOF empowers radio hams to optimize antenna performance and adapt designs for diverse operating conditions with confidence.

See Also:

- [Experimenting with Half-Wave Square Loops: Simulation and Practical Insights]
- [The 17m Band 2-Element Delta Loop Beam: A Compact, High-Gain Antenna for DX Enthusiasts]

About the Author

Tony Golden

RF ENGINEER & PHYSICS PH.D. With 25+ years in Computational Electromagnetics, I'm a passionate researcher focused on antenna modeling and design. As Founder of Golden Engineering LLC, I develop accessible, high-performance simulation tools that help RF engineers optimize their designs, educators teach complex concepts, and hobbyists bring antenna projects to life.

Have a question?

💬 **Ask me** | ✉️ **Email me** | 🌐 **Follow me**

Antennas and Beyond!

Get Exclusive Updates

Share this Article

Efficient NOAA Satellite Signal Reception with the Quadrifilar Helix Antenna

Share this Article

The Quadrifilar Helix antenna (QFH or QHA), with its unique design and circular polarization, ensures efficient NOAA satellite signal reception. This article explores the history, key characteristics, and practical modeling of QFH antennas using AN-SOF, providing valuable insights for RF engineers and enthusiasts.

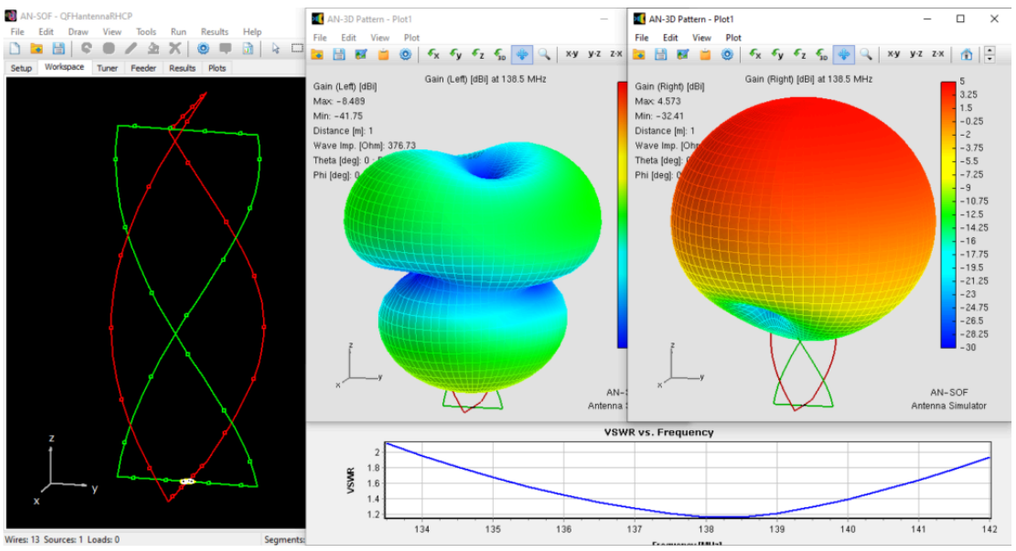

Introduction

The **Quadrifilar Helix (QFH)** antenna, also known as the **QHA**, is an excellent choice for receiving signals from the **National Oceanic and Atmospheric Administration (NOAA) satellites**. This antenna configuration consists of four helically wound monofilar wires that intertwine to form a quadrifilar helix (Fig. 1). This intricate geometric arrangement gives the antenna unique properties in **a compact size:** a directional radiation pattern, circular polarization, and self-resonance with **a feedpoint impedance close to 50 Ohms**. While the QFH antenna's bandwidth is narrower compared to a traveling-wave axial mode helix, its compact form factor makes up for this limitation.

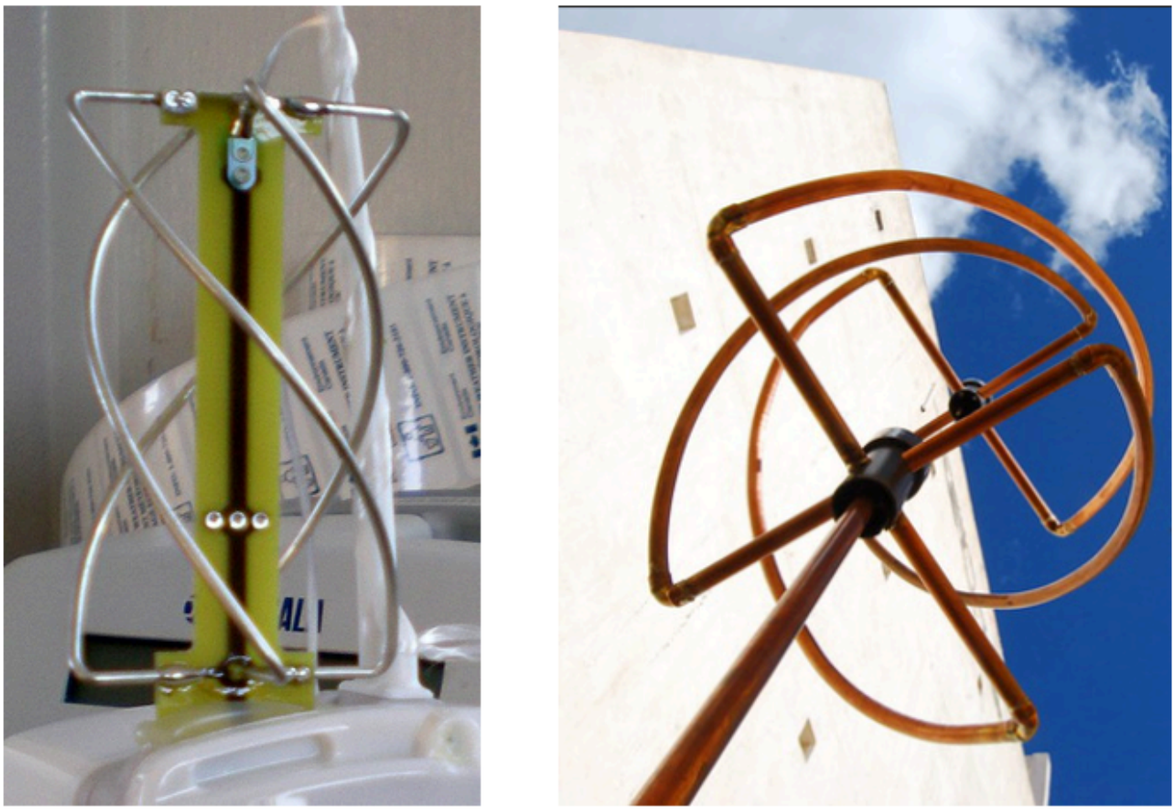

Fig. 1: Quadrifilar Helix Antennas (QFH or QHA) (images licensed under Creative Commons).

Axial Mode Helical Antennas: History and Fundamentals

The **axial mode helical antenna** was invented in 1946 by John Kraus. Inspiration can come when we least expect it:

> *I attended an afternoon lecture on traveling-wave tubes by a famous scientist… In these tubes an electron beam is fired down the inside of a long wire helix for amplification of waves traveling along the helix. The helix is only a small fraction of a wavelength in diameter and acts as a guiding structure. … I asked the visitor if he thought a helix could be used as an antenna. 'No,' he replied, 'I've tried it and it doesn't work.' The finality of his answer set me thinking. If the helix were larger in diameter than in a traveling-wave tube, I felt that it would have to radiate in some way, but how, I did not know. I determined to find out.*
>
> **Dr. John D. Kraus, in "Antennas," 2nd Ed. McGraw-Hill, 1988.**

Today, helical antennas can be easily simulated (Fig. 2). Being **wire antennas**, the most efficient way to simulate them is through **the Method of Moments (MoM)**. However, a poor convergence rate is often obtained for the input impedance when the helix is approximated by straight segments, as is customary. Using **curved segments** that exactly follow the helix contour overcomes this problem.

The axial mode helical antenna is one of the most widely used antennas for UHF and microwave communications. Its robust design makes it ideal for both space and ground applications, contributing significantly to the explosive growth of satellite-based services.

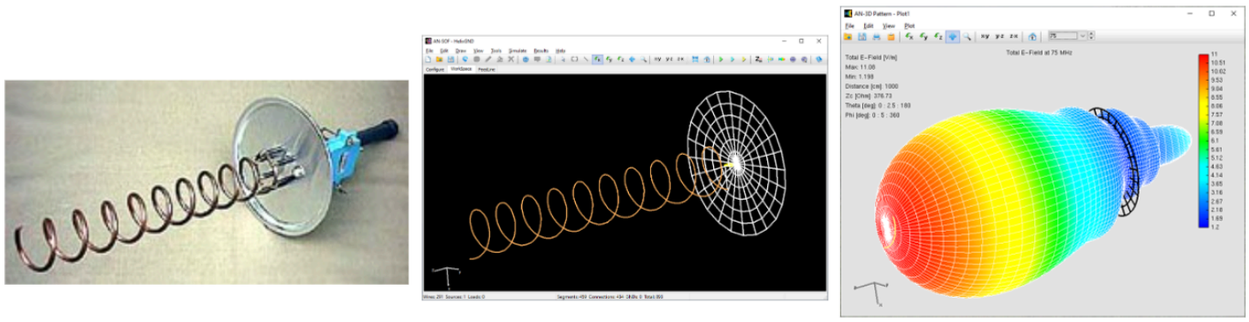

Fig. 2: Axial Mode Helical Antenna. The antenna radiates a beam along its axis. The feedpoint is located between the helix base and the ground plane.

Traveling-Wave Antennas and Axial-Mode Helix: Traveling-wave antennas are a class of antennas where the radio frequency (RF) energy travels along a structure, such as a wire, in a continuous wave. The axial mode helix is a specific type of traveling-wave antenna designed to operate in the axial mode. For a helix to operate in this mode, **the circumference of the helix should be close to one wavelength** of the operating frequency. Additionally, **a metallic ground plane**, often of circular shape, is added to the helix base, as shown in Fig. 2. These conditions allow the antenna to produce a directional radiation pattern with a main beam along the axis of the helix.

Circular Polarization: The axial-mode helical antenna exhibits circular polarization, which can be either right-hand circular polarization (RHCP) or left-hand circular polarization (LHCP), depending on the winding sense of the helix. Circular polarization is achieved when the electric field of the wave rotates in a circular motion as it propagates. The sense of rotation—RHCP or LHCP—is determined by the direction in which the helix is wound. RHCP helical antennas are typically used for transmitting WEFAX pictures due to their reliable performance in space communications.

Importance of Circular Polarization: Circular polarization is crucial in both space communications and terrestrial mobile applications. In space communications, circular polarization helps to mitigate the effects of **Faraday rotation**, an unpredictable phenomenon caused by the ionosphere, which can alter the polarization of the signal. By using circular polarization, satellite communications can maintain consistent signal quality despite these changes. In terrestrial mobile applications, circular polarization helps to reduce signal degradation caused by multipath interference, where signals bounce off various obstacles before reaching the receiver.

Key Characteristics of Quadrifilar Helical Antennas

The axial-mode helix antenna exhibits a consistent input impedance over a wide bandwidth, thanks to its nature as a traveling-wave antenna. For optimal performance, a ground plane with a diameter of about half to one wavelength is required. This antenna type can achieve a gain of 10-17 dBi over a 60% fractional

bandwidth. However, with feedpoint impedances ranging from 150 to 300 Ohms, impedance matching is necessary for efficient operation in 50 Ohm systems.

By adding **extra windings**, the radiation pattern of the axial-mode helix can be tightened, and sidelobes can be reduced compared to a monofilar helix. The **Quadrifilar Helix (QFH)** antenna comprises **four windings of equal torsion**. Unlike long traveling-wave antennas, the QFH can be shortened to sizes commensurate with half a wavelength and operate as a **resonant antenna**, similar to a resonant dipole or loop antenna.

As a resonant antenna, **the QFH has a narrow bandwidth**, requiring careful attention to its dimensions and construction details. Its compactness and ease of integration with mobile systems make the short resonant QFH ideal for portable applications.

Each component helix of a QFH is excited in a **90-degree progression**, either clockwise or counterclockwise, depending on the desired polarization and lobe direction. QFHs can operate in either **endfire** or **backfire** modes, producing a hemispherical directional pattern (Fig. 3). For long quadrifilar antennas, a quadrature feeding network is necessary to generate the 90° phase progressions. This can be achieved using quadrature hybrids and power splitters. For the small resonant helix, using two co-wound half helices with slightly different dimensions can induce quadrature excitation, similar to the "nearly square" method of generating circular polarization in a microstrip patch antenna.

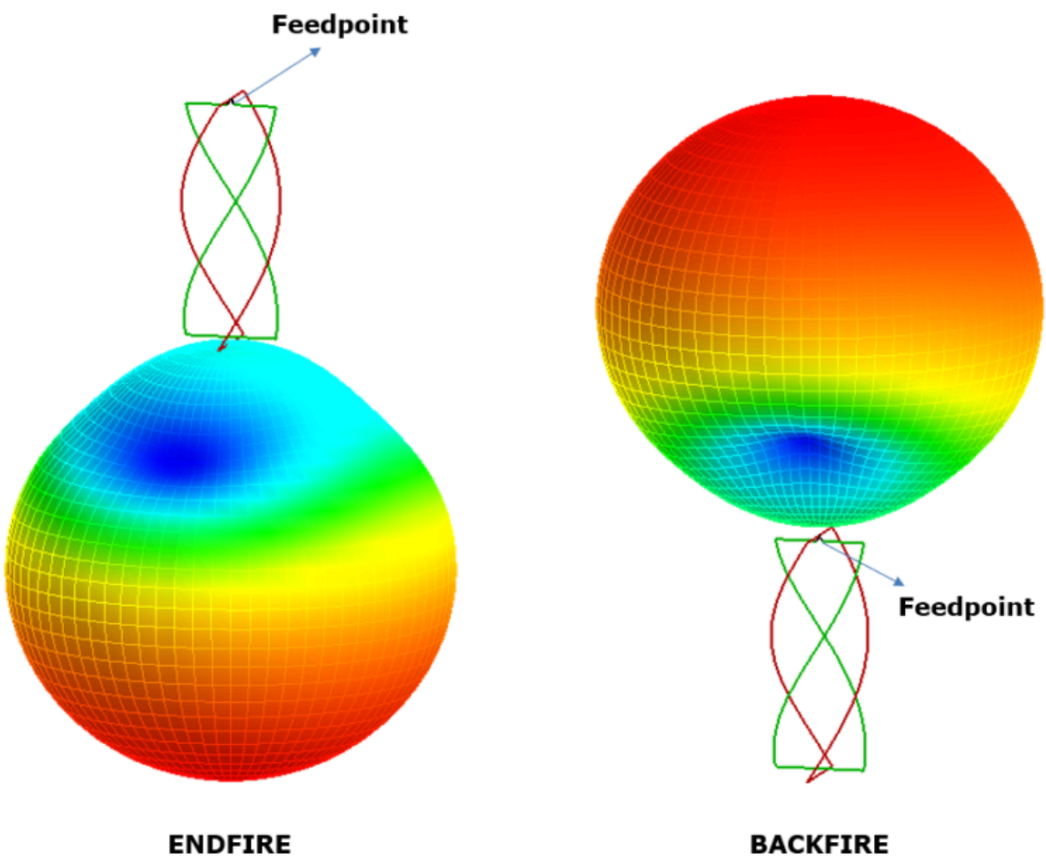

Fig. 3: Endfire (left) and backfire (right) modes of operation of QFH antennas.

The feed phasing sense relative to the QFH winding sense determines the radiation mode: if they match, the antenna will be backfire; if they oppose, the antenna will be endfire. The circular polarization sense of the radiation is always opposite to the helix winding sense, regardless of the feed phasing sense. However, if a backfire helix antenna is used with a reflector or ground plane at the feed, the sense of the circular

polarization is reversed, making the antenna endfire with the polarization sense corresponding to the helix winding.

Summary:

- The helix winding sense is opposed to the desired circular polarization sense. That is to say, left-hand wound helices in a QFH will generate right-hand circular polarization.
- Careful adjustment of the helix dimensions will produce a 50 Ohm feedpoint impedance without the need for external quadrature generating circuits or impedance matching networks.
- The backfire resonant quadrifilar helix antenna is popular for GNSS, communication, and weather satellite receiving stations. This antenna is configured for right-hand circular polarization, with a left-hand winding sense and the feedpoint at the top of the antenna.
- The QFH antenna's ability to provide circular polarization and its compact form factor make it an essential tool for modern communication systems, ensuring reliable performance in a variety of challenging environments.

Input Parameters for Drawing a Helix in AN-SOF

AN-SOF allows you to draw helices quickly. **Right-click on the workspace screen and choose Helix**. There are two options for drawing a helix:

1. **Start – Radius – Pitch – Turns:** In this option, the helix is generated from a starting point along an axis with a defined pitch (distance between turns) and number of turns. The number of turns does not need to be an integer.

- When the pitch is positive, the helix is right-handed, running from the starting point along the +z axis, with the endpoint at z > 0.
- When the pitch is negative, the helix is left-handed, running along the -z axis, with the endpoint at z < 0.

Starting from **AN-SOF version 9.50**, you can enter the helix **diameter**, **pitch angle**, and **filar length** instead of the Radius-Pitch-Turns combination. The **axial height** is automatically calculated. The software warns when the wire diameter is greater than the pitch, preventing the overlapping of the windings.

2. **Start – End – Radius – Turns:** In this option, a helix with an integer number of turns connects the specified start and end points. The straight line connecting these points defines the axis of the helix. Only a helix with an integer number of turns can be mathematically defined between two given points, ensuring that the axis is parallel to the straight line joining them. The helix is right-handed if the number of turns is positive and left-handed if the number of turns is negative. Note that in this option, a pitch cannot be specified, as its value is determined by dividing the distance between the given start and end points (the axial height) by the number of turns (an integer).

A QFH Model for NOAA Satellite Signal Reception

The design depicted in Figure 4 showcases an endfire QFH configuration with a diameter of approximately 0.14 times the wavelength (λ) and helix lengths of 0.4λ. It exhibits a resonant frequency of 138.5 MHz and a fractional bandwidth of 6% (VSWR < 2). The helices composing the QFH antenna are **left-handed**, resulting in a **right-hand circularly polarized (RHCP) field**. This design serves a dual purpose: enabling efficient signal reception from NOAA satellites while effectively mitigating external interference.

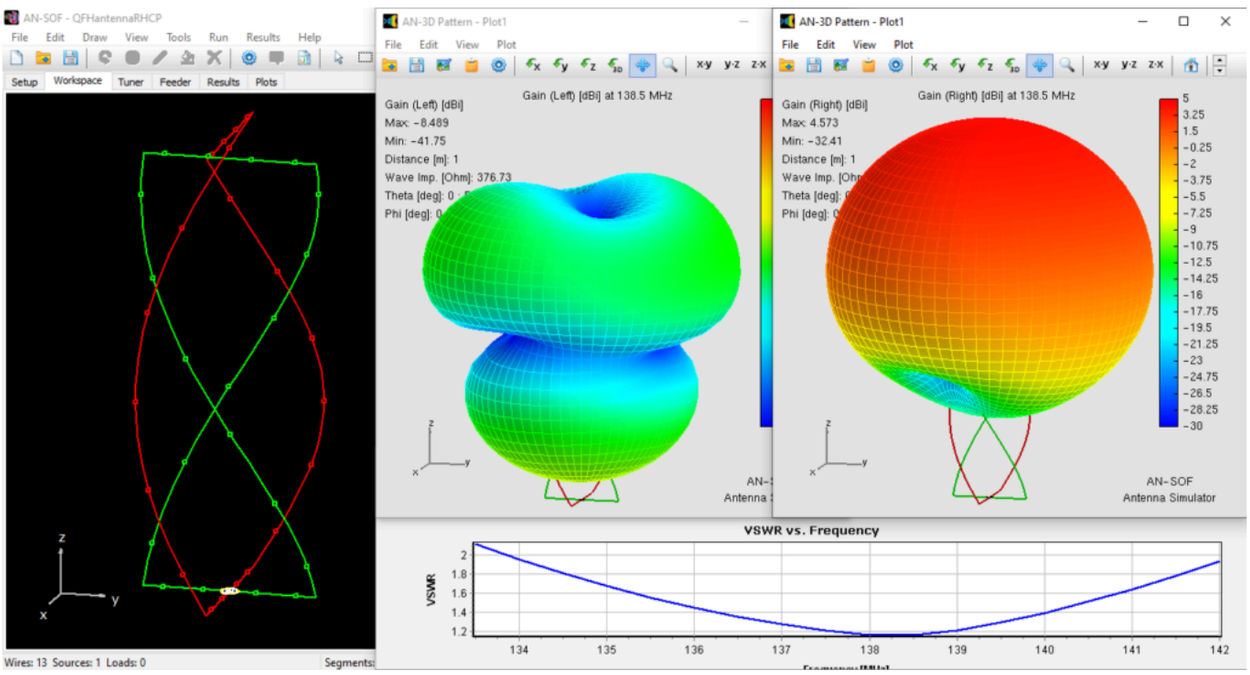

Fig. 4: QFH antenna model in the AN-SOF interface, with the LHCP (center) and RHCP (right) components of the Gain radiation patterns, and the VSWR curve.

Download Model

In free space, the radiation pattern orients upward when the coaxial cable, simulated as a voltage source in the model, connects to the antenna's bottom (endfire mode). **The total gain is 4.6 dBi**. AN-SOF allows for decomposing the gain into right-handed and left-handed polarizations, demonstrating that **the radiated field is RHCP** since the right-hand gain practically equals the total gain and **the left-hand gain is below -8.5 dBi**. The resultant pattern in this configuration is omnidirectional within the azimuth plane, which is invaluable for effectively capturing signals from a variety of satellite orientations.

Thanks to the implementation of **the Conformal Method of Moments (CMoM) in AN-SOF**, we can accurately model the behavior of the QFH **with just 5 segments per helix**, as the **wire segments are curved** and faithfully represent the contour of the helices.

In summary, this Quadrifilar Helix (QFH) antenna model stands as an ingeniously designed configuration. It features a compact form factor, self-resonance, and RHCP, making it adept at capturing signals from NOAA satellites.

Conclusions

The **Quadrifilar Helix antenna (QFH or QHA)** has proven to be an exceptional choice for UHF and microwave communication, particularly in satellite signal reception. Its design, featuring **circular polarization** and **a compact form factor**, ensures reliable performance in various applications, from weather satellite data acquisition to advanced GNSS systems. The historical evolution of the helical antenna highlights its versatility and enduring significance in the field of antenna design.

Utilizing AN-SOF's advanced simulation tools, users can efficiently design and optimize QFH antennas, achieving **precise impedance matching** and robust signal reception. The comprehensive exploration of input parameters and practical examples equips engineers and enthusiasts with the necessary knowledge to fully leverage QFH antennas for their specific needs, cementing their role in the advancement of communication technologies.

See Also:

- **Modeling Helix Antennas in Axial Radiation Mode Using AN-SOF**
- **DIY Helix High Gain Directional Antenna: From Simulation to 3D Printing**
- **Advantages of AN-SOF for Simulating 433 MHz Spring Helical Antennas for ISM & LoRa Applications**

Technical Keywords: Quadrifilar Helix Antenna (QFH, QHA), NOAA Satellite Signal Reception, Circular Polarization (CP), Self-Resonant Antenna, Compact Form Factor, AN-SOF Modeling, Weather Satellite Data Acquisition, Axial Mode, GNSS Systems, Impedance Matching.

About the Author

Tony Golden

RF ENGINEER & PHYSICS PH.D. With 25+ years in Computational Electromagnetics, I'm a passionate researcher focused on antenna modeling and design. As Founder of Golden Engineering LLC, I develop accessible, high-performance simulation tools that help RF engineers optimize their designs, educators teach complex concepts, and hobbyists bring antenna projects to life.

Have a question?

💬 **Ask me** | ✉️ **Email me** | 🌐 **Follow me**

Complete Workflow: Modeling, Feeding, and Tuning a 20m Band Dipole Antenna

Share this Article

Here is a comprehensive guide to modeling, feeding, and tuning half-wave dipoles, offering principles and techniques that can be applied to any antenna system.

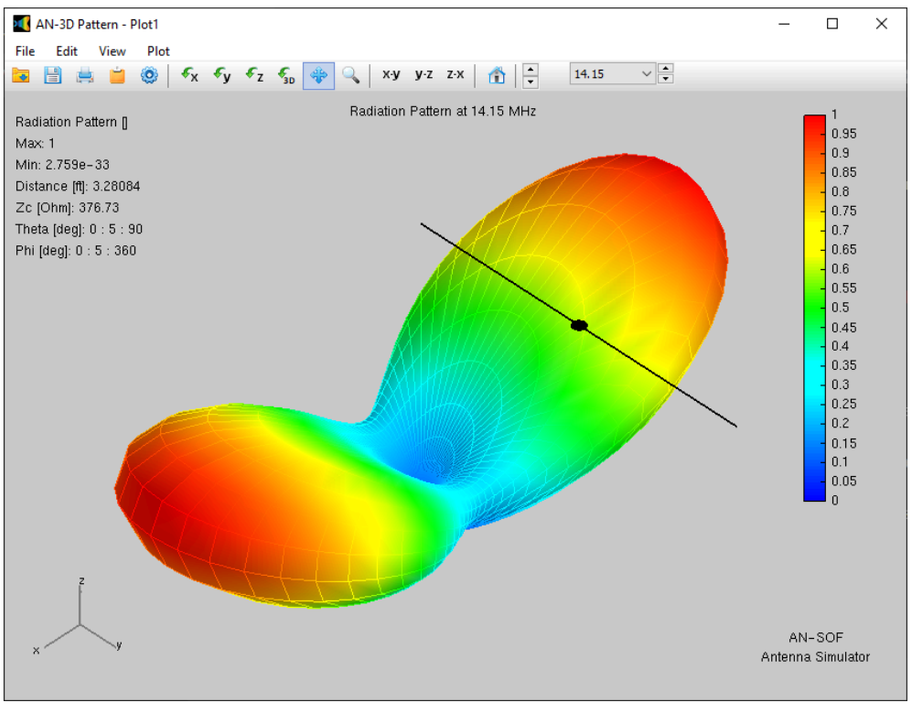

Introduction

With the release of **AN-SOF version 9**, two significant features—**Tuner** and **Feeder**—have been introduced. These additions enable comprehensive modeling of an **entire antenna feeding system**. This includes the power supplied by the transmitter, the impedance matching unit, the feed line, any necessary transformers, and the antenna terminals. In this article, we will model the feeding system for a horizontal half-wave dipole above real ground as an example to demonstrate the extensive options available to users.

Step 1: Modeling a Horizontal Half-Wave Dipole for the 20m Band

We will model a horizontal half-wave dipole for the 20m band, commonly referred to as a **Backyard Dipole** in the ham radio community. To bring the dipole near

resonance, its length will be set to **33.43 feet**, representing 0.48 wavelengths (λ) instead of exactly 0.5λ. The dipole will be constructed using **#12 wire**, which has a radius of 0.0404 inches. It will be positioned **30 feet** (0.43λ) **above the ground**, which has poor conductivity (σ = 0.03 S/m) and a dielectric constant (permittivity) of ε = 20.

The frequency will be varied linearly from **14 to 14.35 MHz** in steps of 0.025 MHz (25 kHz). The wire is divided into **11 segments**, which is sufficient for the purposes of this example. Since the **trial version of AN-SOF** is limited to up to 50 segments, this simulation can be performed with the trial version, including the modeling of the tuner and feeder. The dipole is center-fed by a **1 A current source**.

First, set the model parameters in the **Setup tab**, as shown in Figure 1. Enter the frequency range in the **Frequency panel** and set the ground plane parameters in the **Environment panel**. Note that a "Sommerfeld-Wait/Asymptotic" ground plane with custom conductivity and permittivity has been selected. The rest of the parameters in the Setup tab can be left at their default values.

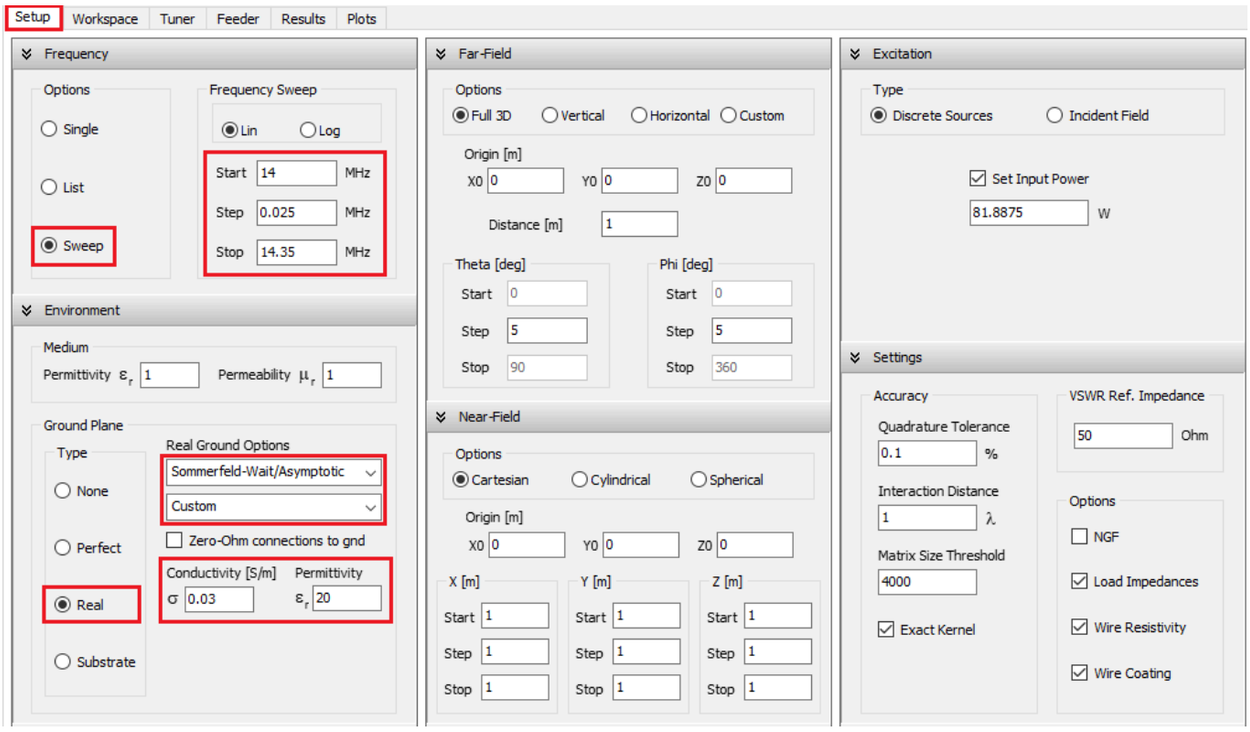

Fig. 1: Setup tab in the AN-SOF interface, where the frequency sweep and ground plane parameters are set.

Download Model

In this example, wire lengths are measured in **feet** and wire cross-section radii in **inches**. To change these units, navigate to the AN-SOF main menu > Tools > **Preferences** and select the desired units in the "Units" tab.

Now, we proceed to the **Workspace tab** to draw a **linear** horizontal wire. Right-click on the screen and choose the "Line" command from the **pop-up menu**. Set the coordinates for the start and end points of the wire, as shown in Figure 2(a). Since we are working with a single wire, we can start the wire at **(0,0,Height)** and end it at **(0,33.43,Height)** feet, where 33.43 feet is the wire length. In this example, **Height = 30 feet**. Next, go to the "Attributes" tab to set the number of segments (11) and the cross-section radius of the wire (0.0404 inches), as illustrated in Figure 2(b). After clicking the OK button, the wire will appear in the Workspace.

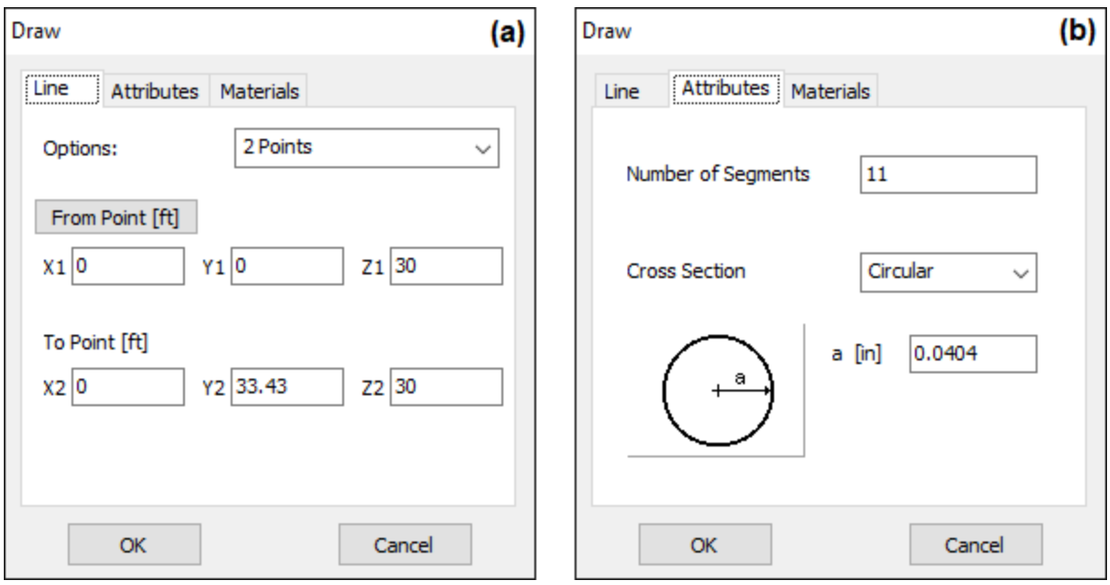

Fig. 2: (a) "Line" tab where the start and end point coordinates of the linear wire are set. (b) "Attributes" tab where the number of segments and cross-section radius for the wire are set.

With the horizontal wire drawn, we need to place a current source at the center of the wire. Right-click on the wire and select the **Source/Load/TL** command. This will display a toolbar at the bottom of the screen with a slider that allows you to select the desired wire segment. Move the slider to the center of the wire or simply click the "50%" button, as shown in Figure 3. Then, click the "Add Source" button and enter a **current source** of 1 A in amplitude, as shown in Figure 4(a). To model an **ideal current source**, add a high internal impedance in parallel by going to the "Impedance Zs" tab and entering **R = 1E6 Ohms**, as shown in Figure 4(b).

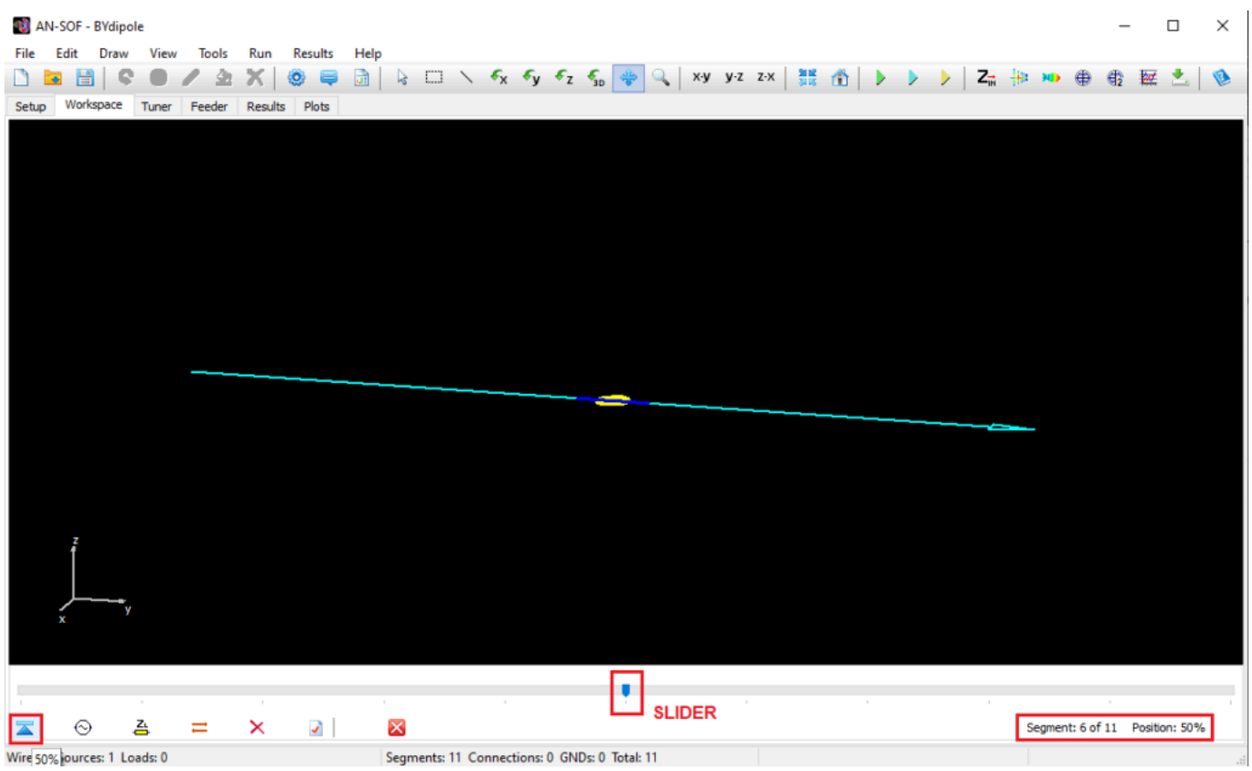

Fig. 3: The center segment of the wire is selected by positioning the slider at the 50% mark in the Source/Load/TL toolbar at the bottom of the screen.

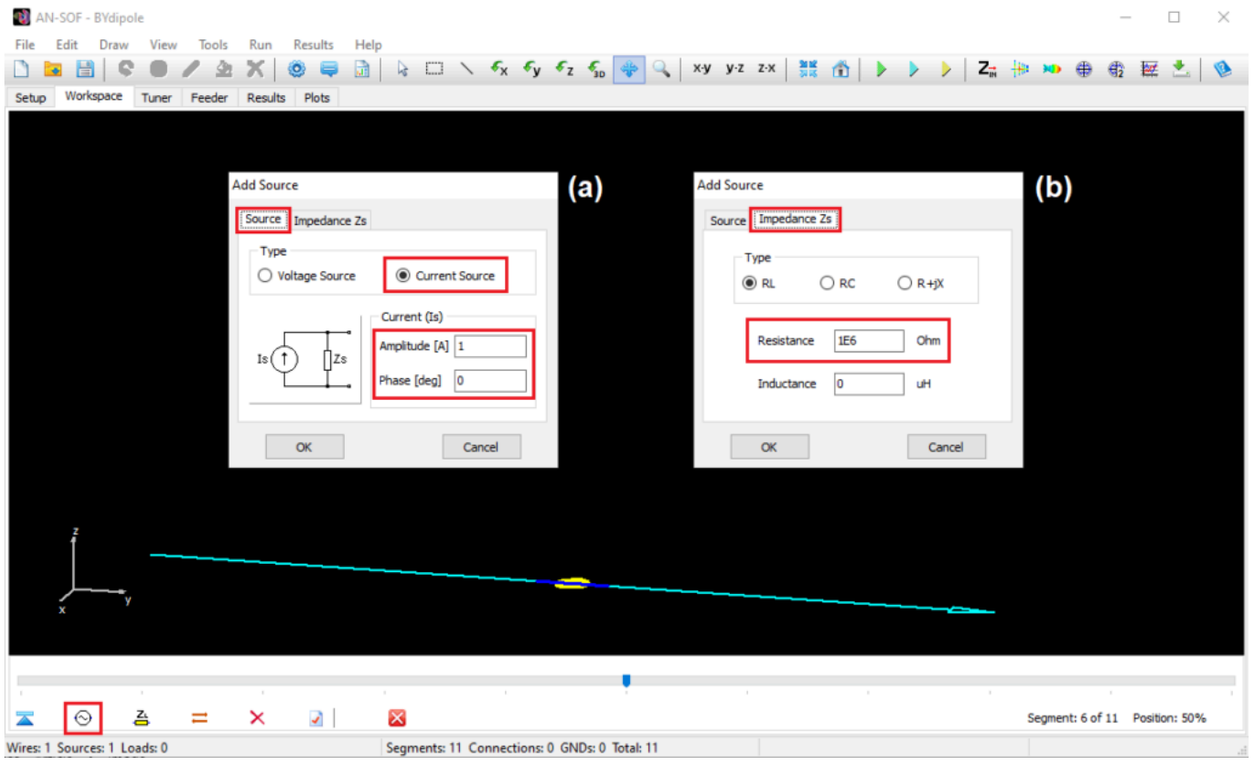

Fig. 4: Adding a current source at the wire center. (a) "Source" tab where the type of source, its amplitude, and phase are set. (b) "Impedance Zs" tab where the source's internal impedance is set.

With the center-fed dipole set up, we can calculate the antenna input impedance ($Z_{in} = R_{in} + jX_{in}$) by pressing **Ctrl + R**. Next, go to the **Plots tab** to view the VSWR curve. Ensure that the **Antenna** option is selected in the "Zin" box at the upper right corner of the screen. The VSWR ranges from approximately 2.5 to 1.8 across the analyzed frequency range, as shown in Figure 5.

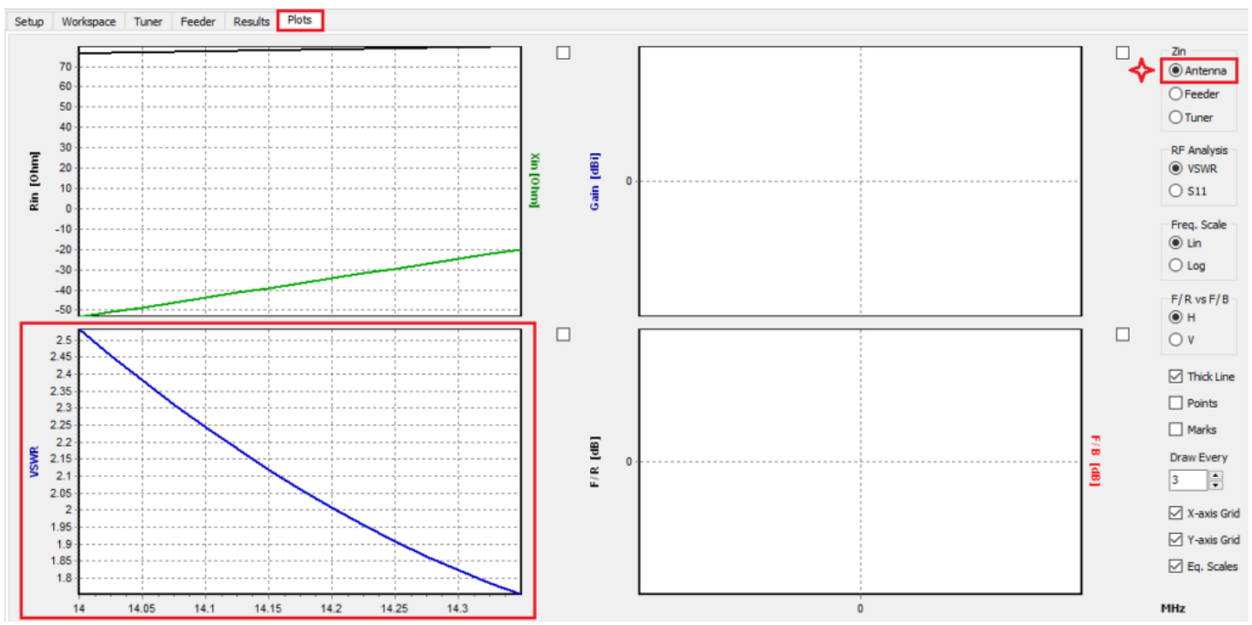

Fig. 5: VSWR curve as a function of frequency in the Plots tab. Click on the "Antenna" option in the "Zin" box to view the VSWR at the antenna terminals.

The current source connected to the antenna terminals helps determine the antenna input impedance. Its addition is purely for defining the position of the **antenna terminals**, from which the input impedance and VSWR are obtained. In the next section, a feeder consisting of a bifilar transmission line will be connected to the antenna terminals.

Step 2: Integrating a Ladder Line Feeder for the Dipole

As commonly used to feed backyard dipoles, we will connect a ladder line to the antenna terminals. Remember, **the antenna terminals in the model are defined by the position of the source**, so there is no need to modify anything in the antenna model already drawn and calculated in the Workspace tab. Although AN-SOF allows for the explicit addition of a **transmission line** in the Workspace, for this example, we will model a single feeder using the parameters available in the **Feeder tab**, so **there is no need to add a transmission line in the Workspace.**

To add the feed line, go to the "Feeder" tab. Under the Cable Type option, select **553 Wireman Ladder Line**, which typically has a characteristic impedance of 450 Ohms, though the **nominal impedance** is lower at **395 Ohms** with a **velocity factor of 0.902**. Enter the line length as **100 feet**. The line length in wavelengths and electrical degrees will be displayed automatically. In the **Matched Loss Curve** box, three parameters, **K0**, **K1**, and **K2**, are shown. These parameters are calculated from the transmission line loss curve provided by the manufacturer. While the computation details are beyond this article's scope, it's worth noting that K0 relates to DC losses, K1 to resistive losses (skin effect), and K2 to dielectric losses in the wire insulation.

Next, choose the **operating frequency**. Here, select the **center frequency** within your range of interest. The frequencies available here are drawn from the list of frequencies previously set in the **Frequency panel** of the Setup tab.

Enter the **input power** to the line. For this step, use **100 W as a reference value**, simplifying quick mental calculations, effectively treating it as a percentage. This input power will automatically adjust when the tuner is connected to the feeder in the next step.

Ensure the **Antenna Impedance** option is selected in the "Load Impedance" box. This option connects the feeder to the antenna terminals, displaying the antenna impedance as a load impedance ($R_L + jX_L$) to the feed line at the selected frequency. Alternatively, selecting the "Custom Load" option allows you to enter any desired impedance value, enabling the use of the Feeder calculator as an independent transmission line calculator, separate from the antenna model.

Note that a **transformer** can be connected between the feed line and the antenna. However, for this example, we will leave this option at its default setting (no transformer added), as we will use a transformer at the tuner's output in the next section.

The feeder parameters are illustrated in Figure 6, where the design frequency is set to **14.15 MHz**.

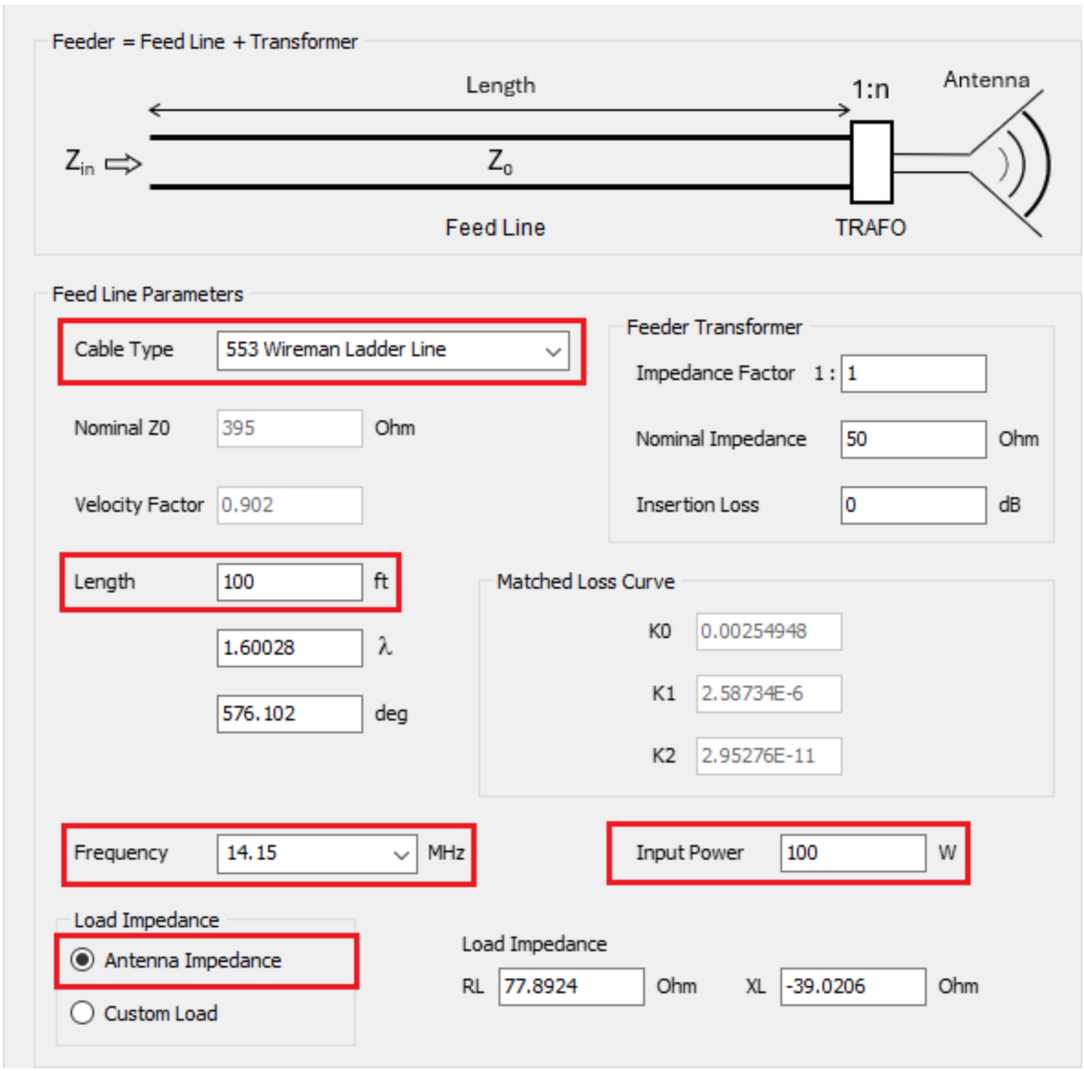

Fig. 6: Feed line parameters set in the "Feeder" tab: cable type, length, design frequency, input power, and load impedance (antenna impedance).

On the right side of the Feeder tab, the calculated results are displayed in the "Results" box. Line losses distort its characteristic impedance, Z_0, and velocity factor, generally resulting in an **imaginary part** in Z_0, with **the real part differing from the nominal impedance**. The **Matched Loss**, in **dB/100 ft**, represents the loss in the line per 100 feet when connected to its characteristic impedance. The **Total Matched Loss** is the matched loss multiplied by the line length.

Next, we examine two sections: **At Feeder Input** and **At Feeder Load**. The "At Feeder Input" section displays the **input impedance seen at the feed line input terminals**. This impedance results from connecting the antenna to the transmission line, thereby transforming the antenna impedance through the line. The feeder input impedance is shown as a **complex number** (real part + j imaginary part) and as a **polar number** (magnitude and phase angle).

Additionally, the **reflection coefficient (Rho)**, **VSWR**, and **return loss (dB)** at the feeder input are displayed. These values refer to the "true" characteristic impedance of the line, which, as previously noted, differs somewhat from the nominal impedance.

The "At Feeder Load" section shows similar values, but the load impedance of the line (the antenna input impedance) is used to compute Rho, VSWR, and return loss.

At the bottom of the "Results" box, several power metrics in Watts are provided. **Power at Load** indicates the power delivered to the load impedance of the transmission line (i.e., the antenna impedance). This power is lower than the input

power due to losses in the line. **Power Lost in Feed Line** represents the power dissipated in the line due to its losses (DC, skin effect, and dielectric losses). **Power Lost in Trafo** indicates the power lost in the transformer between the feed line and the antenna terminals, which will be zero here since no transformer has been added. **Total Feeder Loss** is the total power lost in the feeder system (feed line + transformer), which equals the power lost in the line since there is no transformer.

At the bottom right of the Results box, there are additional power metrics related to the antenna system, which will all show as zero since **we haven't calculated the radiated power yet**. By pressing **Ctrl + R** (or going to the main menu > Run > Run Currents), we have only calculated the antenna **current distribution** and the antenna **input impedance**, not the radiated field. We will calculate the far field after adding the tuner in the next section.

Figure 7 shows the Results box on the right side of the Feeder tab with the described results.

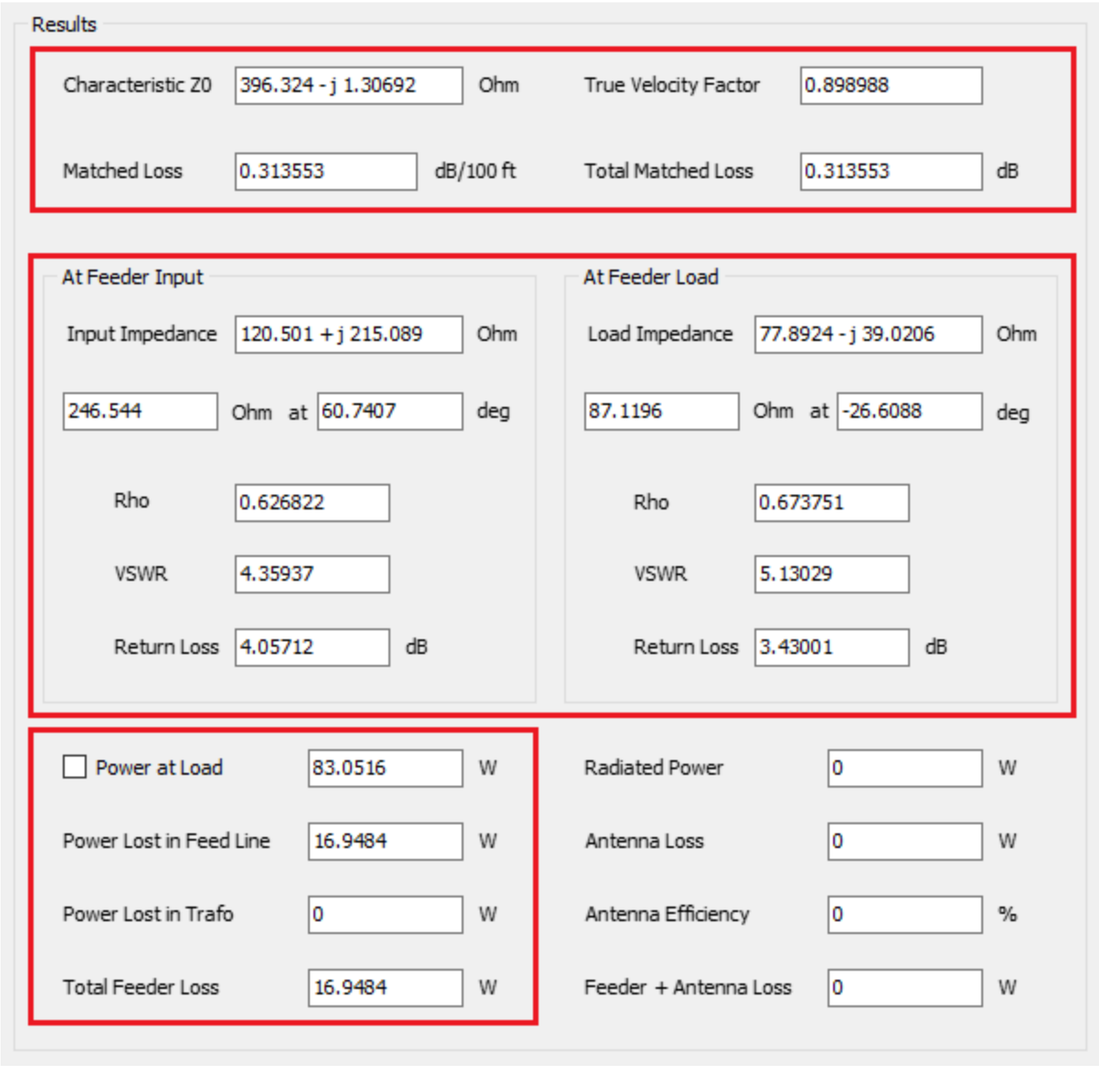

Fig. 7: "Results" box on the right side of the "Feeder" tab displaying the feed line results.

To conclude this section, navigate to the **Plots** tab and select the **Feeder** option in the "Zin" box at the upper right corner of the screen. This will display the input impedance and VSWR of the feeder as a function of frequency, indicating the need to tune the antenna, as **the VSWR values are still high**. Figure 8 illustrates these results.

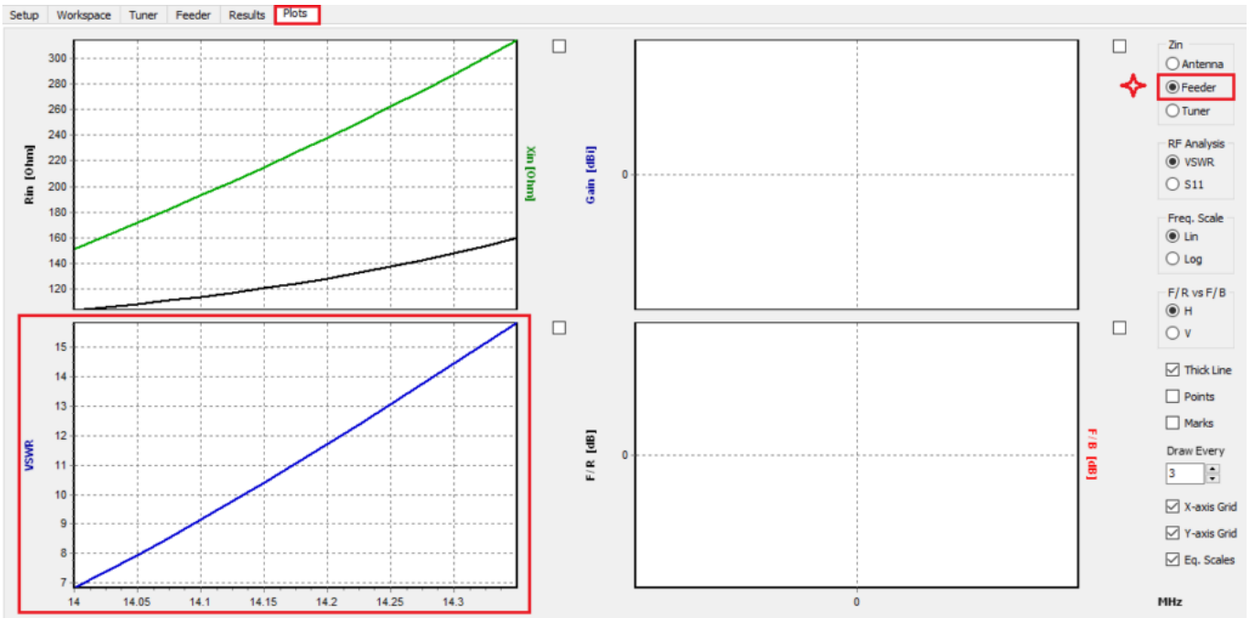

Fig. 8: VSWR curve as a function of frequency in the Plots tab. Click on the "Feeder" option in the "Zin" box to view the VSWR at the feeder terminals.

Note that in the "Feeder" tab, a fixed frequency is chosen to calculate the results, including **the VSWR relative to the line's "true" characteristic impedance**. In the "Plots" tab, the VSWR is shown as a function of frequency, but instead of being referred to the feed line's characteristic impedance, it is referred to **the reference impedance** defined in the **Settings panel** of the Setup tab, which is **50 Ohms**. Therefore, the VSWR at the feeder input shown in the "Feeder" tab at the design frequency will not generally be equal to the VSWR displayed in the "Plots" tab. For practical purposes, we need the VSWR referred to the purely resistive impedance of the transmitter, typically 50 or 75 Ohms. To change this reference impedance, simply adjust it in the Settings panel of the Setup tab.

Step 3: Fine-Tuning the Antenna System with a Transformer and Impedance Matching Network

Given that the input impedance to the "feeder + antenna" system is high, reaching approximately 160 + j 314 Ohms at 14.35 MHz, we will connect a **1:4 balun** to the feeder input to reduce the impedance.

In the **Tuner tab**, you will find a diagram of the tuner system. First, connect the feeder and antenna system to the tuner. At the bottom left corner of the Tuner window, select **Feeder + Antenna** as the load for the tuner in the "Load Impedance" box. The tuner system comprises an **impedance matching network**, **stray capacitance**, and a **transformer**. We will first add a 1:4 balun or impedance transformer. In the "Tuner Transformer" box, enter the impedance factor. If modeling transformer losses, set a **nominal impedance** and an **insertion loss**, but for this example, we'll model an ideal transformer with 0 dB insertion loss.

For this 20m band antenna setup, we'll use a **high-pass T network** for impedance matching. For PI and T networks, we can set a minimum quality factor (Q), which determines the network's bandwidth. However, for L networks, Q is determined by the impedances connected at the network input and output ports, making it meaningless to choose Q for L-type networks. A good practice is to choose an L network to see the available Q, then switch to a PI or T network and enter a Q equal to

or greater than the available Q for the L network. In this example, we will choose **Q = 1.5**. The network **inductors** and **capacitors** will be automatically calculated and displayed on the upper right side of the Tuner tab, along with their corresponding **reactances** (±jX) at the chosen design frequency. Adjust the **minimum Q** value to approximate real-world inductance and capacitance values of standard components.

Inductor Q and **capacitor Q** can be set separately. We'll leave the default values, Inductor Q = 250 and Capacitor Q = 1000, as they are commonly encountered in actual network components.

The frequency at which the impedance matching network's inductors and capacitors are calculated can be set in the **Tuner Parameters** box, along with the tuner **input power**. We'll select **14.15 MHz** as the center frequency and an input power of **100 W**.

By choosing 14.15 MHz, the load impedance for the tuner will automatically be set to 120.5 + j 215.1 Ohms, which is the input impedance to the **feeder + antenna** system, not the input impedance at the antenna terminals (check it in the Feeder tab).

The tuner parameters described are illustrated in Figure 9.

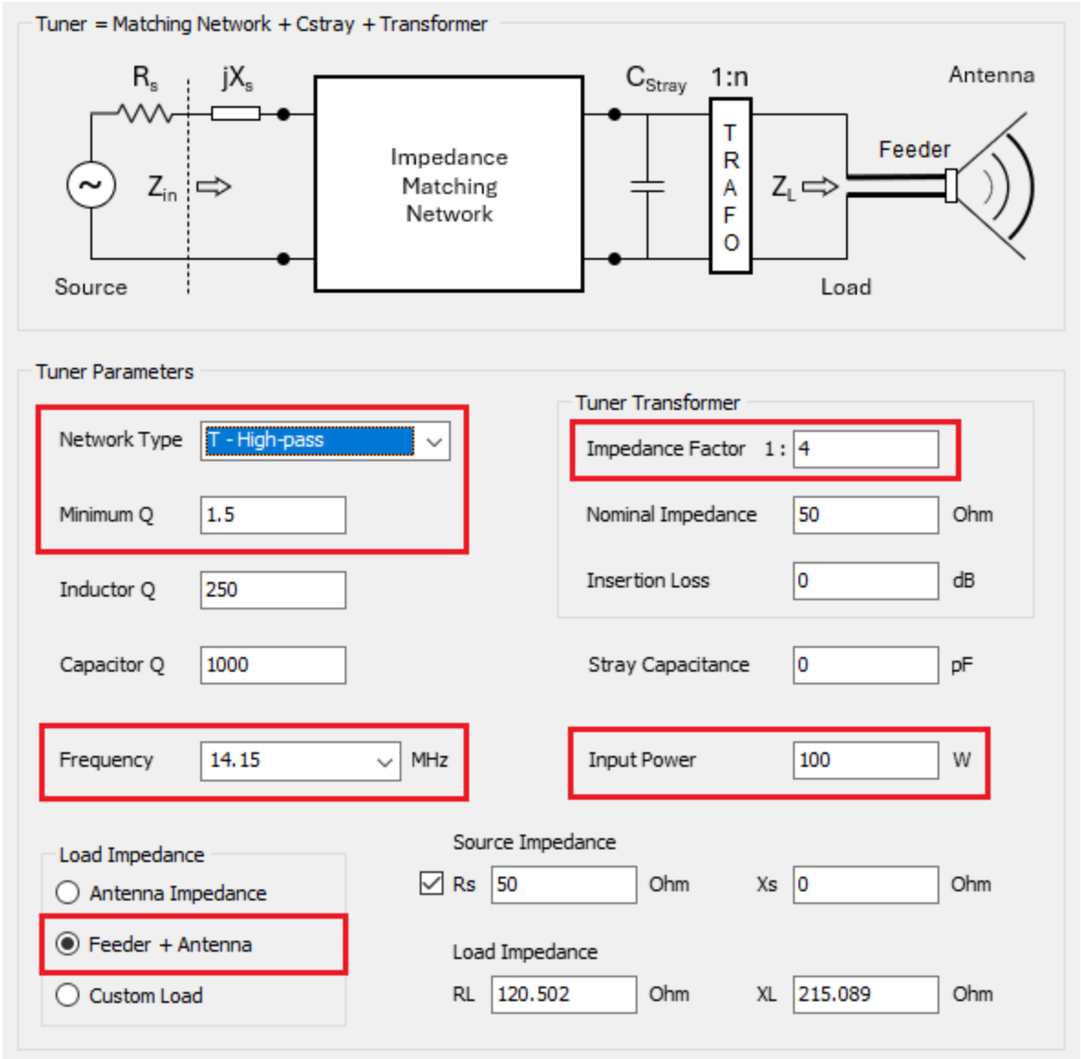

Fig. 9: Tuner parameters set in the "Tuner" tab: network type, minimum Q, transformer factor, design frequency, input power, and load impedance (feeder + antenna impedance).

In the Tuner tab's **Results** box, a diagram of the **high-pass T network** is displayed, showing two series capacitors of approximately 230 pF and 114 pF, and a parallel inductor of 0.44 µH. Below this diagram, the input and load impedances of the tuner

system are shown, along with the reflection coefficient (Rho), VSWR, and return loss at each side of the tuner. We see that an input impedance of **49.9 – j 0.55 Ohms** is achieved, **nearly matching the 50 Ohm source impedance**. The resulting **VSWR at 14.15 MHz is 1.01**, indicating an almost perfect match. However, on the load side of the tuner, the VSWR is 10.4, demonstrating the tuner's impact on the VSWR at each side.

It's important to note that the input impedance of the **Tuner + Feeder + Antenna** system is 49.9 – j 0.55 Ohms, not exactly 50 Ohms, **due to losses in the tuner components**, not numerical errors.

At the bottom of the Results box, various power metrics are shown. **Power at Load** is the power delivered to the tuner load, which is the "feeder + antenna" system connected to the tuner's output. By clicking the checkbox next to the "Power at Load" label, you can set this power as the **input power to the feeder**. This adjustment results in the "feeder + antenna" system being fed by the power from the tuner output port. **Verify in the Feeder tab that the input power to the feeder has changed to 98.6 W.**

Power Lost in Network shows the power lost in the impedance matching network, which is **1.4 W** for the high-pass T network in this example. Since the transformer at the tuner output has 0 dB insertion loss, the **Power Lost in Trafo** will be zero. Consequently, the **Total Tuner Loss**, which is the sum of network and transformer losses, equals **1.4 W**. Four additional power metrics related to the antenna system remain to be calculated, which will require computing the antenna radiated and lost powers.

Figure 10 illustrates the Results box on the right side of the Tuner tab with the described results.

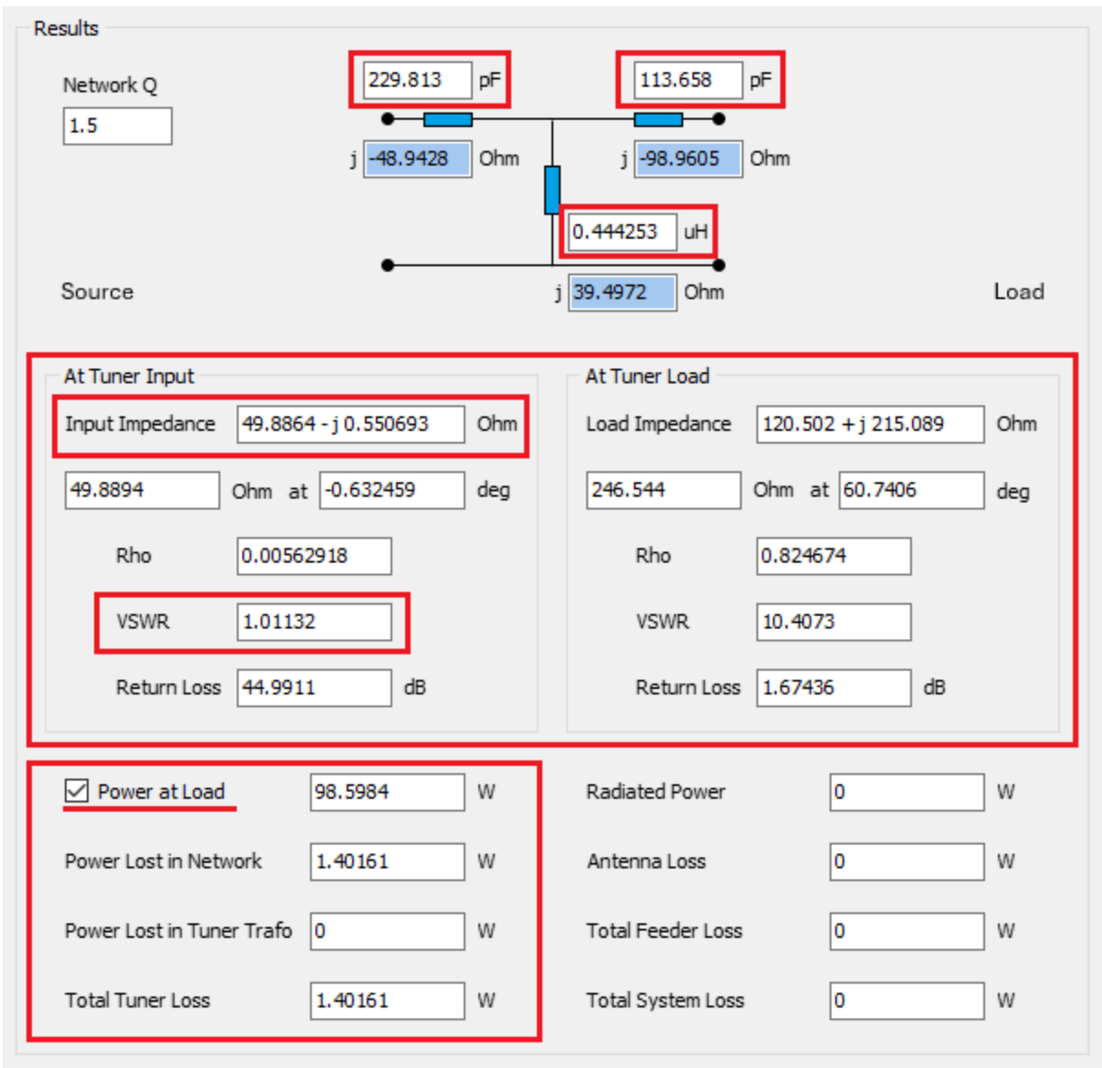

Fig. 10: "Results" box on the right side of the "Tuner" tab displaying the tuner results.

Now, navigate to the **Plots** tab and select the **Tuner** option in the "Zin" box at the upper right corner of the window. **A V-shaped VSWR plot will appear, centered at the design frequency of 14.15 MHz, where a VSWR of 1.01 is obtained.** Figure 11 illustrates these results.

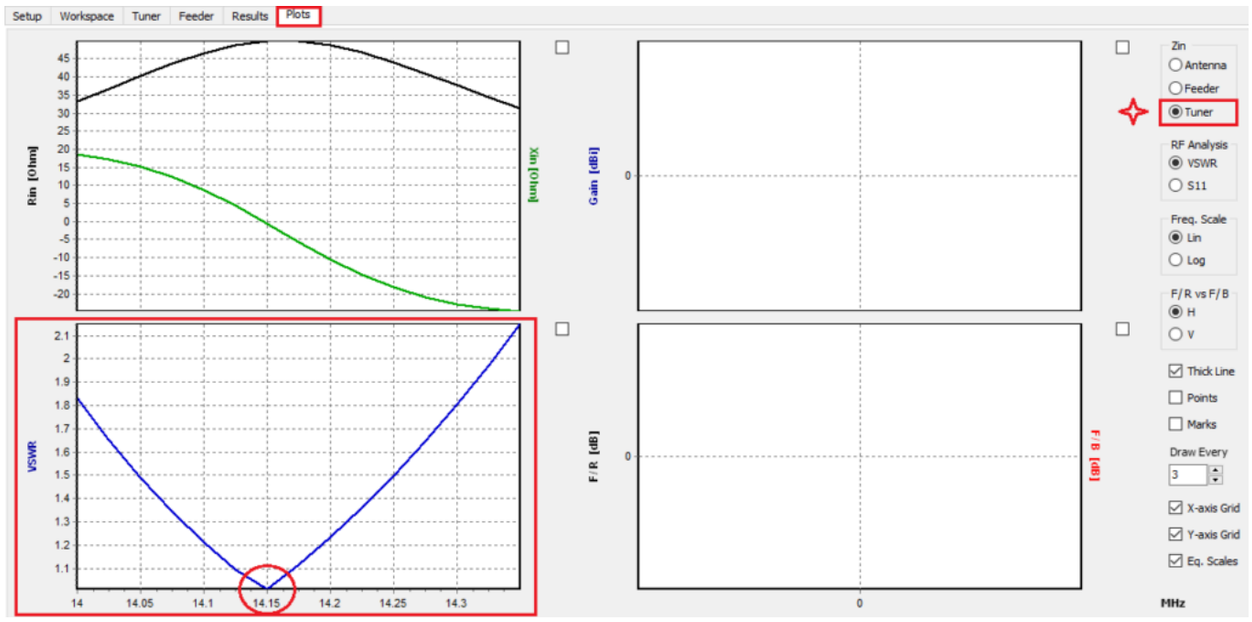

Fig. 11: VSWR curve as a function of frequency in the Plots tab. Click on the "Tuner" option in the "Zin" box to view the VSWR at the tuner input port.

From the perspective of the **antenna feeding system**, our design is complete. We've added a **feeder** to the antenna terminals, a **transformer**, and an **impedance matching network**. The next step is to calculate the far-field radiation pattern to determine the antenna radiated and lost powers. Typically, multiple iterations of the antenna feeding system design process are required. Switch back and forth between the **Feeder** and **Tuner** tabs to adjust their parameters until you achieve the desired results. **This process is quick since it does not require recalculating the antenna model.** If recalculating the antenna input impedance is necessary, press **Ctrl + R** (or navigate to the main menu > Run > Run Currents) to compute only the antenna current distribution and input impedance. This approach saves time as the far-field calculation is not needed at this step. The next section will focus on the radiated far-field.

Evaluating the Backyard Dipole's Radiation Performance

Now that we have completed the design of the backyard dipole feeding system, we are ready to compute its **radiation pattern**. Press **F11** (or navigate to the main menu and select Run > Run Far-Field) to calculate the radiated far-field. Click on the **Far-Field 3D Plot** button on the main toolbar to display a 3D representation of the radiation pattern. Instead of the typical donut-shaped pattern of a half-wave dipole (with a horizontal axis in this case), **two radiation lobes pointing upwards are obtained**, as Figure 12 shows. This is an expected result due to reflections of the electromagnetic waves at the air-ground interface.

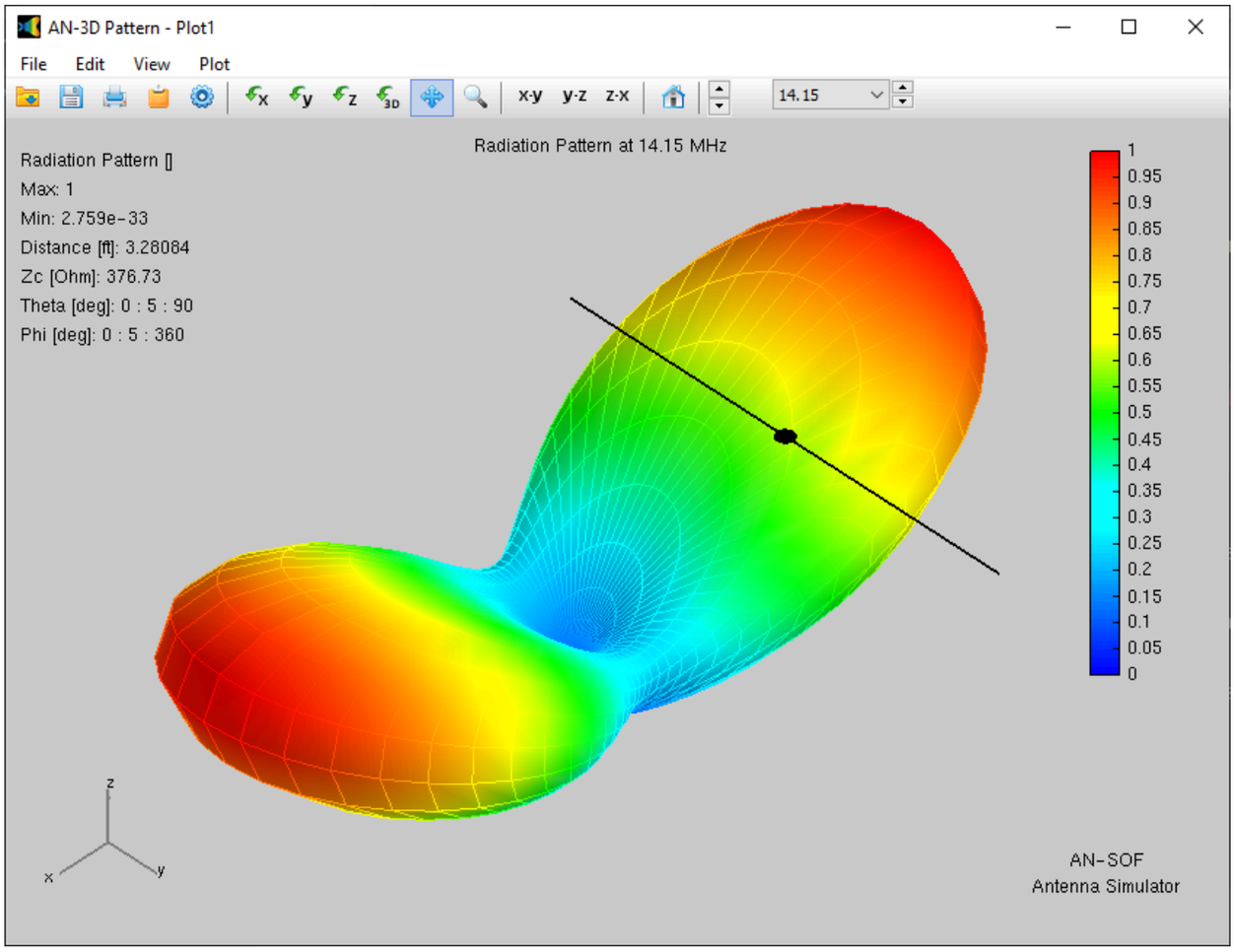

Fig. 12: 3D radiation pattern of the designed horizontal half-wave dipole antenna above ground.

Download Model

To plot the antenna **gain in dBi**, go to the "Plot" menu in the displayed radiation pattern and select the **Gain [dBi]** option. We can see that a **maximum gain of 6.9 dBi** is obtained. If we select the **Directivity [dBi]** option instead, we will see a **maximum directivity of 7.8 dBi**. This means that **the 0.9 dB difference between the directivity and gain is due to power losses in the ground**. Figure 13 illustrates these results.

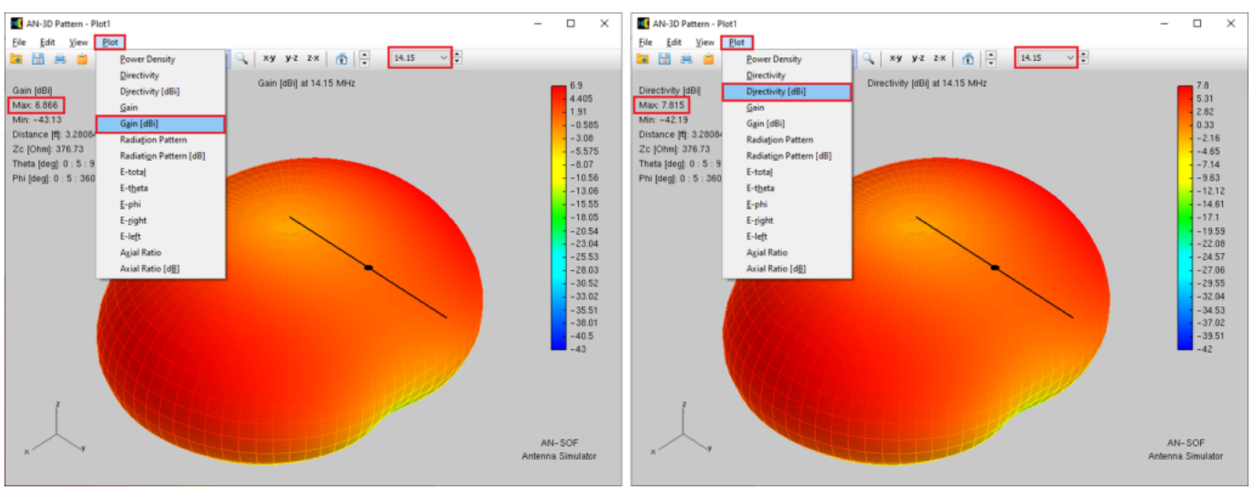

Fig. 13: Gain (left) and directivity (right) patterns at 14.15 MHz of the designed horizontal half-wave dipole antenna above ground. The 0.9 dB difference between the maximum gain and directivity is attributed to ground losses.

If we return to AN-SOF and access the “Results” tab, we will find a column labeled **Eff.** that displays the **antenna efficiency** as a function of frequency (see Fig. 14). Here, we observe **a consistent efficiency of 80%**, indicating that **20% of the power delivered to the antenna terminals dissipates as heat into the ground below**.

Setup | Workspace | Tuner | Feeder | Results | Plots

No.	Freq.	Rin	Xin	VSWR	S11	Dir.	Gain	Eff.	F/R H	F/B H	F/R V	F/B V
---	MHz	Ohm	Ohm	---	dB	dBi	dBi	%	dB	dB	dB	dB
1	14	33.2046	18.4753	1.82865	-10.6641	7.75692	6.81103	80.4287	9.64327E-16	9.64327E-16	9.64327E-16	0
2	14.025	36.7612	17.2368	1.65148	-12.1918	7.76666	6.82025	80.419	9.64327E-16	9.64327E-16	9.64327E-16	0
3	14.05	40.3361	15.2387	1.49056	-14.1121	7.77637	6.82945	80.4097	0	0	0	0
4	14.075	43.7101	12.4002	1.34492	-16.6482	7.78605	6.83865	80.4007	9.64327E-16	9.64327E-16	9.64327E-16	0
5	14.1	46.6099	8.72294	1.21356	-20.3115	7.7957	6.84783	80.392	0	0	0	0
6	14.125	48.7482	4.32489	1.09545	-26.83	7.80532	6.857	80.3837	0	0	0	0
7	14.15	49.8867	-0.550601	1.01132	-44.9933	7.8149	6.86615	80.3757	0	0	0	0
8	14.175	49.9007	-5.56743	1.11786	-25.0904	7.82446	6.87529	80.3681	9.64327E-16	9.64327E-16	9.64327E-16	0
9	14.2	48.8159	-10.3655	1.23465	-19.5759	7.83398	6.88442	80.3608	0	0	0	0
10	14.225	46.7975	-14.6389	1.36146	-16.3023	7.84346	6.89353	80.3538	0	0	0	0
11	14.25	44.0978	-18.1892	1.49853	-13.9999	7.85292	6.90262	80.3472	9.64327E-16	9.64327E-16	9.64327E-16	0
12	14.275	40.9919	-20.9393	1.64597	-12.2475	7.86233	6.9117	80.3409	9.64327E-16	9.64327E-16	9.64327E-16	0
13	14.3	37.7248	-22.9121	1.80381	-10.8519	7.87171	6.92076	80.3349	0	0	0	0
14	14.325	34.4844	-24.1943	1.97202	-9.70753	7.88106	6.9298	80.3294	9.64327E-16	9.64327E-16	9.64327E-16	0
15	14.35	31.3966	-24.9014	2.15044	-8.75017	7.89037	6.93883	80.3241	0	0	0	0

Fig. 14: Antenna efficiency (%) versus frequency displayed in the ‘Results’ tab.

If we go to the “Tuner” tab, “Results” box, we will see that the four powers that remained to be calculated now appear with non-null values (see Fig. 15). At the center frequency of 14.15 MHz, the **radiated power equals 65.8 W**, the **antenna loss is 16.1 W**, the **total feeder loss is 16.7 W**, and the **total system loss is 34.2 W**. The total system loss is the sum of the tuner, feeder, and antenna losses. **Since the input power to the tuner has been set to 100 W, this means that 34.2% of this power is lost in the antenna feeding system we have designed.**

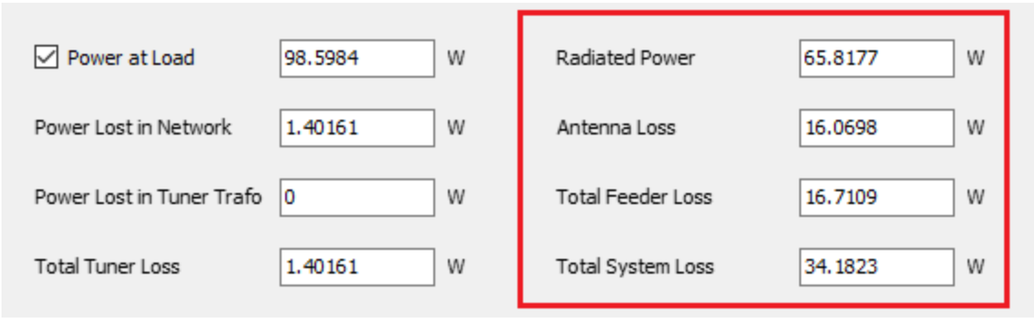

Fig. 15: Power metrics displayed in the bottom right corner of the “Tuner” tab after computing the far-field, including radiated power, antenna losses, feeder losses, and total system loss.

It is interesting to go to the “Feeder” tab to see the power metrics (see Fig. 16). The **feeder input power is 98.6 W**, which is the power delivered by the tuner (remember that 1.4 W are lost inside the tuner). The **Power at Load is 81.9 W**, which is the power delivered to the antenna terminals by the feeder. Therefore, of the 100 W originally injected to the tuner input, **we have already lost 100 W – 81.9 W = 18.1 W inside the tuner and feeder together**.

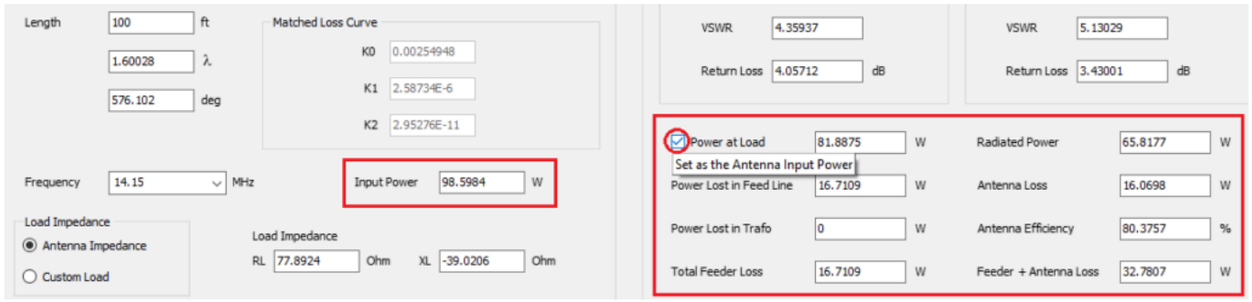

Fig. 16: Bottom section of the "Feeder" tab displaying input power to the feeder, power metrics such as power delivered to the antenna terminals (Power at Load), power lost in the feed line, and details of antenna radiated and lost powers.

The **antenna radiated power is 65.8 W** and the **antenna losses are 16.1 W** (just like on the Tuner tab, of course). The antenna efficiency of 80% is also shown. To verify this value, we must take into account that the antenna input power is 81.9 W, so we have Eff = 100 x 65.8 / 81.9 = 80% (rounded to two digits). The sum of the **feeder plus antenna losses is shown to be 32.8 W**. All these powers correspond to the **design frequency of 14.15 MHz**.

Hover your mouse over the check box next to the "Power at Load" label in the Feeder tab and you will see a hint message that reads **"Set as the Antenna Input Power"** (see Fig. 16). Click on this check box to set this power, **81.9 W**, as the input power delivered to the antenna terminals in the antenna model drawn in the Workspace tab. In this way, **all the plots related to the antenna radiated power will be scaled to the actual antenna input power after discounting losses in the feeding system**. This is of particular importance when we need to calculate the **EIRP** (Effective Isotropic Radiated Power) in order to evaluate **Electromagnetic Field (EMF) compliance** and perform far-field RF exposure assessments. For instance, to plot the EIRP versus frequency after having set 81.9 W as the antenna input power, navigate to the main menu > Results > **Power Budget** and find the **Peak EIRP** column in the displayed table (see Fig. 17). We should not be surprised that the peak EIRP takes values close to **400 W**, since this figure represents the power that the antenna would radiate if it radiated the maximum radiation intensity **isotropically** in all directions, and is obtained **by multiplying the numerical gain by the antenna input power**.

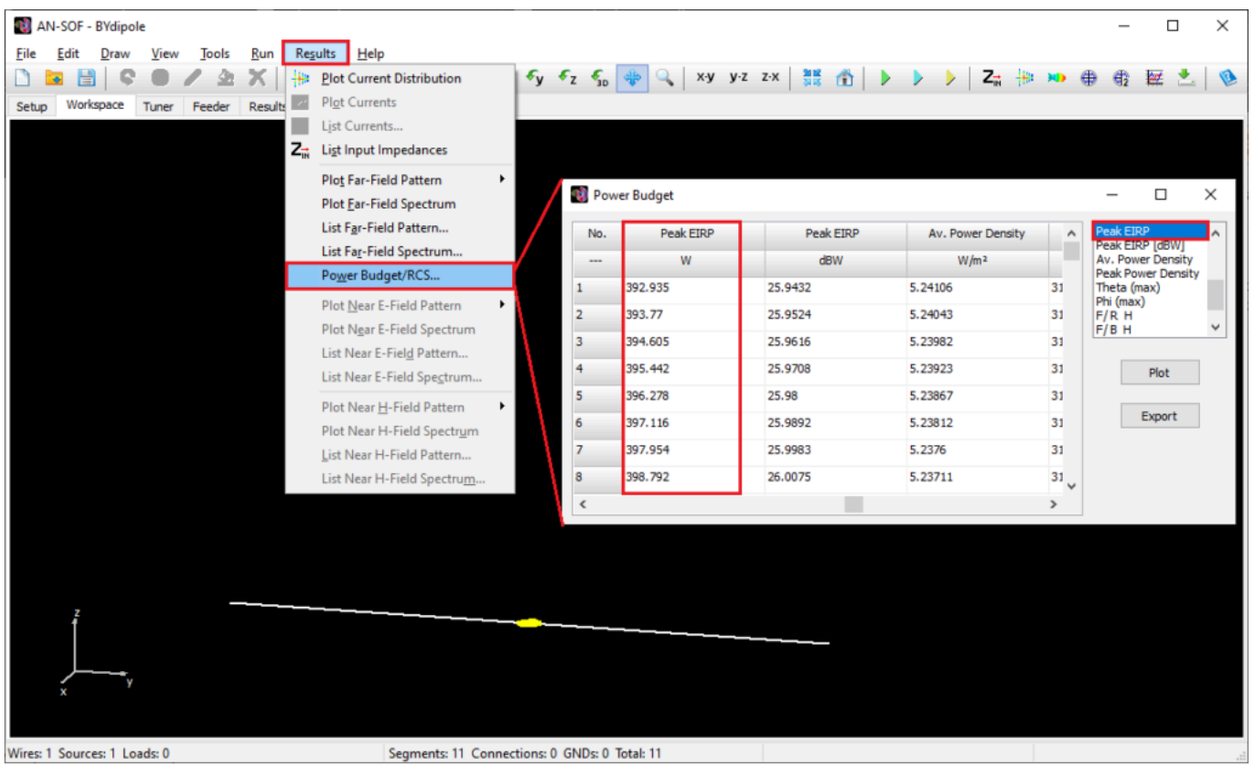

Fig. 17: Power Budget table showing Peak EIRP (Effective Isotropic Radiated Power) as a function of frequency, used for evaluating Electromagnetic Field (EMF) compliance.

With this section, we have concluded the necessary calculations to obtain the powers involved in the entire radiating system that we have designed.

Conclusions

In this article, we have meticulously walked through the **complete workflow** of designing, modeling, feeding, and tuning a **20m band backyard dipole antenna**. Starting with the **Setup** and **Workspace** tabs in AN-SOF, we quickly constructed a horizontal half-wave dipole. We then integrated a **ladder line feeder**, essential for power delivery to the antenna terminals, and analyzed its effects on the system's impedance and performance.

Next, we incorporated a **tuner system** composed of a **transformer** and an **impedance matching network**, demonstrating how to tune the antenna system to achieve optimal impedance matching and **minimize VSWR**.

Finally, we evaluated the **radiation performance** of the backyard dipole antenna. Through far-field calculations, we visualized the antenna's radiation pattern and quantified its **gain** and **directivity**. This comprehensive analysis highlighted the real-world performance metrics of the antenna, including its **efficiency** and **effective isotropic radiated power (EIRP)**, which are vital for compliance with electromagnetic field (EMF) regulations and for practical communication purposes.

By following this complete workflow, enthusiasts and professionals alike can design, implement, and optimize antenna systems that meet their specific requirements, whether for amateur radio, professional communication, or educational purposes. The principles outlined in this article serve as a reference for modeling, feeding, and tuning any antenna system.

AN-SOF Feeder and Tuner FAQs

Here are frequently asked questions related to the Feeder and Tuner features:

1. What value should I set for 'VSWR Ref. Impedance' in Setup > Settings?

VSWR (Voltage Standing Wave Ratio) measures the standing wave ratio on a transmission line and indicates the impedance match between a load and a reference impedance. For instance, an open-wire line with a characteristic impedance of 450 Ohms will exhibit a VSWR of 1 when terminated with a 450-Ohm load (under ideal conditions). To replicate this in AN-SOF, set the 'VSWR Ref. Impedance' to 450 Ohms. However, the VSWR is commonly measured at the transmitter end of a feeding system, typically using 50 or 75 Ohms as reference impedances. AN-SOF's flexibility in setting the VSWR reference impedance allows users to analyze VSWR at various points in the antenna feeding system relative to the desired reference value.

2. On the Feeder tab, the feeder diagram shows the transformer (TRAFO) positioned between the feedline and the antenna, resulting in the sequence: feedline + transformer + antenna. How can I add a transformer before the feedline, so that the sequence becomes: transformer + feedline + antenna?

If a transformer between the feedline and antenna is unnecessary, configure a 1:1 transformer with 0 dB insertion loss. To introduce a transformer at the feeder input, access the 'Tuner' tab and define the desired transformer parameters (see Fig. 18). If no additional impedance matching network is required, select the 'No Network' option and set the 'Stray Capacitance' to 0. This configuration effectively places the transformer at the feeder input without introducing other components.

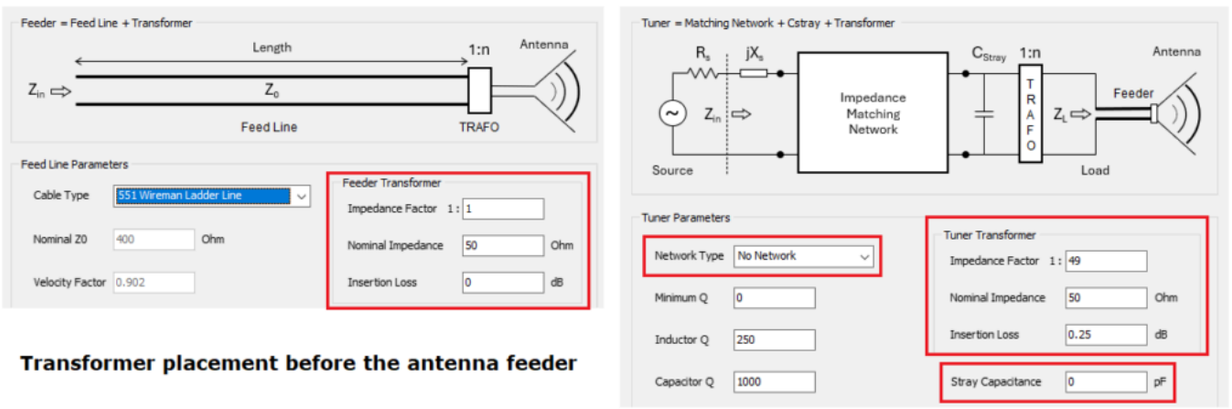

Fig. 18: Transformer placement before the antenna feeder.

3. What should I enter for the nominal impedance of a transformer?

The nominal impedance is only relevant when a transformer exhibits insertion loss. For ideal transformers (0 dB insertion loss), the default value of 50 Ohms can be retained. The nominal impedance is typically specified in transformer datasheets. For example, an unun with a 1:49 ratio, designed to reduce a high impedance to 50 Ohms, would have a nominal impedance of 50 Ohms.

Insertion loss quantifies the power reduction within a transformer relative to the input power. It is expressed in decibels (dB). Consequently, the output power delivered to the load is lower than the input power due to energy dissipation within the transformer's materials (conductor and core losses).

See Also:

- **Explore 5 Antenna Models with Less Than 50 Segments in AN-SOF Trial Version**
- **Simple Dual Band Vertical Dipole for the 2m and 70cm Bands**
- **Precision Simulations with AN-SOF for Magnetic Loop Antennas**

About the Author

Tony Golden

RF ENGINEER & PHYSICS PH.D. With 25+ years in Computational Electromagnetics, I'm a passionate researcher focused on antenna modeling and design. As Founder of Golden Engineering LLC, I develop accessible, high-performance simulation tools that help RF engineers optimize their designs, educators teach complex concepts, and hobbyists bring antenna projects to life.

Have a question?

💬 **Ask me** | ✉️ **Email me** | 🌐 **Follow me**

Antennas and Beyond!

Get Exclusive Updates

Share this Article

Understanding the Antenna Near Field: Key Concepts Every Ham Radio Operator Should Know

Share this Article

Learn the essentials of the antenna near field! This guide explains key concepts for ham radio operators, from reactive fields to EMF safety, helping you better understand antenna radiation and ensure compliance. Ideal for both beginners and experienced hams alike!

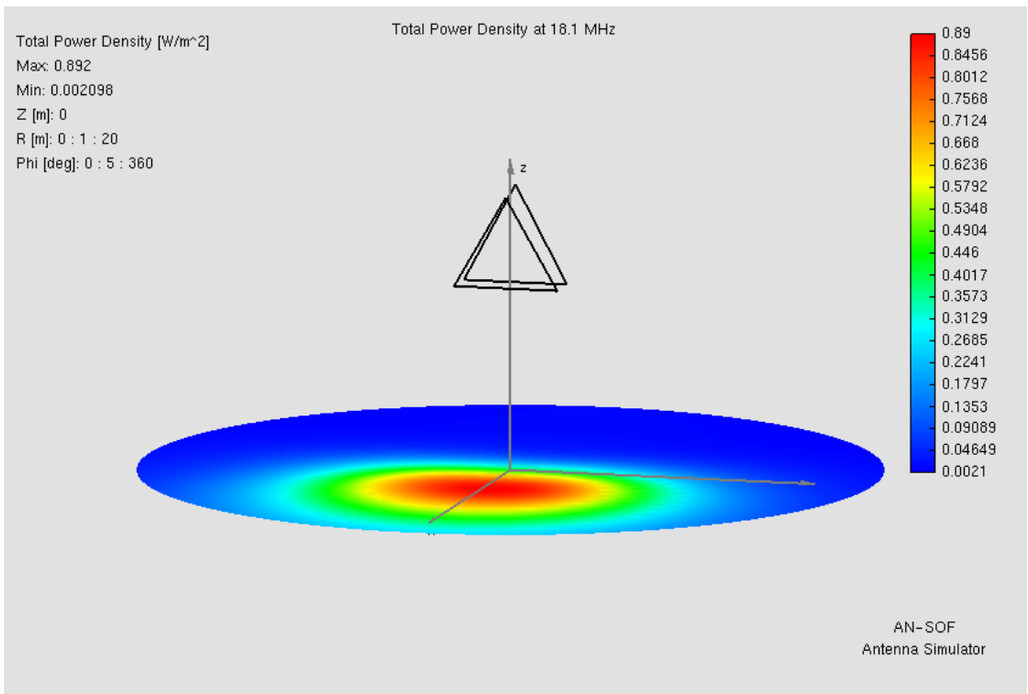

Introduction: Demystifying the Near Field of Antennas for Ham Radio Enthusiasts

For ham radio operators and those venturing into the world of antennas, terms like **near field** and **far field** often arise in discussions about antenna performance and electromagnetic radiation. But what do these terms truly mean, and why are they important? This article aims to provide a clear and accessible explanation of these concepts, avoiding complex equations or advanced physics.

The near field is a crucial region surrounding an antenna where electromagnetic fields exhibit unique behaviors distinct from those in the far field. A solid understanding of this region is vital not only for optimizing antenna performance but also for ensuring compliance with electromagnetic field (EMF) safety standards, a key consideration for safe operation. While a comprehensive understanding of

antenna theory involves Maxwell's equations and advanced mathematical analysis (as detailed in authoritative texts like *Antennas* by John D. Kraus), this article focuses on conveying the fundamental principles in a straightforward manner. Whether you are new to ham radio or seeking to enhance your conceptual knowledge, this guide will help you grasp the essentials of near field, far field, and wave propagation in a practical and approachable way.

Understanding the Near-Field Region: A Conceptual Overview

When transmitting a signal using your ham radio, the antenna serves as the critical interface between your radio and the surrounding space, radiating electromagnetic energy into the air. But what occurs in the immediate vicinity of the antenna? This is where the *near-field region* becomes significant—a complex yet fascinating area essential to understanding antenna operation.

Energy Flow from Radio to Antenna

Antennas, often referred to as *aerials*, are typically fed by **transmission lines** such as open-wire lines or coaxial cables. These lines deliver radio frequency (RF) power from your radio to the antenna. In an ideal scenario—where the antenna is perfectly matched to the transmission line and losses are negligible—all the power supplied to the line reaches the antenna's feedpoint. From this point, the process of energy transformation and radiation begins.

At the antenna's feedpoint, electromagnetic energy is released into the surrounding space, establishing a distribution of electric (*E*) and magnetic (*H*) fields. This process creates a **current distribution** along the antenna's metallic structure, which in turn generates these fields around the antenna. These fields are fundamental to the propagation of your signal through space.

The Interaction of Electric and Magnetic Fields

The behavior of the fields near the antenna is intricate. Electric field lines originate perpendicularly from regions of the antenna with a positive charge and terminate at areas with a negative charge. Since RF signals oscillate with time, the currents, charges, and both electric and magnetic fields fluctuate in sync. This oscillation enables your signal to carry information across distances.

Magnetic fields, however, exhibit a different behavior. Unlike electric fields, which begin and end at specific points, magnetic field lines form continuous loops around the antenna. To visualize this, consider a simple **half-wave dipole antenna** (Figure 1). The electric field lines radiate outward, while the magnetic field lines encircle the antenna in closed loops.

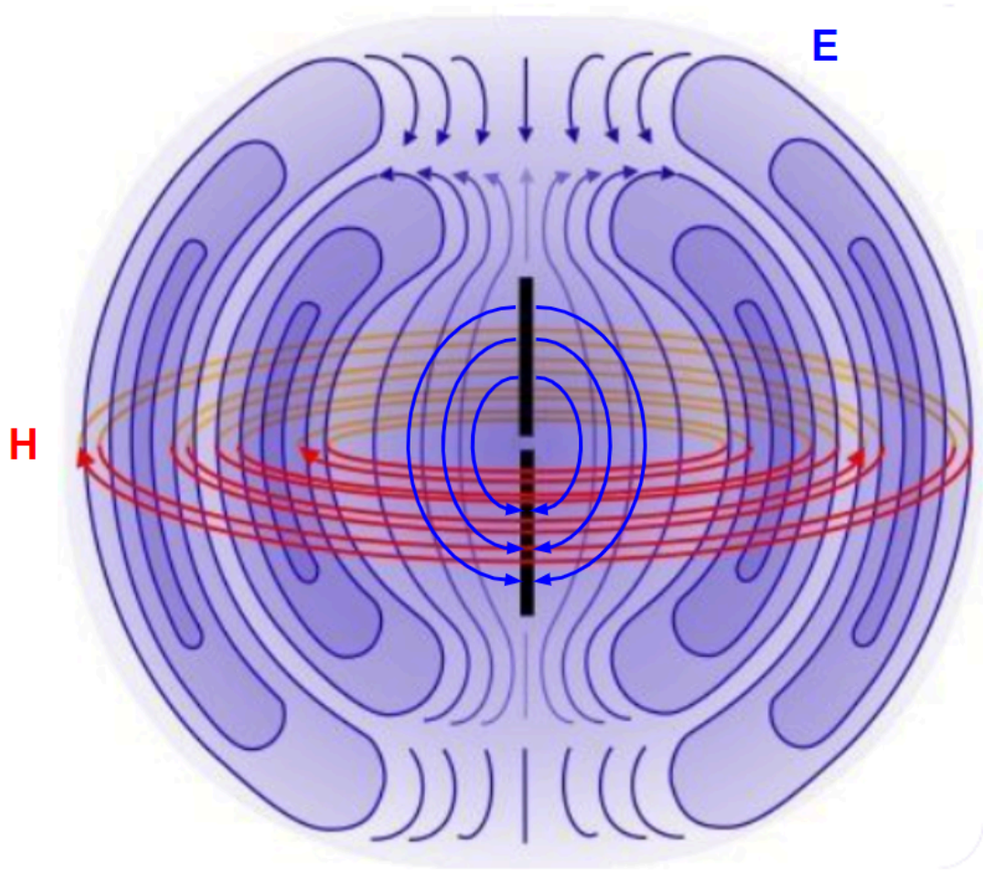

Fig. 1: Electric (E) and magnetic (H) field lines near a dipole antenna, illustrating the near-field region where energy is stored and exchanged between electric and magnetic fields.

Stored Energy in the Near Field

A defining characteristic of the near-field region is its ability to store energy. This energy exists in two distinct forms:

1. **Electric Energy**: Associated with the electric field lines.
2. **Magnetic Energy**: Associated with the magnetic field lines.

To better understand this, the near field can be likened to an electric circuit. The electric energy is analogous to the energy stored in a capacitor (C), while the magnetic energy resembles the energy stored in an inductor (L). When these components are combined in an LC circuit, their energies interact. If the electric and magnetic energies are equal, the system achieves resonance, and the reactances cancel each other out. This does not imply the absence of energy—rather, the energies are balanced.

For instance, in a half-wave dipole antenna, the feedpoint reactance is typically **positive**, indicating that **magnetic energy dominates over electric energy**. Nevertheless, both forms of energy coexist in the space surrounding the antenna, interacting in a precise balance that facilitates effective signal propagation.

The LC Oscillator Bubble: The Heart of the Near-Field Region

To fully comprehend the near-field region of an antenna, it is helpful to conceptualize it as an **LC oscillator bubble**. This bubble represents the space surrounding the antenna where electromagnetic energy is stored and exchanged

between electric and magnetic fields, akin to the energy exchange in an inductor-capacitor (LC) circuit. Let's explore this concept in detail.

What is the LC Oscillator Bubble?

The near-field region is characterized by the concentration of the antenna's reactive fields—the electric and magnetic fields. These fields are tightly bound to the antenna's structure and do not extend far into the surrounding space. The electric field lines are anchored to the antenna's metallic surface, originating from areas of positive charge and terminating at regions of negative charge. Simultaneously, the magnetic field lines form closed loops around the antenna, linked to the currents flowing through its structure.

This interplay of electric and magnetic fields creates a dynamic energy exchange. Electric energy transforms into magnetic energy, and vice versa, oscillating at the frequency of the RF signal. In essence, **the near-field region is an extension of the antenna itself**, where the antenna's materials define the boundaries of these electromagnetic fields. This region acts like an invisible bubble, storing and cyclically transforming energy, much like an LC circuit.

Accounting for the Radiated Power

While the LC oscillator bubble provides a useful framework for understanding the near-field region, it does not fully capture the antenna's function. Antennas are designed to radiate power, and this radiated power escapes the LC oscillator bubble, propagating outward into space. From the perspective of the antenna's feedpoint, this radiated power is represented by the resistive component of the antenna's input impedance.

However, not all the power delivered to the antenna is radiated. A portion is lost as heat due to the resistance of the antenna's metallic structure, a phenomenon known as **skin effect losses**. To complete the picture, two types of resistance must be considered:

1. **Radiation Resistance**: This represents the power successfully radiated into space.
2. **Loss Resistance**: This accounts for the power dissipated as heat in the antenna's conductors.

Figure 2 depicts how the radiated power density propagates beyond the LC oscillator bubble as a **Transverse Electromagnetic (TEM)** wave. This wave carries energy away from the antenna, and its power density is described by the Poynting vector (**S**). (The Poynting vector can be thought of as the directional flow of electromagnetic energy, analogous to the way sunlight carries energy to warm the Earth's surface.)

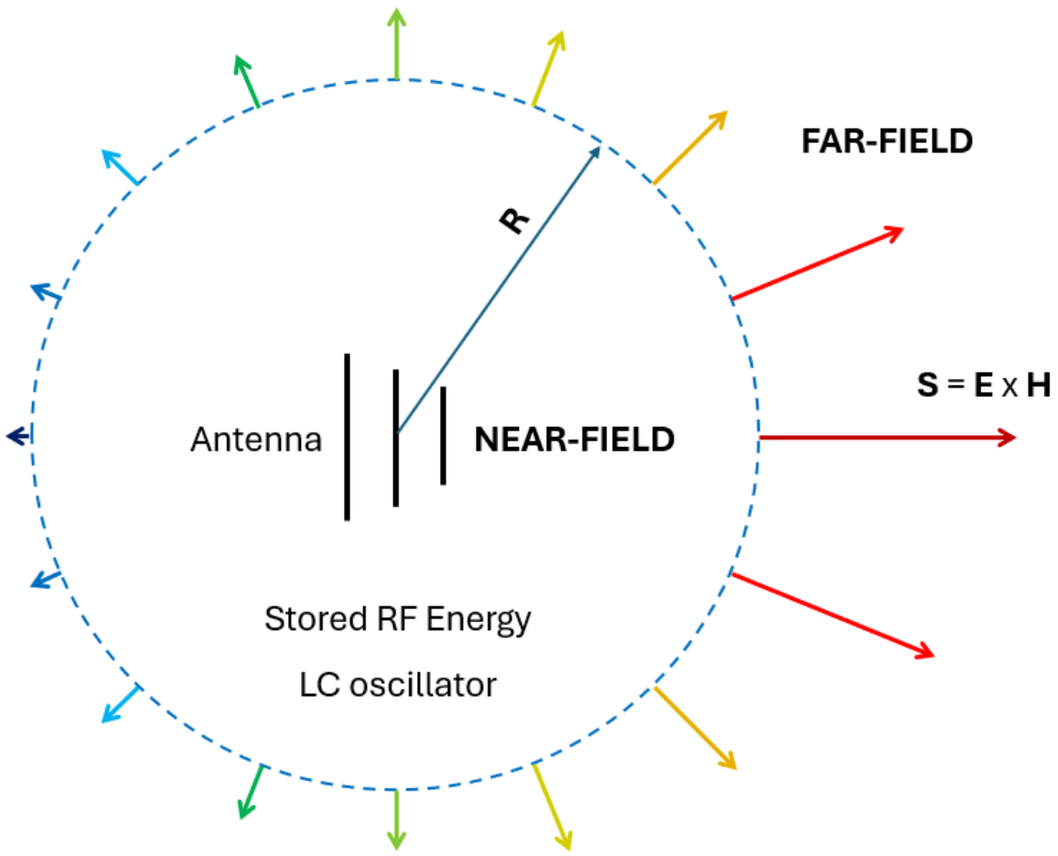

Fig. 2: Power density distribution (S) on a spherical wavefront around an antenna. The electric (E) and magnetic (H) fields are mutually perpendicular and orthogonal to the Poynting vector (S), representing the direction of energy flow.

Transitioning to the Far-Field Region

Beyond the LC oscillator bubble lies the **far-field region**. Here, the radiated wave fully detaches from the antenna and propagates as a self-sustaining TEM wave. In the far field, the electric (E) and magnetic (H) fields oscillate in phase, are perpendicular to each other, and are also perpendicular to the direction of wave propagation, as indicated by the Poynting vector.

In this region, the wavefront becomes spherical, and the fields no longer depend on the antenna's structure. The electric field lines close on themselves, and the magnetic field lines are no longer tied to the antenna's currents. Instead, the wave sustains itself through the mutual generation of electric and magnetic fields—each field creating the other as the wave propagates through space.

Power Density vs. Radiated Power: Understanding the Distinction

When analyzing antennas and electromagnetic waves, it is essential to differentiate between **power density** and **radiated power**. While these concepts are interrelated, they describe distinct aspects of how energy propagates from an antenna. Let's examine this distinction in detail.

Power Density in the Far Field

In the far-field region, the electromagnetic wave radiated by the antenna propagates outward, and its electric (E) and magnetic (H) fields weaken as they travel. Specifically, the fields attenuate according to the **inverse distance law**: doubling the distance from the antenna reduces the field strength to half its original value.

Power density, represented by the Poynting vector (S), quantifies the energy flow per unit area and is calculated by multiplying the E and H fields. Its units are Watts per square meter (W/m^2). Power density follows the **inverse square law**: doubling the distance from the antenna reduces the power density to one-fourth of its original value. This occurs because the energy spreads over a larger wavefront area as the wave propagates.

For example, consider the sun radiating energy. At Earth's surface, after accounting for atmospheric absorption and scattering, we receive approximately 1,000 W/m^2 on a clear day. If you had a 1 m^2 solar cell with 100% efficiency, oriented perpendicularly to the incoming sunlight, it would collect 1,000 Watts of power. Doubling the solar cell's area to 2 m^2 would yield 2,000 Watts. This example highlights the importance of distinguishing between *power density*, measured in Watts per square meter (W/m^2), and *power*, measured in Watts (W), which represents the total energy received by the solar cell.

Similarly, in the context of antennas, we must not confuse the **power density**, represented by the Poynting vector radiating from a transmitting antenna, with the **radiated power**. Radiated power is calculated by integrating the power density over a spherical wavefront—essentially summing the power density contributions across each square meter of the sphere's surface. This distinction is crucial for understanding how energy propagates from an antenna and how it is measured in both near-field and far-field regions.

Power Density in the Near Field

The concept of power density also applies in the near-field region, but the situation is more complex. Inside the "LC oscillator bubble," the fields remain concentrated around the antenna, and the energy exchange between electric and magnetic fields dominates. If a receiving antenna is placed in the near-field region of a transmitting antenna, it becomes part of the transmitting antenna's electromagnetic environment.

In this scenario, the receiving antenna does not simply capture power density as it would in the far field. Instead, it interacts with the transmitting antenna through **induction**, creating a current distribution in the receiver. This interaction makes near-field calculations significantly more challenging, as the fields are non-uniform and depend on the specific geometry and placement of the antennas.

Radiated Power: The Broader Perspective

Radiated power refers to the total energy that escapes the antenna and propagates into space. It represents the power that ultimately reaches the far field and can be received by distant antennas. However, a distant receiving antenna will not capture the total radiated power but only a fraction of it. This fraction is determined by multiplying the power density at the receiver's location by the antenna's effective area, much like calculating the power received by a solar cell based on the power density of sunlight at its location.

That said, not all the power delivered to a transmitting antenna is radiated. Some is lost as heat due to the resistance of the antenna's conductors (skin effect or ohmic losses). Understanding these losses is essential for optimizing antenna efficiency and ensuring effective energy transfer.

To summarize:

- **Power Density (S)**: Describes the energy flow per unit area (W/m^2) and follows the inverse square law with distance in the far field.
- **Radiated Power**: Represents the total power that escapes the antenna and propagates into space, accounting for losses in the antenna's structure. Unlike power density, the radiated power, measured in Watts, remains constant regardless of distance (principle of energy conservation).

Calculating the Near Field in AN-SOF

To calculate the near field in AN-SOF, you must first define a grid of points in space where the electric (*E*), magnetic (*H*), and power density (*S*) fields will be computed. To set up the grid for the near field, navigate to the **Setup tab > Near Field panel**. Here, you'll find three coordinate system options: **Cartesian**, **Cylindrical**, and **Spherical**.

For a transmitting antenna positioned above a ground plane, the near field at ground level as a function of distance from the antenna is often of particular interest. To analyze this, select the *Spherical* option and set *Theta = 90°* (ground level). The angle *Phi* (azimuth) indicates the direction on the xy-plane, starting from *Phi = 0°* at the x-axis and increasing to *Phi = 90°* at the y-axis, *Phi = 180°* at the -x axis, *Phi = 270°* at the -y axis, and returning to the positive x-axis at *Phi = 360°* (which coincides with *Phi = 0°*).

After specifying the observation direction, you can set the range for the distance *R* from the antenna. As a practical example, Figure 3 shows the power density as a function of distance in the direction of maximum radiation (where the main lobe points in the far-field region) for a **17m band delta loop beam**. The details of the model can be found in the following articles:

- **Evaluating EMF Compliance – Part 1: A Guide to Far-Field RF Exposure Assessments**
- **Evaluating EMF Compliance – Part 2: Using Near-Field Calculations to Determine Exclusion Zones**

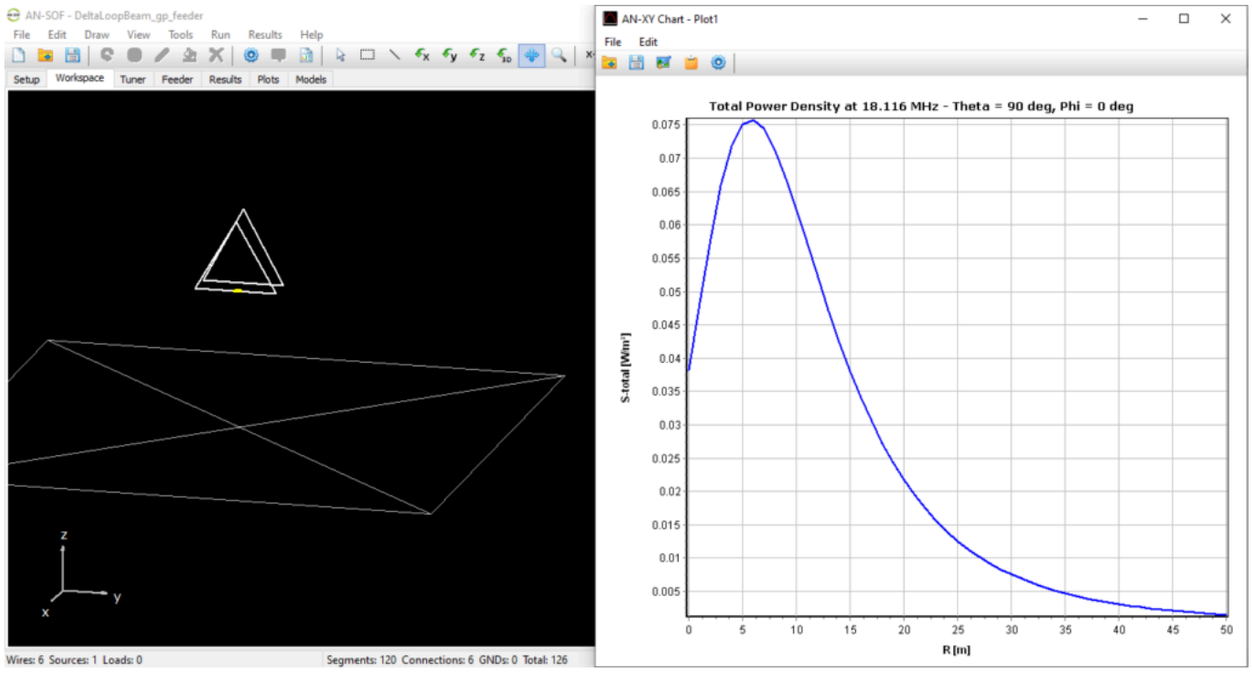

Fig. 3: A 17m band delta loop beam positioned above a ground plane, with its power density (S) plotted as a function of distance at ground level.

Download Model

Figure 3 illustrates the power density, which peaks near the antenna and then decays following the inverse square law with distance. In this model, the input power to the feeder is set to 100 W, with 84.6 W delivered to the antenna feedpoint at the resonant frequency and 15.4 W lost in the feeder. By navigating to the **Results menu › Power Budget**, you can see that the radiated power is 62.1 W. The difference between the antenna input power (84.6 W) and the radiated power represents the power lost as ohmic losses in the antenna structure and as heat in the ground plane below the antenna. As explained earlier, the radiated power remains constant across all field regions (principle of energy conservation), while the power density, as illustrated in Figure 3, varies with distance.

Insights on the Boundary Between the Near and Far Field Regions

At this point, we recognize that the near-field region is characterized by electric and magnetic field lines closely linked to the antenna's metallic structure, where energy is stored in the electric and magnetic fields. **But how far does this region extend?** This question has been a long-standing topic of discussion and continues to generate debate among RF professionals.

There is no abrupt boundary between the near and far field regions; instead, the near electromagnetic field gradually transforms into a TEM wave as distance from the antenna increases. Traditional formulas, which remain widely accepted, are still published in antenna textbooks. An online calculator implementing these formulas is available at this link:

Antenna Near – Far Field Boundary Calculator

A more accurate method to determine the practical boundary between field regions is based on the concept of **wave impedance**, defined as the ratio between the electric (E) and magnetic (H) fields. In the far-field region, the wave impedance approaches **377 Ohms** for a TEM wave propagating in free space. Thus, the onset of the far field can be identified when the wave impedance consistently reaches 377 Ohms within a given margin of error.

In AN-SOF, the wave impedance (Z_w) is calculated alongside the power density, as well as a parameter called the **Wave Matching Coefficient (WMC)**. The WMC, expressed in decibels, is analogous to the return loss in a transmission line and measures the mismatch between the actual wave impedance and 377 Ohms. To access the power density (S), Z_w, and WMC, navigate to the AN-SOF main menu > Results > **List Power Density Pattern** (fixed frequency, varying point coordinates) or **List Power Density Spectrum** (fixed point coordinates, varying frequency).

Using the WMC provides a straightforward way to determine the boundary between the near and far field regions. **When the WMC exceeds 20 dB, it indicates that we are in the far-field region**.

Frequently Asked Questions About the Near Field of Antennas

Now that we've explored the conceptual framework of the near-field and far-field regions, let's address some common questions from the ham radio community.

---

1. If the power density in the near field is stronger than predicted by the inverse-square law, doesn't that violate the conservation of energy?

This question stems from a common confusion between *power* (measured in Watts) and *power density* (measured in Watts per square meter). In the near-field region, the power density is indeed stronger than in the far field and does not follow the inverse-square law. This is because the electric (E) and magnetic (H) fields are significantly more intense close to the antenna.

However, this does not imply a violation of energy conservation. The near-field power density includes *reactive components*—parts of the fields associated with stored energy rather than radiated power. These reactive components oscillate locally, creating strong fields near the antenna, but they do not contribute to energy propagation. When you calculate the total radiated power by integrating the power density over a sphere surrounding the antenna, the result remains constant, regardless of the sphere's size. This consistency is a direct consequence of the *conservation of energy*: energy is neither created nor destroyed; it is simply distributed differently between the near and far fields.

---

2. If the electromagnetic wave in the near field isn't a Transverse Electromagnetic (TEM) wave, how can a receiver pick up a signal when placed close to a transmitting antenna?

A common misconception is that only TEM waves can induce signals in a receiver. While TEM waves dominate in the far field, the near field operates differently. In the near-field region, the electric and magnetic fields do not form a perfect TEM wave, but they still interact with a receiving antenna through *induction*.

When a receiving antenna is placed in the near field, the oscillating electric and magnetic fields induce currents in its structure. These currents generate a voltage and current at the receiver's terminals, enabling it to detect the signal. This process does not require a TEM wave; instead, it relies on the coupling between the fields and the receiver's conductive elements. Thus, even though the near-field wave is not TEM, it can effectively transfer energy to a nearby receiver.

---

3. If the near field is such a concern, shouldn't cellular phones—which operate at microwave frequencies and are held close to the brain—be banned? Why do ham radio operators need to worry about EMF compliance?

This is a valid point, and it's important to note that cellular phones are subject to stringent EMF compliance regulations in most countries. These regulations ensure that the electric (E), magnetic (H), and power density (S) fields emitted by phones remain below established safety limits to protect users from potential health risks.

For ham radio operators, EMF compliance is equally critical, particularly when transmitting at high power levels. The near-field region is where field strengths are highest, and prolonged exposure to strong fields can pose health hazards. By understanding and adhering to EMF safety guidelines, ham radio operators can ensure their activities are safe for themselves and those around them.

The primary factor influencing field strength is transmit power: higher power levels result in stronger fields. By calculating field levels and ensuring they remain below safety thresholds, operators can enjoy their hobby responsibly. Tools such as field strength meters, compliance calculators, and antenna simulations can assist in this process.

Why Is the Near Field Important for Ham Radio Operators?

Understanding the near field is crucial for ham radio operators because it directly impacts antenna performance, safety, and operational efficiency. This region, where electromagnetic energy is stored and exchanged between electric and magnetic fields, influences key factors such as **impedance matching** and **radiation efficiency**. Additionally, the near field is where electromagnetic field (EMF) strengths are highest, making it essential to assess and manage exposure levels **to comply with safety standards**, especially when transmitting at high power.

The near field also affects how antennas interact with their environment, including nearby objects and other antennas. This knowledge helps operators minimize interference and maximize performance in complex setups. In short, mastering the near field enables ham radio enthusiasts to enhance their technical skills, ensure safe operation, and achieve better results in their radio communications.

About the Author

Tony Golden

RF ENGINEER & PHYSICS PH.D. With 25+ years in Computational Electromagnetics, I'm a passionate researcher focused on antenna modeling and design. As Founder of Golden Engineering LLC, I develop accessible, high-performance simulation tools that help RF engineers optimize their designs, educators teach complex concepts, and hobbyists bring antenna projects to life.

Have a question?

💬 **Ask me** | ✉️ **Email me** | 🌐 **Follow me**

Antennas and Beyond!

Get Exclusive Updates

Share this Article

A Simple, Low-Cost Approach to Simulating Solid Wheel Antennas at 2.4 GHz

Share this Article

Explore a simple, low-cost method to simulate 2.4 GHz solid wheel antennas with reliable first-order accuracy and practical efficiency.

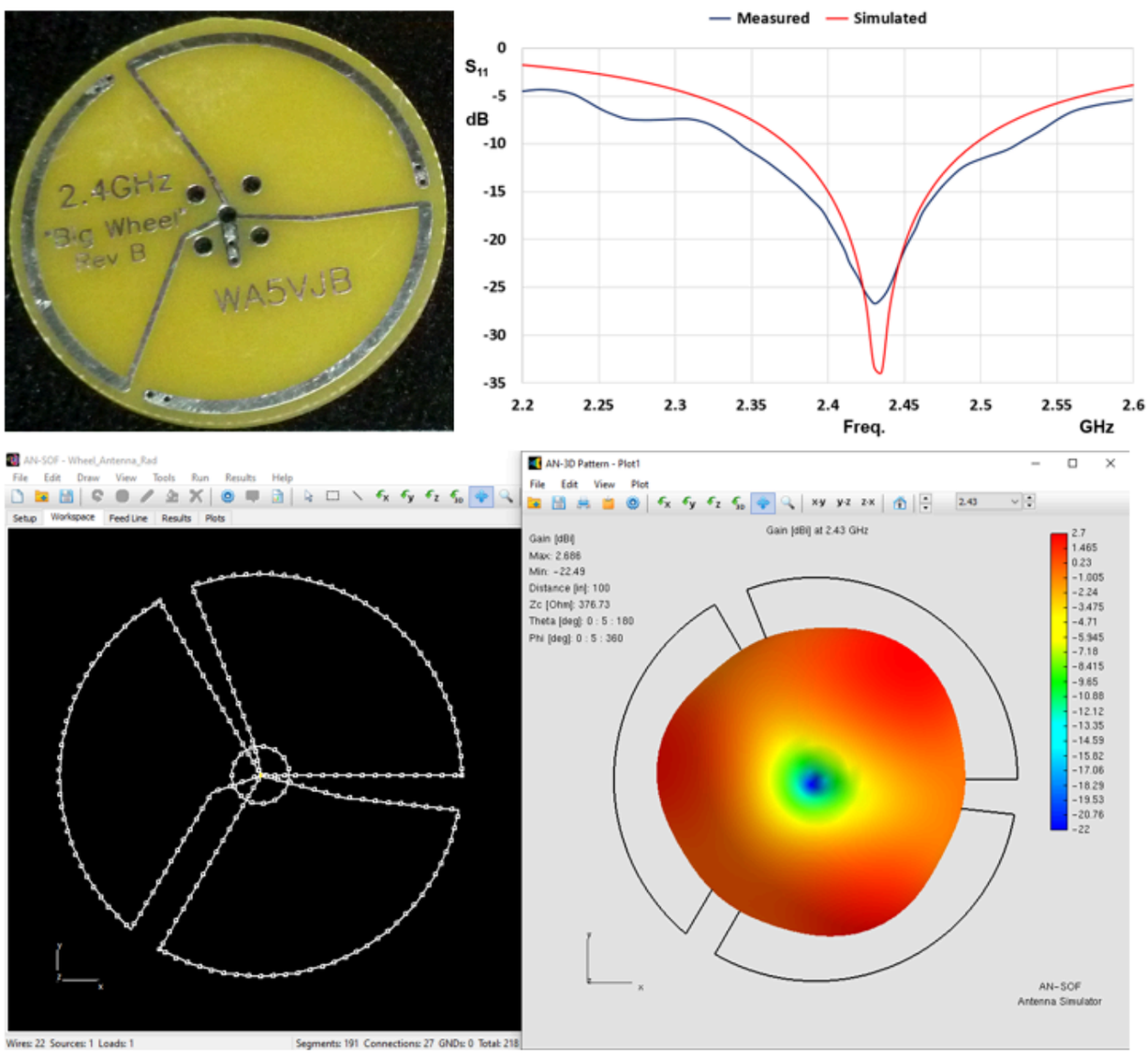

Fig. 1: 2.4 GHz Wheel Antenna with return loss curves from the datasheet and AN-SOF simulation, alongside the AN-SOF model and gain pattern. Photo and measured data courtesy of Kent Electronics (WA5VJB).

This article presents calculated **return loss** and **gain** results in the 2.4 GHz band for Wheel antennas. Using a simplified approach for simulating **planar antennas on ungrounded dielectric substrates** with sufficiently high permittivity, the results closely replicate the measured data published

by the antenna manufacturer, achieving practical engineering accuracy. A summary of these results is shown in Figure 1. The proposed method is not only straightforward but also enables the use of cost-effective simulation tools.

Introduction

Wheel antennas derive their name from their circular configuration and the presence of spokes akin to a cartwheel. Among wheel antenna designs, **solid wheel antennas** feature flat metallic traces printed on a singular dielectric substrate. Typically, these substrates are circular and crafted from materials such as **FR4**. Solid wheel antennas are known for their compact dimensions and frequent application in **ISM (industrial, scientific, and medical) frequency bands** spanning from approximately 900 to 2400 MHz, primarily within **wireless network** contexts. In the plane of the wheel, these antennas offer **omnidirectional** coverage and exhibit **horizontal polarization**. Moreover, the radiation pattern in the plane perpendicular to the wheel closely resembles that of a magnetic dipole, taking on a distinctive donut-like shape.

This article centers on the examination of a 2.4 GHz wheel antenna manufactured by **Kent Electronics (WA5VJB)**. Our primary objective is to replicate the measured return loss data (S_{11}) for the **Big Wheel Rev B** antenna variant as provided by the manufacturer, available at **this link**.

Calculation Method

Given the **planar** nature of wheel antennas, fabricated on an **ungrounded dielectric substrate**, we can employ a straightforward method for simulating these microstrip antennas. This approach is outlined in the article **Simplified Modeling of Microstrip Antennas on Ungrounded Dielectric Substrates: A Practical First-Order Approach**, which offers a **cost-effective** means of modeling such antennas. This methodology capitalizes on the capabilities of wire antenna simulation software, such as **AN-SOF**.

The initial step involves defining the **frequency range** of interest, which, in this instance, spans from **2.2 to 2.6 GHz**. Subsequently, the antenna structure is created within AN-SOF. This process is relatively uncomplicated and entails the addition of **Line** objects to represent the straight metallic strips and **Arc** objects to replicate the curved sections of the antenna. This wheel antenna boasts a diameter of approximately **1.5 inches**. At the center of this circular structure, the feed point is positioned.

Radiating outward from the antenna's center, there are **spokes** that connect to the arcs on the antenna's periphery, situated above the dielectric substrate. Additionally, there are **spokes that return beneath the substrate** to close the electrical circuit of the antenna. For the sake of facilitating external connectivity, the manufacturer typically incorporates a coaxial connector at the antenna's central point, enabling a straightforward connection to a coaxial cable.

AN-SOF, operating on the **Conformal Method of Moments**, mandates the division of wires into shorter **segments** relative to the wavelength. In the case of the antenna printed on FR4, which possesses a **dielectric constant of 4.6**, the applicable wavelength must be that of free space divided by **$\sqrt{(4.6)} = 2.14$**. Consequently, for the uppermost frequency within the specified range, 2.6 GHz, the wires have been

partitioned into segments measuring 2% of the wavelength within the substrate. This aligns with the same criterion employed for planar dipoles, as detailed in **the previously referenced article**.

In accordance with the manufacturer's datasheet, this antenna is tunable through the introduction of a **capacitor** with an approximate value of **1 pF**. This tuning capacitor has been incorporated into the model at the feed point, inserted in series with a **voltage source**. By configuring a **medium** characterized by a permittivity of 4.6, as depicted in Figure 2, and initiating the calculations with a **Ctrl + R** command, we have ascertained that **the antenna resonates at 2.43 GHz** when equipped with a **0.7 pF capacitor**, consistent with the datasheet's specifications. Consequently, there is no necessity to determine the resonance frequency in free space, as elucidated in the simplified method. This instance exemplifies **an alignment between the effective permittivity and the substrate's permittivity**.

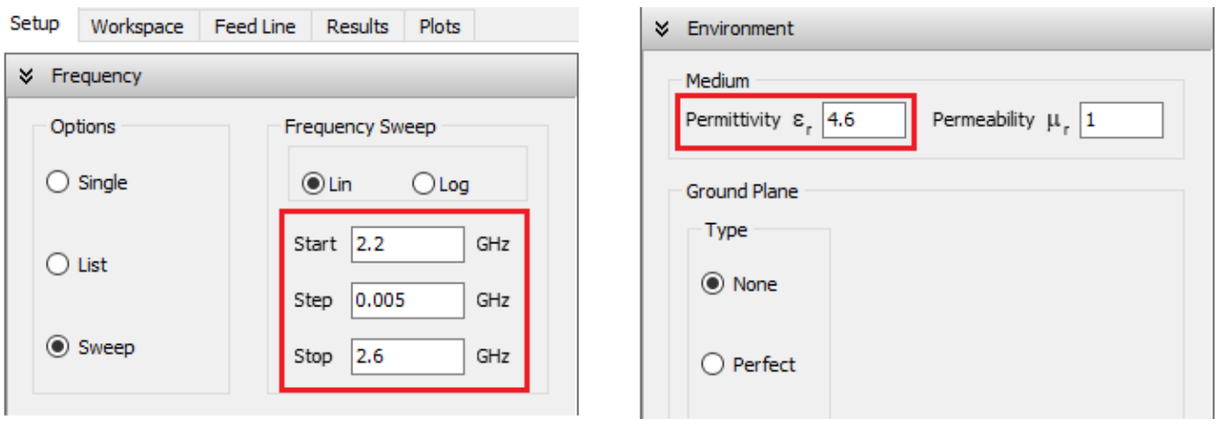

Fig. 2: Frequency and medium specification in the AN-SOF 'Setup' tab to calculate the antenna input impedance.

Figure 3, included below, presents a photograph of the physical wheel antenna, sourced from the manufacturer's website, alongside the corresponding AN-SOF model, illustrating the employed **segment density**.

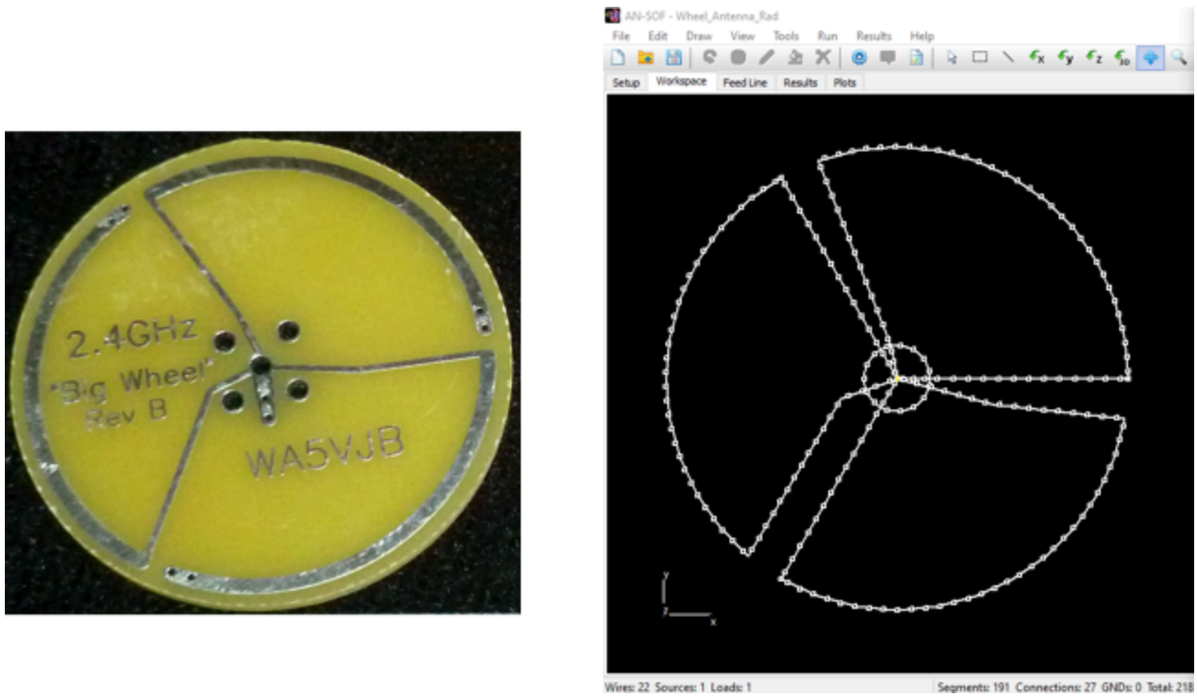

Fig. 3: Photo of the actual 2.4 GHz wheel antenna by Kent Electronics (WA5VJB) and model of the antenna in the AN-SOF's workspace showing segmentation density. The wheel diameter is about 1.5".

Comparison with Measured Data

Initiating the **input impedance** calculation with a **Ctrl + R** command, within the scrutinized frequency span of 2.2 to 2.6 GHz and employing a medium permittivity of 4.6, we generate the S_{11} curve presented in Figure 4. This figure also overlays the measured S_{11} curve, extracted from the manufacturer's **datasheet**. It is evident that the agreement between the simulated and measured outcomes is remarkably robust, particularly in the vicinity of the resonance frequency. It is worth noting that the model maintains good agreement with measurements, even though it completely neglects the dielectric substrate's thickness and contour.

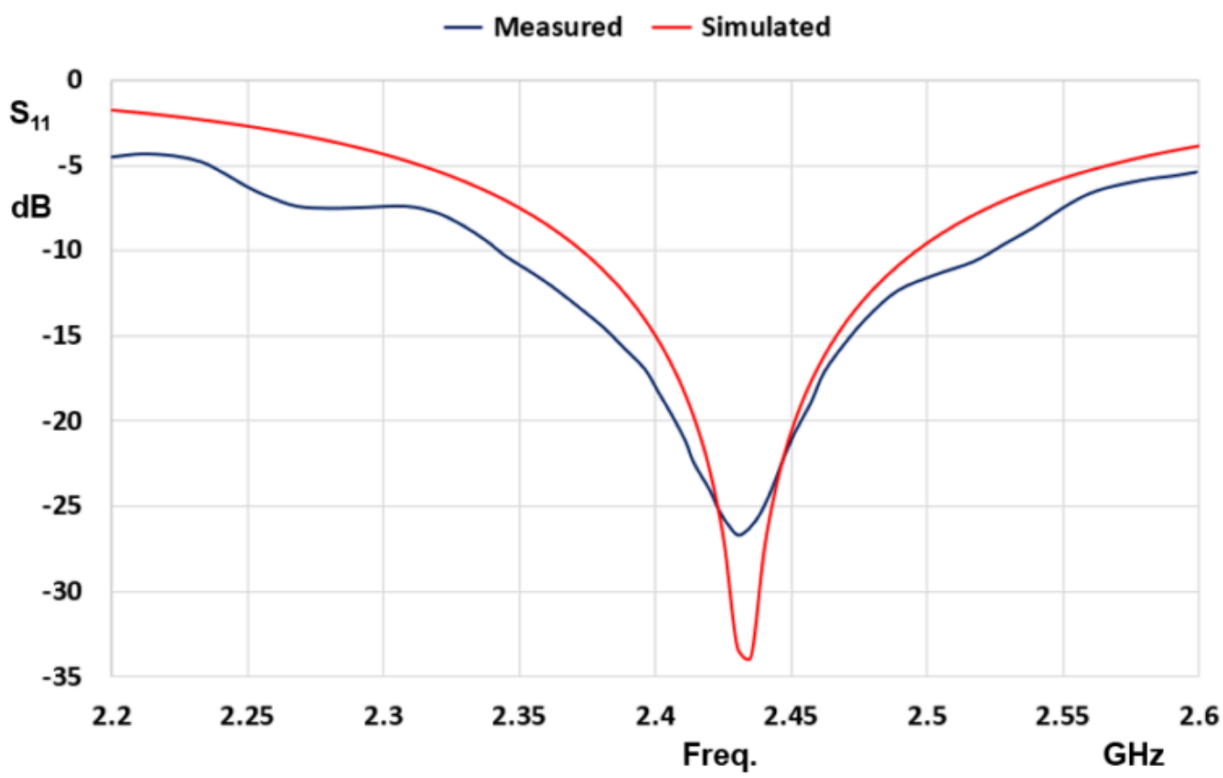

Fig. 4: Measured and Simulated Return Loss (S_{11}) for the 'Big Wheel Rev B' Antenna by Kent Electronics. Measured curve extracted from the antenna datasheet and simulated results obtained from AN-SOF.

Download Model

To calculate the radiation pattern, we must set the **permittivity of the medium (free space) to 1**, and then **rescale the antenna's dimensions** by a factor of **√(4.6) = 2.14**. This can be achieved by first clicking on the "Selection Box" button within the AN-SOF toolbar. Subsequently, draw a box around the entire antenna using the mouse and then proceed to Edit > **Scale Wires** in the main menu. Here, input the scaling factor of 2.14, ensuring that you adjust the wire cross-section accordingly, as depicted in Figure 5. Furthermore, it is necessary to modify the value of the tuning capacitor, reducing it from 0.7 pF to **0.7/2.14 = 0.33 pF**.

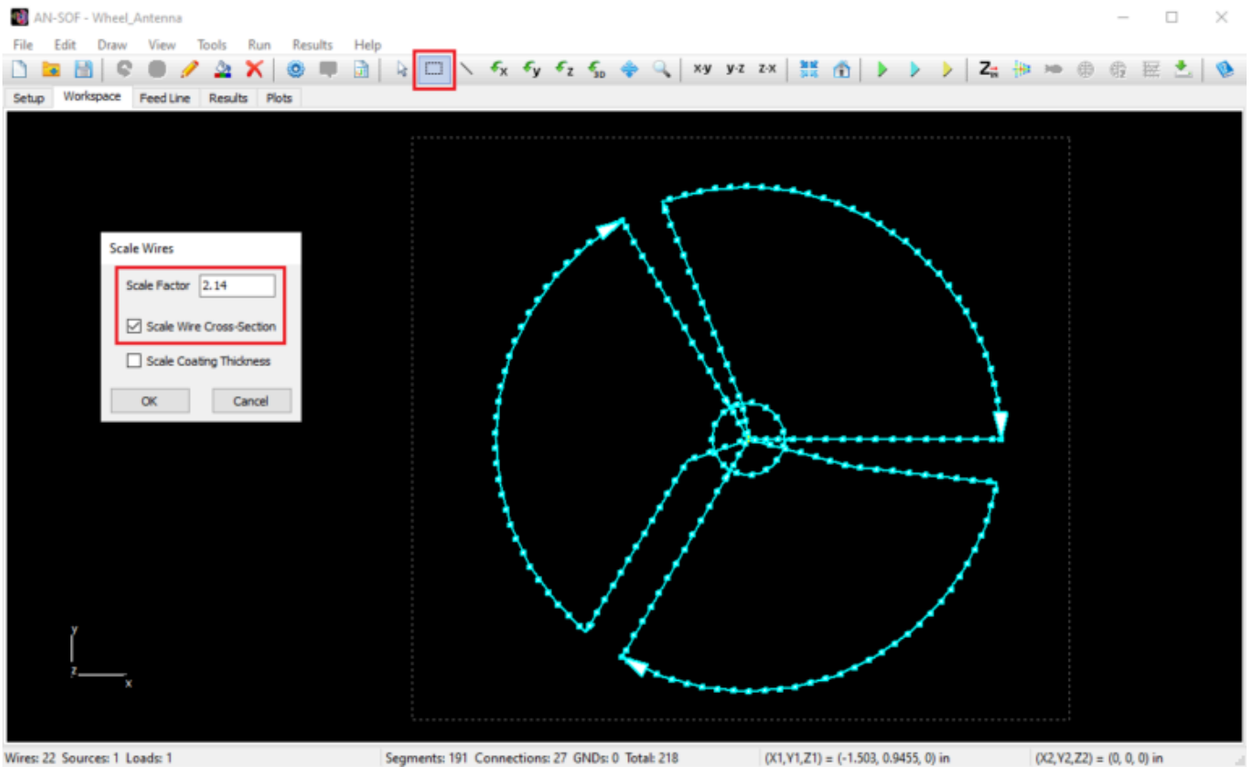

Fig. 5: Rescaling the antenna dimensions involves selecting the entire structure and navigating to Edit > Scale Wires in the AN-SOF main menu to enter the scaling factor.

Once these adjustments are made, the calculation is tailored to the single frequency of **2.43 GHz**, since our primary interest lies in the radiation pattern at the resonance frequency. With this configuration, we proceed with the calculations by pressing **F11**. The outcome, illustrated in Figure 6 (left), portrays the **gain pattern** in decibels (dBi), which, as anticipated, exhibits **near-omnidirectional coverage** within the plane of the antenna. Furthermore, the polarization is predominantly horizontal, evident from the dominance of the $\mathbf{E}_{\varphi}$ (azimuthal) component over the $\mathbf{E}_{\Theta}$ (zenithal) component of the electric field, as shown in Figure 6 (right). The $\mathbf{E}_{\varphi}$ component of the electric field reveals that there are **three directions with radiation peaks**, corresponding to each wheel arch, indicating that the radiation pattern is not perfectly omnidirectional.

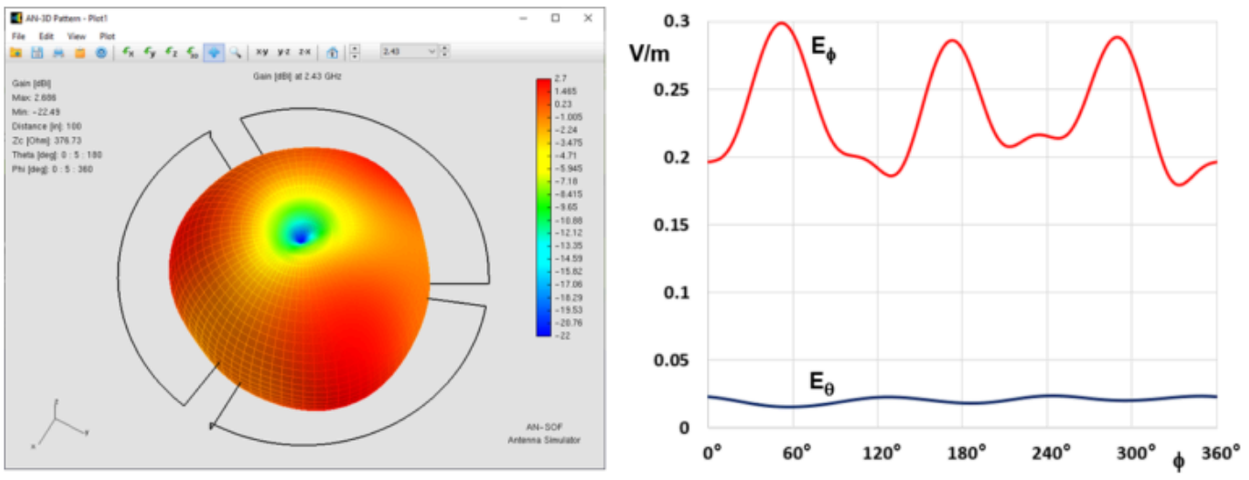

Fig. 6: Gain pattern in dBi at 2.43 GHz (left) and electric field components on the horizontal plane (Θ = 90°, varying φ) for an input voltage of 1V at the antenna feed point.

Download Model

The calculated **peak gain** registers at **2.7 dBi**, slightly surpassing the manufacturer's specification of 2 dBi. It is essential to acknowledge that this computed gain **does not account for all potential power losses** within the actual antenna, particularly within components such as the coaxial connector and the substrate (incorporating loss tangent). These factors have been omitted in our model, wherein solely a **resistivity** matching that of aluminum has been introduced for the metal traces.

Conclusions

In this article, we have introduced a simplified method for the modeling of **solid wheel antennas**, enabling the calculation of their **return loss** and **radiation pattern**. We have employed this method to simulate the performance of the Big Wheel Rev B antenna designed for the 2.4 GHz band, as provided by **Kent Electronics**. The results obtained through AN-SOF simulation have been compared with the measured data furnished by the manufacturer, and a high degree of agreement has been achieved.

This study clearly demonstrates AN-SOF's capability to model planar antennas printed on ungrounded dielectric substrates, such as FR4. The presented method combines simplicity with practical accuracy, making it a valuable tool for antenna engineers and researchers seeking **cost-effective** and reliable solutions for design and analysis.

See Also:

- **Simplified Modeling of Microstrip Antennas on Ungrounded Dielectric Substrates: A Practical First-Order Approach**

About the Author

Tony Golden

RF ENGINEER & PHYSICS PH.D. With 25+ years in Computational Electromagnetics, I'm a passionate researcher focused on antenna modeling and design. As Founder of Golden Engineering LLC, I develop accessible, high-performance simulation tools that help RF engineers optimize their designs, educators teach complex concepts, and hobbyists bring antenna projects to life.

Have a question?

💬 **Ask me** | ✉️ **Email me** | 🌐 **Follow me**

High-Performance Impedance Matching in Microstrip Antennas: The Role of Capacitive Feeding

Share this Article

Overcome probe inductance and simplify your antenna designs with capacitive feeding. This study demonstrates how to utilize proximity coupling to achieve a perfect 50-Ohm match and 10 dBi gain. Validated against classic experimental benchmarks, our simulation shows how internal reactance cancellation enables wideband performance in microstrip patches without external matching networks.

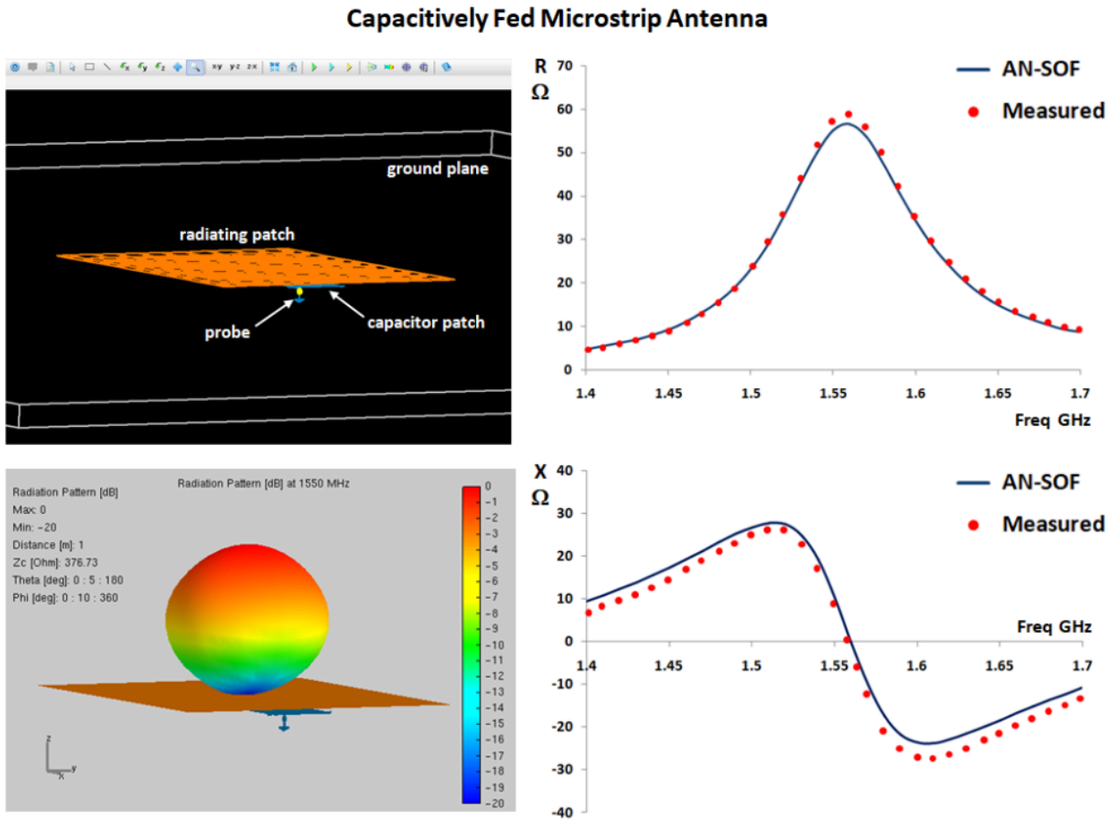

The Evolution of Microstrip Feeding Techniques

Microstrip patch antennas are ubiquitous in modern wireless communication due to their low profile and ease of integration. However, as applications demand wider bandwidths, designers typically increase the substrate thickness. This physical

change introduces a significant electromagnetic penalty: **the coaxial feed probe becomes electrically long,** introducing an unwanted **inductive reactance**. This parasitic inductance shifts the resonance and degrades the Voltage Standing Wave Ratio (VSWR), traditionally necessitating external impedance-matching networks that increase complexity and footprint.

The capacitive feeding method represents a sophisticated solution to this challenge. By decoupling the physical connection between the probe and the radiating element, and instead utilizing proximity coupling through a small intermediate patch, the inherent inductance of the feed can be neutralized internally.

Understanding the Physics of Capacitive Cancellation

In a capacitively fed architecture, the coaxial probe terminates at a small "capacitor patch" situated between the ground plane and the main radiating element (**Fig. 1**). This configuration creates a series capacitance that acts as a compensator. From a circuit perspective, the inductive reactance of the feed probe is canceled by the negative reactance of the capacitive gap.

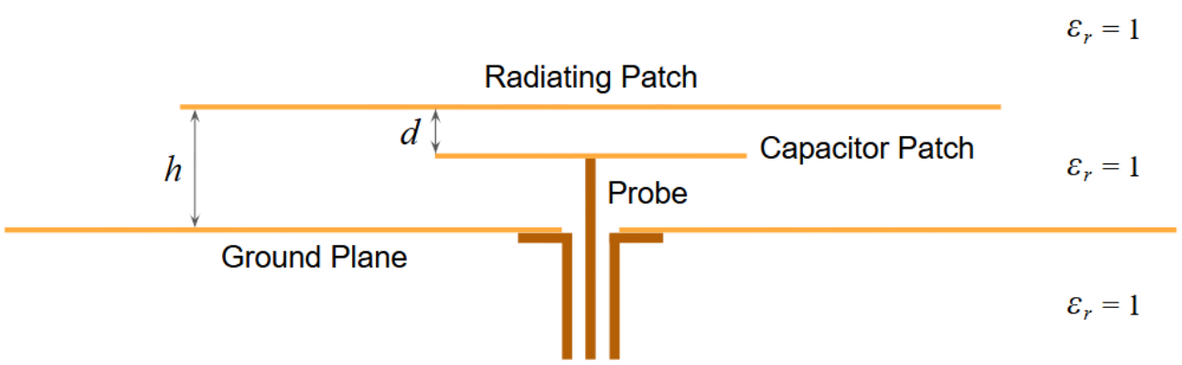

Fig. 1: *Side view of the components for a capacitively-fed patch antenna.*

The primary advantage of this approach is the ability to achieve a perfect 50-Ohm match at the desired frequency simply by adjusting the geometry of the coupling patches, rather than relying on external stubs or **transformers**. This has been a critical breakthrough for the development of Planar Inverted-F Antennas (PIFAs) and other compact radiators used extensively in the mobile phone industry.

Geometric Configuration and Model Setup

To demonstrate the precision of this technique, a suspended patch model was analyzed using the AN-SOF simulation engine (**Fig. 2**). Modeling the structure in air ($\epsilon_r = 1$) allows for a pure examination of the coupling dynamics without the influence of substrate losses or dielectric uncertainty.

Detailed Model Dimensions:

- **Radiating Element:** A square PEC patch measuring 82.5×82.5 mm.
- **Capacitor Patch:** A square PEC patch measuring 20×20 mm.

- **Ground Plane:** A large square PEC surface of 600×600 mm (approx. 3λ at the center frequency).
- **Vertical Stacking:** The radiating patch is positioned $h = 6.85$ mm above the ground plane. The capacitor patch is suspended $d = 2.25$ mm below the radiating patch.
- **Feed Offset:** To achieve the required resistance, the capacitor patch is offset 22 mm from the center of the radiating patch.

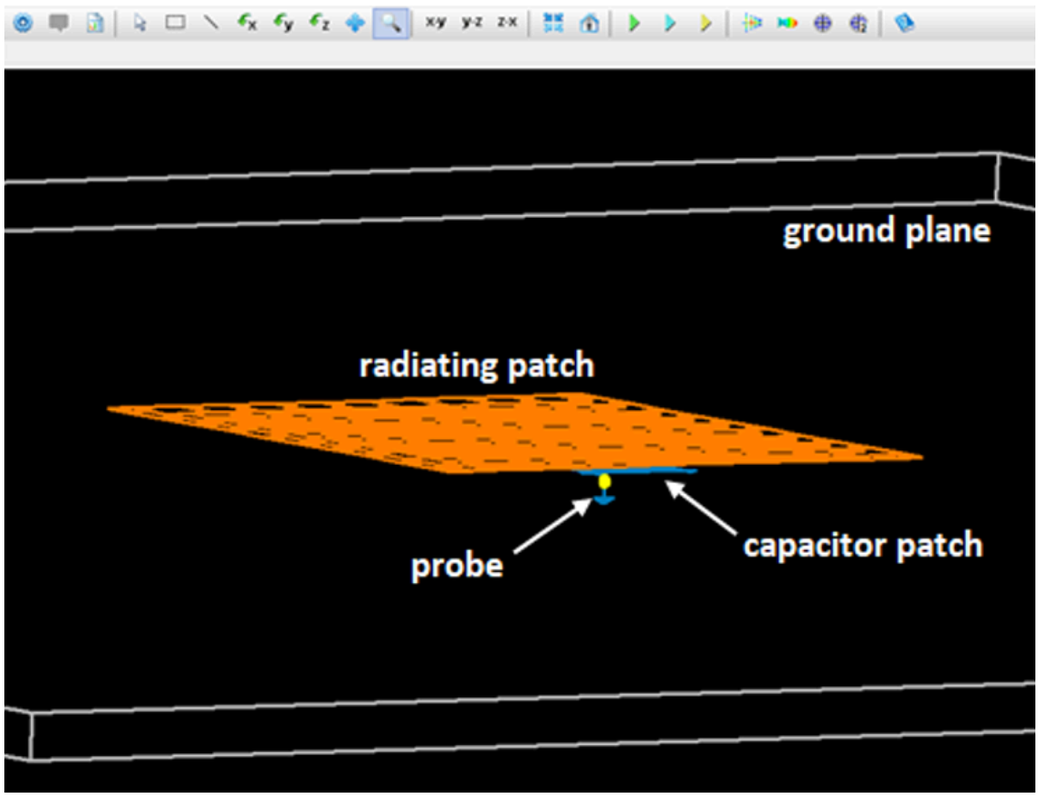

Fig. 2: AN-SOF model of a capacitively-fed patch antenna.

Download Model

The model shown in **Fig. 2** was constructed by defining a **Patch** with 10×10 facets for the radiating patch and a wire grid representing a solid surface with 5×5 facets for the capacitor patch. A finite PEC ground plane was set under the **Substrate** option in the **Environment** panel. The model can be downloaded via the button below the figure.

Input Impedance and Resonance Analysis

To verify the predictive capabilities of the AN-SOF engine, the antenna geometry and experimental results for this study were sourced from the paper by G.A.E. Vandenbosch and A.R. Van de Capelle, *"Study of the Capacitively Fed Microstrip Antenna Element" (IEEE Trans. Ant. Propag., vol. 42, no. 12, 1994)*. This publication serves as a primary benchmark in the field of computational electromagnetics, providing a rigorous set of measured data for suspended microstrip patches. By utilizing these specific dimensions and empirical results, this simulation acts as a formal validation of the software's ability to model proximity-coupled structures with high precision.

The simulation was conducted across a frequency sweep from 1.4 to 1.7 GHz. The resulting input impedance data reveals the classic signature of a high-performance resonant structure (**Fig. 3**).

The real part of the input impedance follows a bell-shaped curve, reaching a peak of approximately **60 Ohms at 1.56 GHz**. Simultaneously, the input reactance exhibits a *parallel resonant transition*, crossing the zero-Ohm axis at 1.56 GHz. This alignment confirms that the capacitive feed has successfully tuned the antenna to a purely resistive state at its primary resonance.

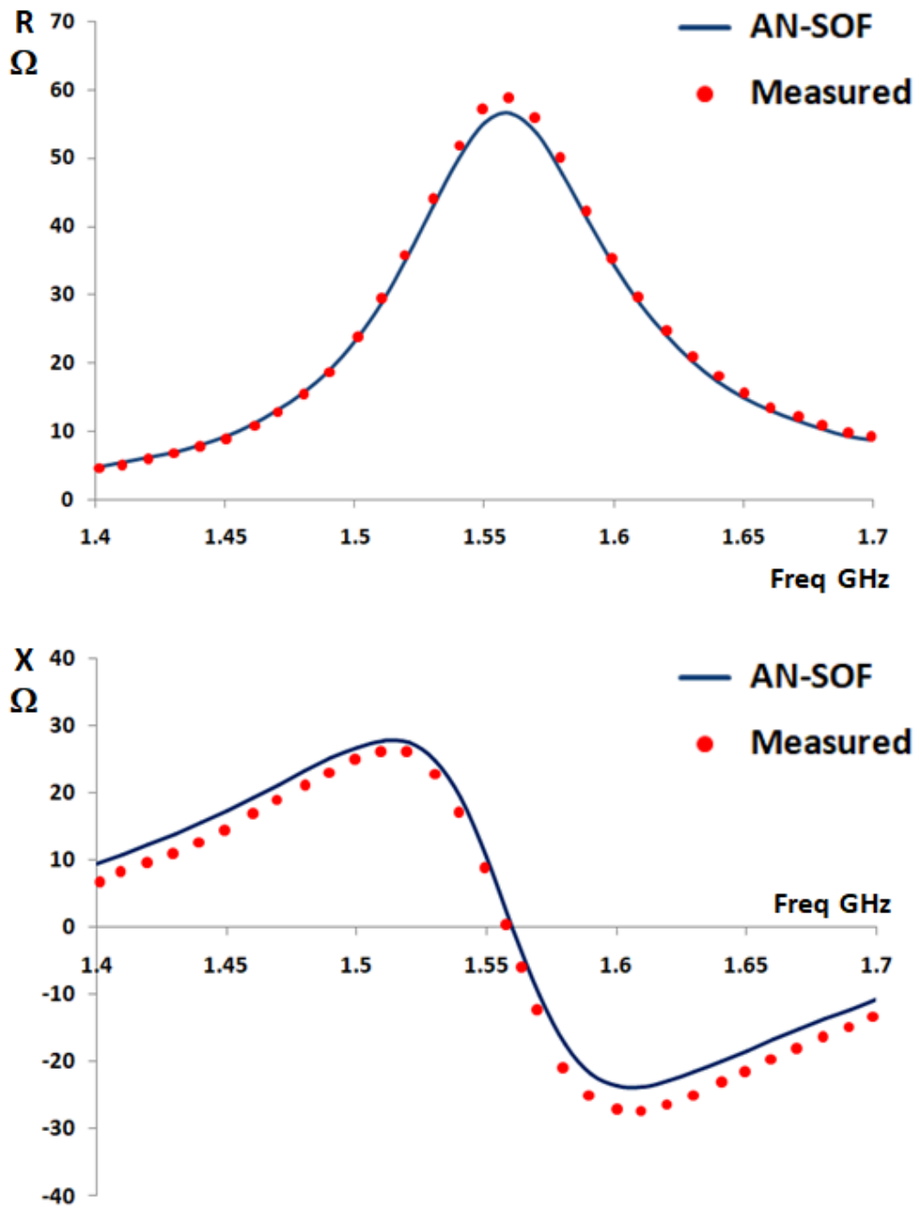

Fig. 3: *Measured and calculated input resistance (top) and input reactance (bottom) as a function of frequency for the capacitively-fed patch antenna.*

The bandwidth performance is equally impressive. For a 2:1 VSWR relative to a 50-Ohm system, the antenna achieves a **5% fractional bandwidth**. This capability to maintain a stable match over a significant range is a direct result of the optimized proximity coupling.

Validation Against Empirical Data

A critical aspect of this study is the comparison between AN-SOF numerical results and established experimental measurements for this specific geometry.

Numerical results show that the calculated real and imaginary parts of the input impedance are nearly *coincident* with measured data reported by G.A.E. Vandenbosch and A.R. Van de Capelle, as shown in **Fig. 3**. Specifically, the resonance frequency of **1.56 GHz** matches the empirical benchmark with negligible error. Notably, the AN-SOF implementation provides a higher degree of correlation to the measured curves than the original theoretical calculations proposed in early literature. This precision underscores the effectiveness of the **Conformal Method of Moments (CMoM)** in capturing the complex near-field interactions between overlapping metallic layers.

Radiation Patterns and Gain Efficiency

The electromagnetic performance extends beyond impedance matching to highly efficient radiation characteristics. Throughout the 1.4 to 1.7 GHz band, the gain remains stable between **9 and 10 dBi**.

The radiation pattern is characterized by a clean, broadside main lobe directed perpendicularly away from the ground plane (**Fig. 4**). No significant side lobes or grating lobes are observed, indicating a well-behaved current distribution on the radiating patch.

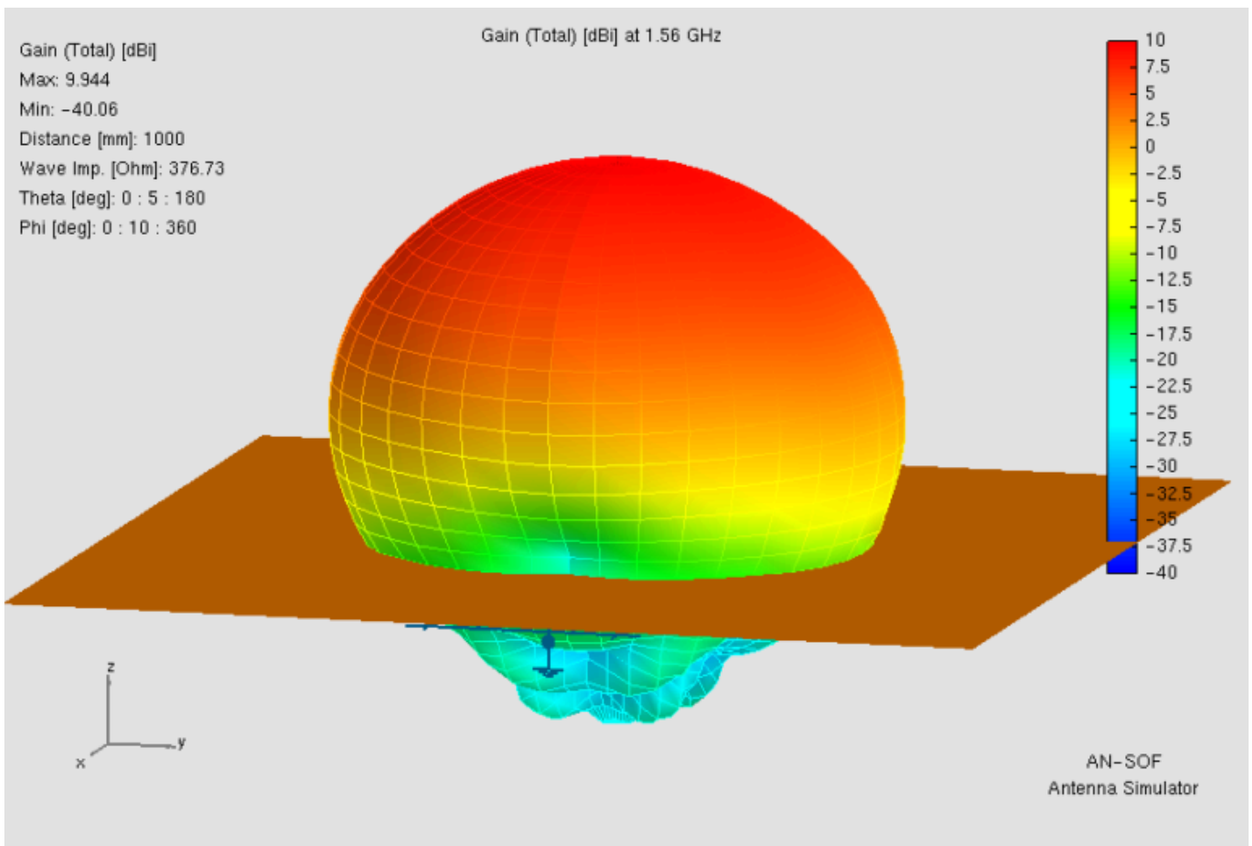

Fig. 4: *Gain pattern (in dBi) of the capacitively-fed patch antenna.*

The impact of the ground plane size is evident in the Front-to-Back (F/B) ratio. Although some diffraction occurs at the edges of the 600 mm ground plane, the energy leaked into the back hemisphere is suppressed to approximately **-30 dB** relative to the peak gain. This high degree of isolation is ideal for applications requiring unidirectional coverage and minimal interference with electronics located behind the antenna.

Conclusion

The study of capacitively fed microstrip elements confirms that proximity coupling is an exceptionally effective method for managing feed probe reactance. By integrating a capacitor patch into the antenna's internal architecture, designers can achieve wideband performance and a stable 50-Ohm match without the need for external tuning components. The perfect agreement between simulation and measurement validates this model as a benchmark for engineers designing advanced, compact radiators for the next generation of wireless devices.

See Also:

- **Learning Antennas Through Simulation: 4.8 Microstrip and Printed Antennas**

Technical Keywords: Microstrip Patch Antenna, Capacitive Feeding, Impedance Matching, Probe Reactance Cancellation, Resonant Resistance, AN-SOF Simulation, PIFA Design.

About the Author

Tony Golden

RF ENGINEER & PHYSICS PH.D. With 25+ years in Computational Electromagnetics, I'm a passionate researcher focused on antenna modeling and design. As Founder of Golden Engineering LLC, I develop accessible, high-performance simulation tools that help RF engineers optimize their designs, educators teach complex concepts, and hobbyists bring antenna projects to life.

Have a question?

💬 **Ask me** | ✉️ **Email me** | 🌐 **Follow me**

Explicit Modeling of a 9-Element LPDA: Capturing Real-World Wideband Performance

Share this Article

Explore the precision of explicit boom modeling in this 9-element LPDA study. Using AN-SOF, we analyze a 200-800 MHz log-periodic array, demonstrating how the ‘active region’ shifts with frequency to maintain stable gain and VSWR. Learn why modeling feed lines as physical wires provides a superior analysis of wideband antenna performance.

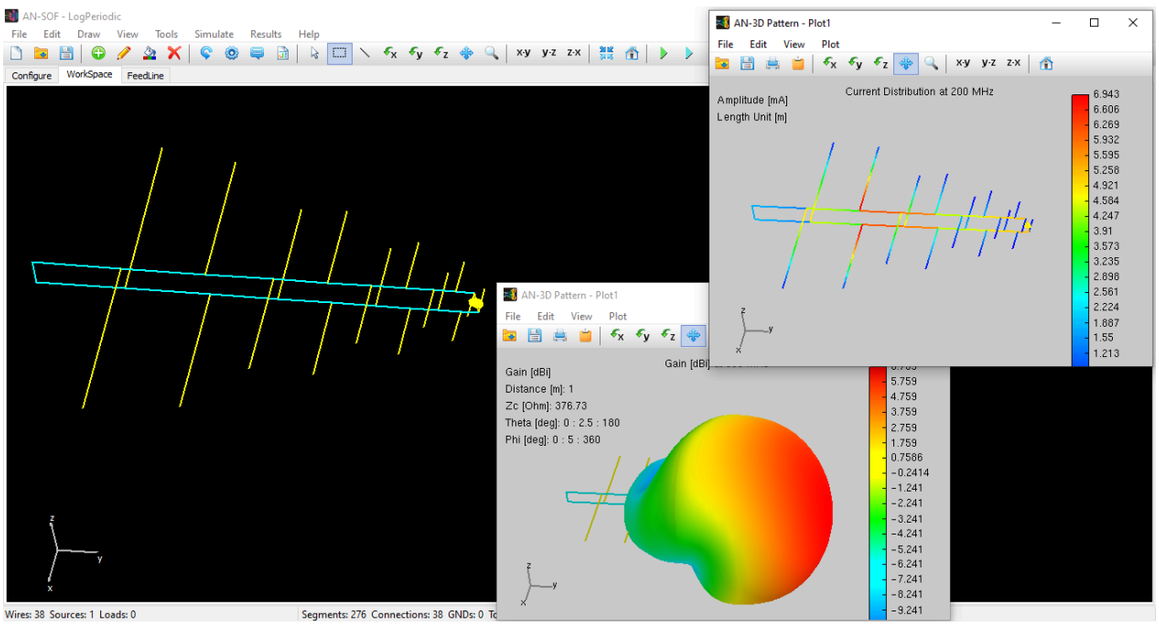

The Principles of Frequency-Independent Design

The **Log-Periodic Dipole Array (LPDA)** belongs to a class of **“frequency-independent”** antennas. The fundamental requirement for such an antenna is that its electrical properties remain invariant when its physical dimensions are **scaled**. While a truly frequency-independent antenna would need to be infinite in size, the LPDA approximates this behavior by employing a self-similar, truncated geometry.

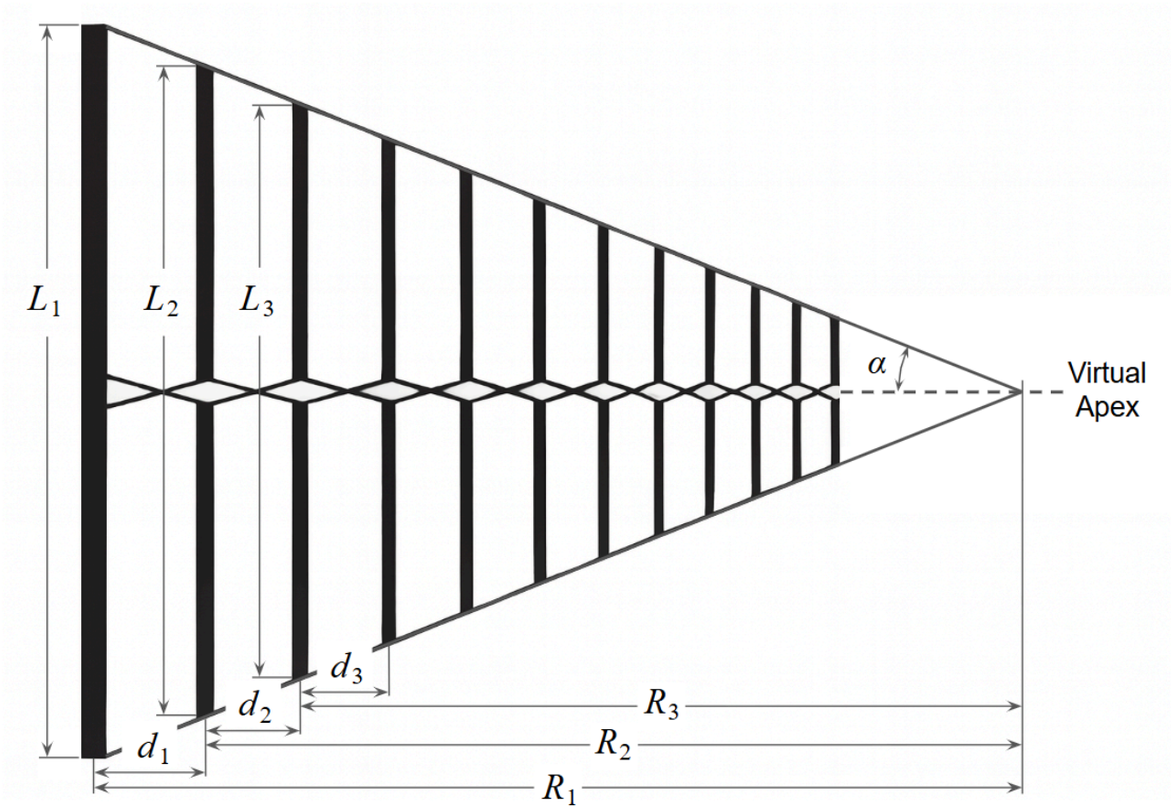

Fig. 1: *Geometrical parameters of an LPDA antenna.*

The design is governed by two primary dimensionless parameters (**Fig. 1**):

1. The Scaling Factor (τ): Defines the ratio of lengths (L) and distances from the apex (R) of adjacent elements:

$$\tau = \frac{L_{n+1}}{L_n} = \frac{R_{n+1}}{R_n} < 1$$

2. The Spacing Factor (σ): Relates the element spacing to the length of the adjacent element:

$$\sigma = \frac{R_n - R_{n+1}}{2L_n} = \frac{d_n}{2L_n}$$

An LPDA is therefore fully specified by the two dimensionless constants τ and σ. The half-apex angle α is related to these parameters by

$$\alpha = \arctan\left(\frac{1-\tau}{4\sigma}\right)$$

Because the geometry repeats at intervals of $\ln(\tau)$, the antenna's performance, including its input impedance and radiation pattern, oscillates periodically when plotted against the logarithm of the frequency. By carefully choosing τ and σ (in this model, optimized for the 200–800 MHz range), these oscillations are minimized, resulting in a remarkably stable VSWR and gain across a 4:1 bandwidth.

Beyond the Ideal: Explicit Boom Modeling in AN-SOF

The LPDA boom, i.e., the transmission line feeding the dipoles, can be implicitly modeled using telegrapher's equations (the standard equations of transmission line theory). In AN-SOF, these **implicit transmission line models** can be used to feed an LPDA, which is computationally inexpensive. A tutorial for connecting the elements of an LPDA using implicit lines is provided here:

- **Linking Log-Periodic Antenna Elements Using Transmission Lines**

This is a good modeling technique as a first approach. However, it ignores the physical reality of the boom as a radiating and coupling structure.

In this 9-element model, we have instead modeled the boom **explicitly using wires** (**Fig. 2**). This ensures that the **Conformal Method of Moments (CMoM)** solver accounts for the physical proximity of the feed line to the elements, providing a more accurate prediction of the antenna's real-world behavior, especially at the higher end of the 200–800 MHz sweep.

Model Specifications:

- **Element Count:** 9
- **Bandwidth:** 200 to 800 MHz
- **Longest Element:** $0.75\ \mathrm{m}$ (Resonant near the lower cutoff)
- **Shortest Element:** $0.1258\ \mathrm{m}$ (Resonant near the upper cutoff)
- **Feeding:** Explicit wire boom with a $200\,\Omega$ reference impedance (simulating a 4:1 impedance transformer to a $50\,\Omega$ system).

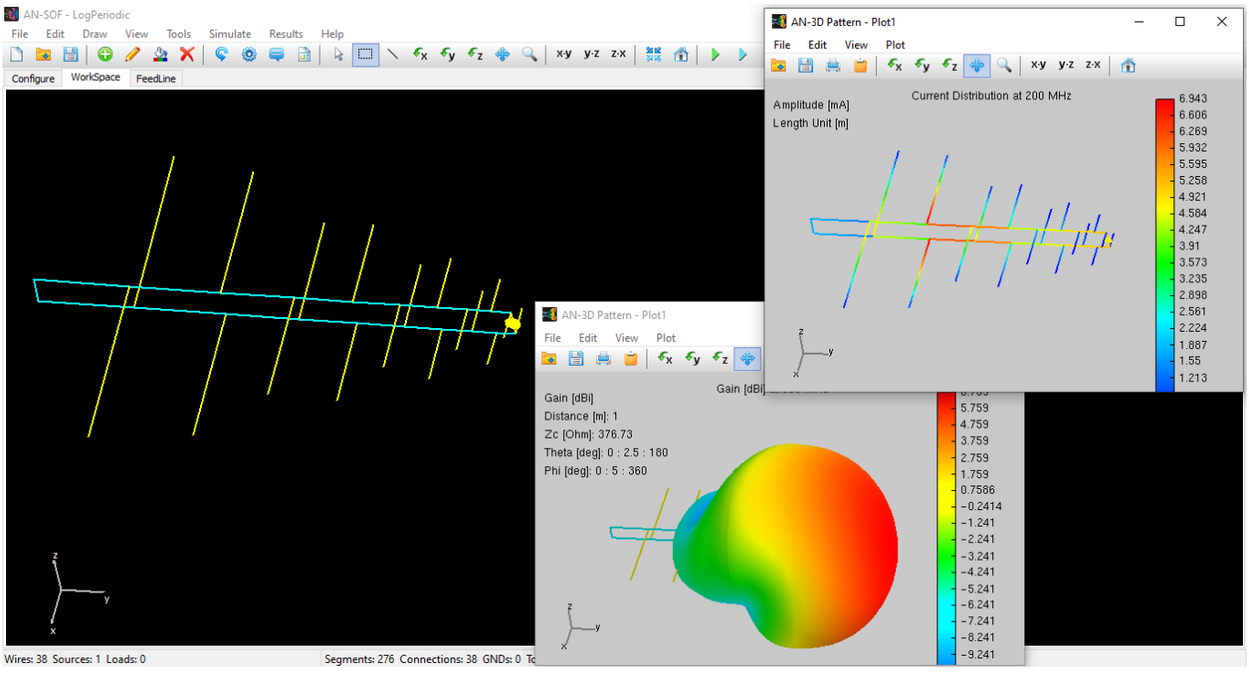

Fig. 2: AN-SOF model of the 9-element LPDA, showing the resulting current distribution and gain pattern at 200 MHz.

Download Model

Analysis of the “Active Region”

The magic of the LPDA lies in the **Active Region**. As the frequency increases, the cluster of near-resonant elements “moves” from the longer elements toward the shorter ones.

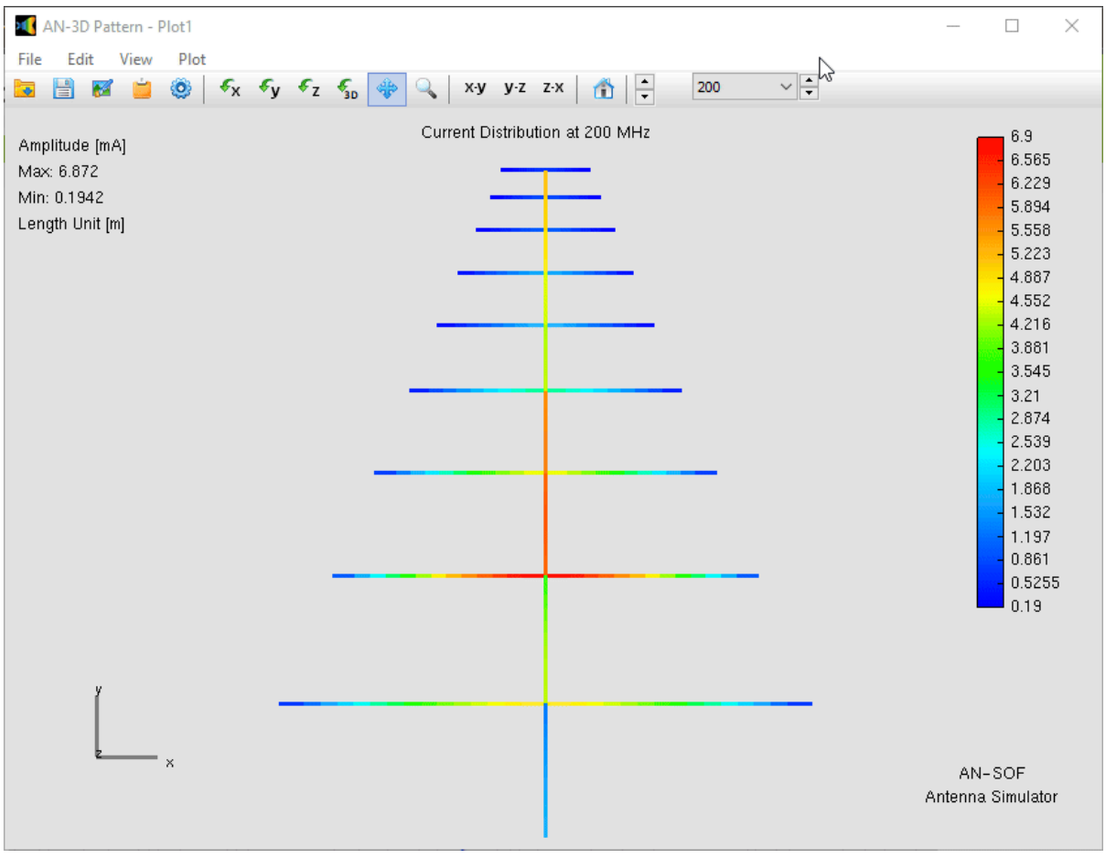

Fig. 3: Variation of current distribution on the LPDA with frequency.

In **Fig. 3**, this shift can clearly be observed in the current distribution on the antenna. At any given frequency, only about three elements are actively contributing to the radiation, while the others act as directors or reflectors, or remain electrically inactive. This localized resonance is the reason the radiation pattern shape remains stable, as **Fig. 4** shows, with a gain between **5.2 and 7.5 dBi** across a 4:1 frequency range.

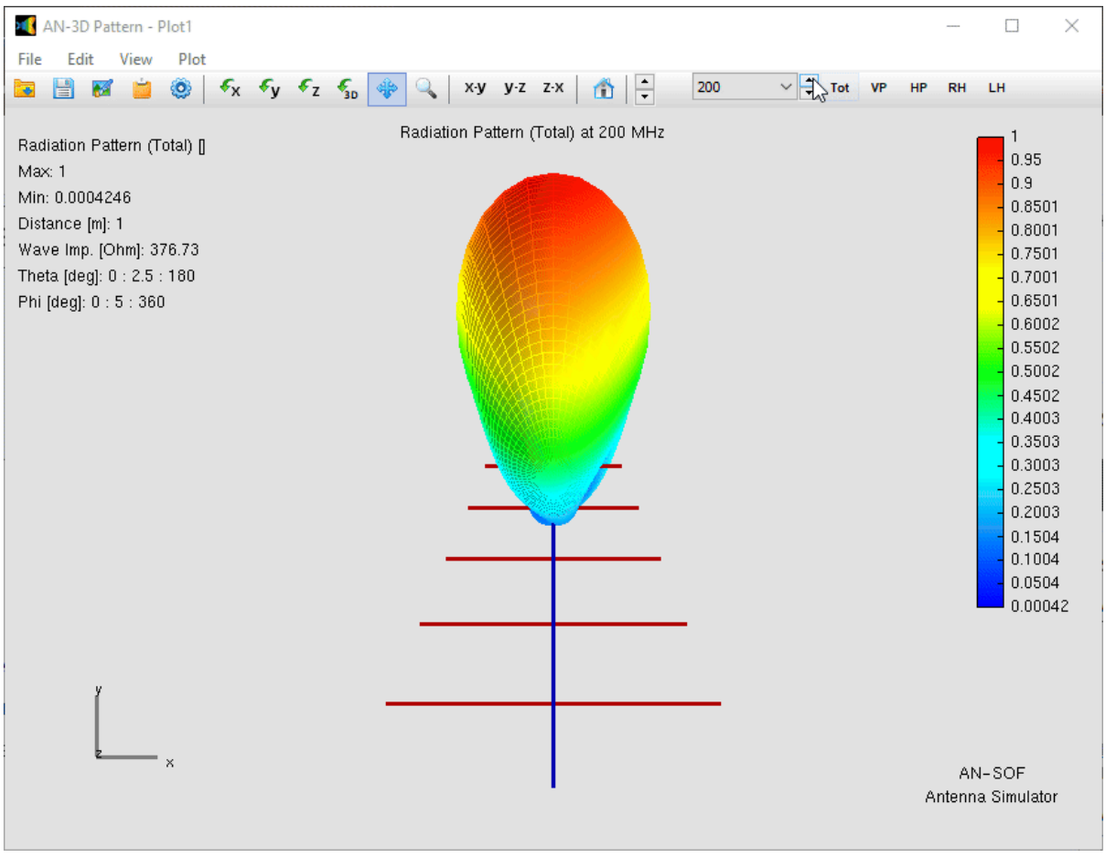

Fig. 4: Variation of the radiation pattern of the LPDA with frequency (linear scale).

Performance Metrics

The simulation results confirm the robust nature of this design (**Fig. 5**):

- **VSWR:** Oscillates between **1.05 and 1.6**, indicating an excellent match across the entire band when referenced to $200\,\Omega$.
- **Front-to-Back (F/B) Ratio:** Achieves peak performance of **>15 dB** between 300 and 700 MHz, maintaining high directivity before tapering to roughly 10 dB at the band edges.

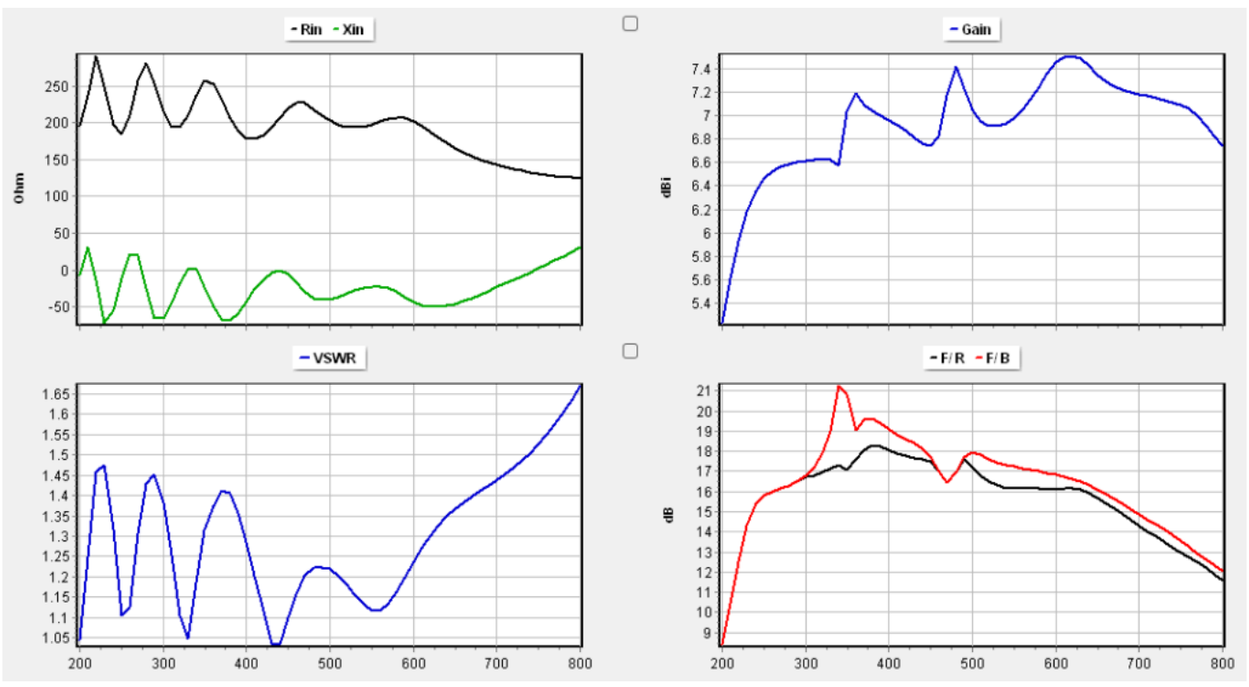

Fig. 5: Input impedance, Voltage Standing Wave Ratio (VSWR), gain, and Front-to-Back (F/B) and Front-to-Rear (F/R) ratios as a function of frequency for the LPDA.

Conclusions

The simulation of this 9-element LPDA within AN-SOF demonstrates that this type of antenna can be modeled completely using wires for both **the dipole elements and the boom** closely approaching real world engineering. By explicitly modeling the transmission line boom with wires instead of using implicit transmission line models, the complex mutual coupling and proximity effects can be accurately captured.

The results confirm that:

- **Active Region Dynamics:** The antenna successfully maintains an "Active Region" that migrates from the 0.75m element down to the 0.1258m element as frequency increases, ensuring consistent directivity.
- **Impedance Stability:** Referencing the system to $200\,\Omega$ effectively demonstrates how a 4:1 balun would stabilize the VSWR between 1.05 and 1.6 across the entire multi-octave range.
- **Modeling Accuracy:** The stable Gain (5.2–7.5 dBi) and high Front-to-Back ratio (>15 dB) calculated by AN-SOF's CMoM solver provide a high-fidelity benchmark for physical prototyping.

See Also:

- **Exploring an HF Log-Periodic Sawtooth Array: Insights from Geometry to Simulation**
- **Linking Log-Periodic Antenna Elements Using Transmission Lines**

Technical Keywords: LPDA, Log-Periodic Dipole Array, Active Region, Explicit Boom Modeling, Wideband Antenna, VSWR, Frequency Sweep.

About the Author

Tony Golden

RF ENGINEER & PHYSICS PH.D. With 25+ years in Computational Electromagnetics, I'm a passionate researcher focused on antenna modeling and design. As Founder of Golden Engineering LLC, I develop accessible, high-performance simulation tools that help RF engineers optimize their designs, educators teach complex concepts, and hobbyists bring antenna projects to life.

Have a question?

💬 **Ask me** | ✉️ **Email me** | 🌐 **Follow me**

Antennas and Beyond!

High-Gain Biquad Antenna with Planar Reflector: Analysis and Applications for the 866.5 MHz ISM Band

Share this Article

Discover the design and performance characteristics of a high-gain Biquad antenna with a planar reflector for the 866.5 MHz ISM band. This AN-SOF analysis details the antenna's 10.5 dBi gain, 10% impedance bandwidth, and exceptional beam symmetry, providing a professional-grade directional solution for LoRaWAN, UHF RFID, and long-range telemetry applications.

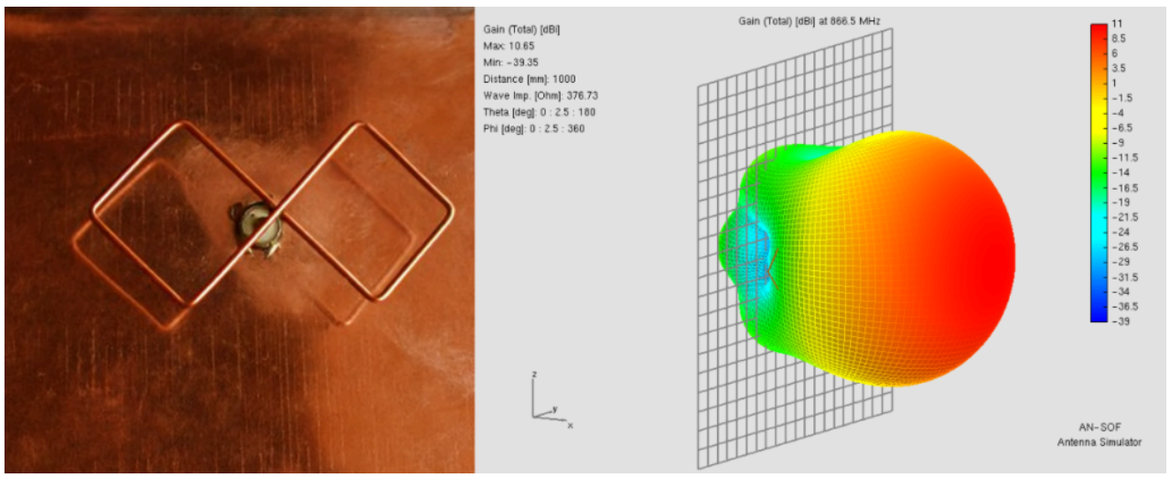

Introduction to the Biquad Radiator

The Biquad antenna, often referred to as a *Harchenko antenna*, is a high-gain directional radiator consisting of two loop elements configured in a "figure-eight" shape (**Fig. 1**). Traditionally favored in the microwave and UHF communities for its simplicity and robustness, the Biquad provides a significant performance boost over standard dipoles. When placed in front of a metallic reflector, the antenna transitions from an omnidirectional radiator to a highly directional system, making it an ideal candidate for point-to-point communication, telemetry, and long-range sensing in the $866.5\ \mathrm{MHz}$ Industrial, Scientific, and Medical (ISM) band.

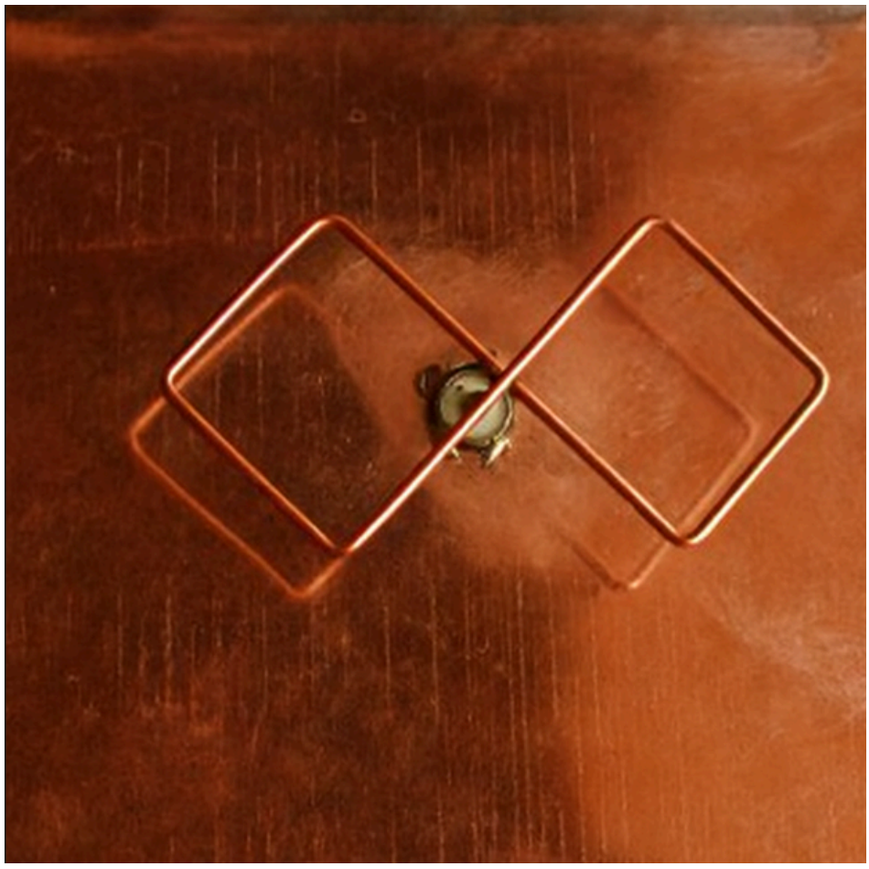

***Fig. 1**: Biquad or Harchenko antenna with a reflector.*

Design Specifications and Geometric Configuration

For operation at a center frequency of $866.5\ \mathrm{MHz}$ ($\lambda \approx 346\ \mathrm{mm}$), the antenna must be precisely dimensioned to ensure resonance and optimal coupling with the reflector. The model presented here is constructed from $3\ \mathrm{mm}$ diameter conductive wire, providing structural rigidity and a stable surface area for current distribution (**Fig. 2**).

The Radiating Element:

- **Quad Side**: $S = 89.1\ \mathrm{mm}$ (approximately 0.258λ).
- **Quad Diagonal:** $D = 126\ \mathrm{mm}$.
- **Total Length:** $L = 2D = 252\ \mathrm{mm}$. The geometry consists of two interconnected square loops. The choice of 89.1 mm for each side ensures that the total perimeter of each loop is approximately **one wavelength**, the fundamental condition for the Biquad's resonant mode.

The Reflector System:

The backplane reflector is a square PEC (Perfect Electric Conductor) surface, measuring $380\ \mathrm{mm} \times 380\ \mathrm{mm}$ ($W = 380\ \mathrm{mm}$ in **Fig. 2**), which represents approximately $1.1\lambda \times 1.1\lambda$. The reflector is positioned at a distance of $h = 42\ \mathrm{mm}$ ($\approx 0.12\lambda$) from the biquad radiator. This spacing is a critical design variable; at 0.12λ, the reflected wave reinforces the forward radiation through constructive interference while maintaining a manageable input impedance close to the 50-Ohm standard.

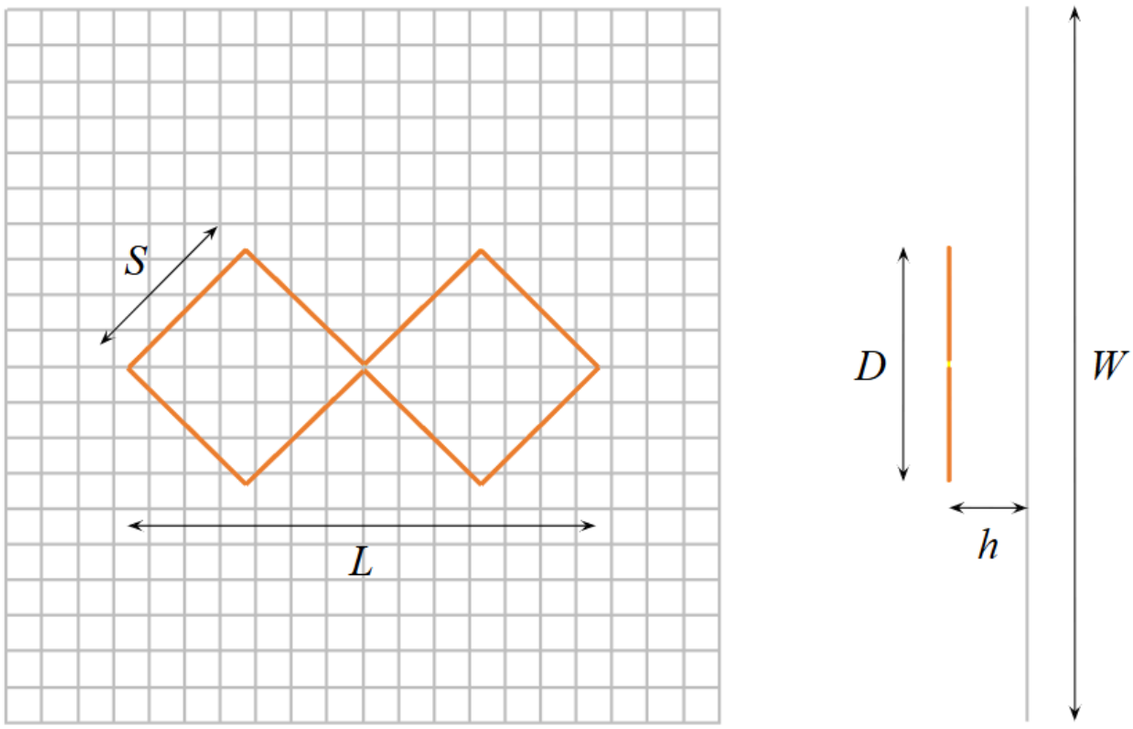

Fig. 2: Relevant geometric parameters of the biquad antenna with a reflector.

Download Model

The reflector in AN-SOF is modeled as a **solid surface** composed of 20 x 20 facets. The antenna is fed by connecting a short vertical wire with a 1V voltage source at the center of the biquad, which is the point where the two square loops meet.

Numerical Analysis and Impedance Characterization

The antenna performance was evaluated using a frequency sweep from $816.5\ \mathrm{MHz}$ to $916.5\ \mathrm{MHz}$. The simulation captures the transition of the antenna through its resonant state, revealing a highly stable impedance profile (**Fig. 3**).

- **Input Impedance:** At the target frequency of $866.5\ \mathrm{MHz}$, the calculated input impedance is $48 + j5\ \Omega$. This results in a Voltage Standing Wave Ratio (VSWR) of 1.1, indicating an nearly perfect match to a standard 50-Ohm feedline.
- **Impedance Dynamics:** Throughout the sweep, the input resistance varies between 35 and 70 Ohms, while the reactance ranges from -35 to $+45$ Ohms (series resonance at $866.5\ \mathrm{MHz}$). This smooth variation, typical of a **series resonance**, demonstrates the "wideband" nature of the biquad compared to **narrow-band patches** that operate around a parallel resonance.
- **Operating Bandwidth:** For a VSWR threshold of ≤ 2, the antenna exhibits an operational bandwidth of $85\ \mathrm{MHz}$ (approximately 10%). This bandwidth is sufficient to cover the entire European LoRaWAN and RFID spectrum without requiring additional tuning.

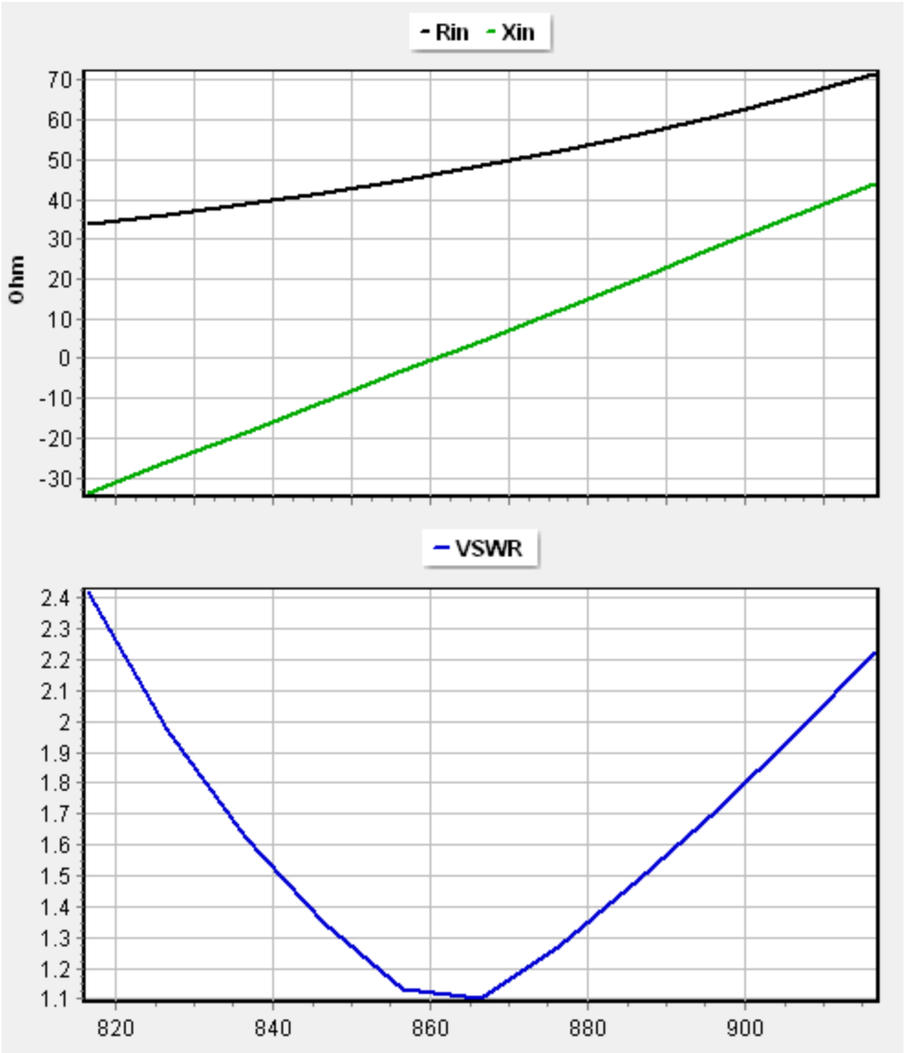

***Fig. 3**: Input impedance (top) and VSWR (bottom) of the biquad antenna with reflector, as modeled in AN-SOF, shown as a function of frequency (in MHz).*

Radiation Pattern and Far-Field Performance

One of the most striking features of the Biquad with a reflector is the high degree of symmetry in its radiation characteristics. The simulation reports a gain that remains remarkably constant across the band, averaging 10.5 dBi.

Pattern Symmetry and Beamwidth:

The main lobe is well-defined and points perpendicularly away from the reflector (**Fig. 4**). A key advantage of this design is its **rotational symmetry**; the half-power beamwidths (HPBW) in both the vertical and horizontal planes are identical at 55°. This symmetry is particularly beneficial for applications where the orientation of the receiving antenna might fluctuate, as it ensures a consistent signal link budget.

Sidelobe and Backlobe Suppression:

The design eliminates secondary forward-pointing lobes, focusing all energy into a single aperture. Due to the optimized reflector size, the Front-to-Back (F/B) and Front-to-Rear (F/R) ratios are maintained at approximately 20 dB. While some back radiation exists due to edge diffraction at the 380 mm plate, the isolation is more

than sufficient for mounting the antenna on walls or masts without significant interference from rearward objects.

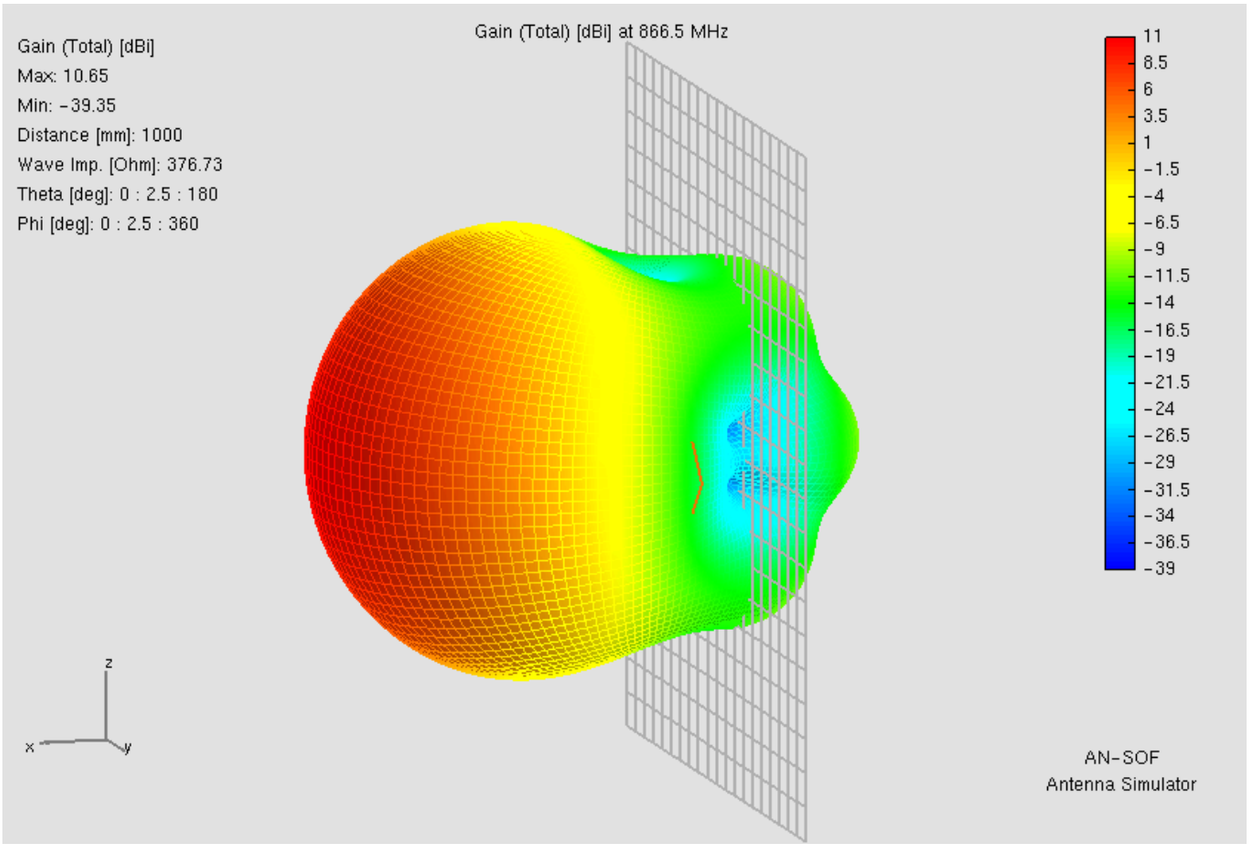

Fig. 4: *Gain pattern (in dBi) of the biquad antenna with a reflector, modeled in AN-SOF.*

Practical Applications at 866.5 MHz

The 866.5 MHz frequency is a critical window within the EU863-870 MHz band. The 10.5 dBi gain of this Biquad antenna makes it a powerful tool for several key industries:

1. **LoRaWAN and LPWAN Gateways:** In IoT (Internet of Things) deployments, gateways often need to reach sensors located several kilometers away. This antenna's 10.5 dBi gain can significantly extend the range of a LoRa gateway compared to a standard omnidirectional whip antenna, especially in sectorized coverage or point-to-point relay links.
2. **UHF RFID Systems:** The 865–868 MHz range is used for passive RFID tag reading. The rotational symmetry of the Biquad's beamwidth is ideal for "portal" style readers where tags pass through a specific area. The high gain ensures that even small, low-power tags can be energized and read from a distance.
3. **Industrial Telemetry:** For SCADA systems and remote industrial monitoring, the Biquad offers a robust, high-directivity solution that is less sensitive to nearby metallic structures than a Yagi-Uda antenna, thanks to its wide-aperture reflector.

Conclusion

The Biquad antenna with a planar reflector is a highly efficient aperture-style radiator that balances high gain with ease of matching. By achieving 10.5 dBi gain and a 10% bandwidth with a VSWR of 1.1, this design provides a "plug-and-play" solution for the 866.5 MHz band. Its symmetrical radiation pattern and high F/B ratio

make it one of the most reliable directional antennas in the “Apertures and Reflectors” category of modern CEM study.

See Also:

- **Design and Analysis of a Parabolic Cylinder Reflector with a Back-Firing Primary Radiator**
- **Learning Antennas Through Simulation: 1.8 Ground Plane and Image Theory**

Technical Keywords: Biquad Antenna, Harchenko Radiator, Planar Reflector, 866.5 MHz, ISM Band, LoRaWAN, UHF RFID, Impedance Matching, Front-to-Back Ratio.

About the Author

Tony Golden

RF ENGINEER & PHYSICS PH.D. With 25+ years in Computational Electromagnetics, I’m a passionate researcher focused on antenna modeling and design. As Founder of Golden Engineering LLC, I develop accessible, high-performance simulation tools that help RF engineers optimize their designs, educators teach complex concepts, and hobbyists bring antenna projects to life.

Have a question?

💬 **Ask me** | ✉️ **Email me** | 🌐 **Follow me**

Wave Matching Coefficient: Defining the Practical Near-Far Field Boundary

Share this Article

Discover how the Wave Matching Coefficient (WMC) redefines near-far field boundaries. Using a 20 dB threshold, we uncover new distances for elementary antennas and a consistent method to define non-spherical boundaries for antennas of any size or complexity relative to the wavelength.

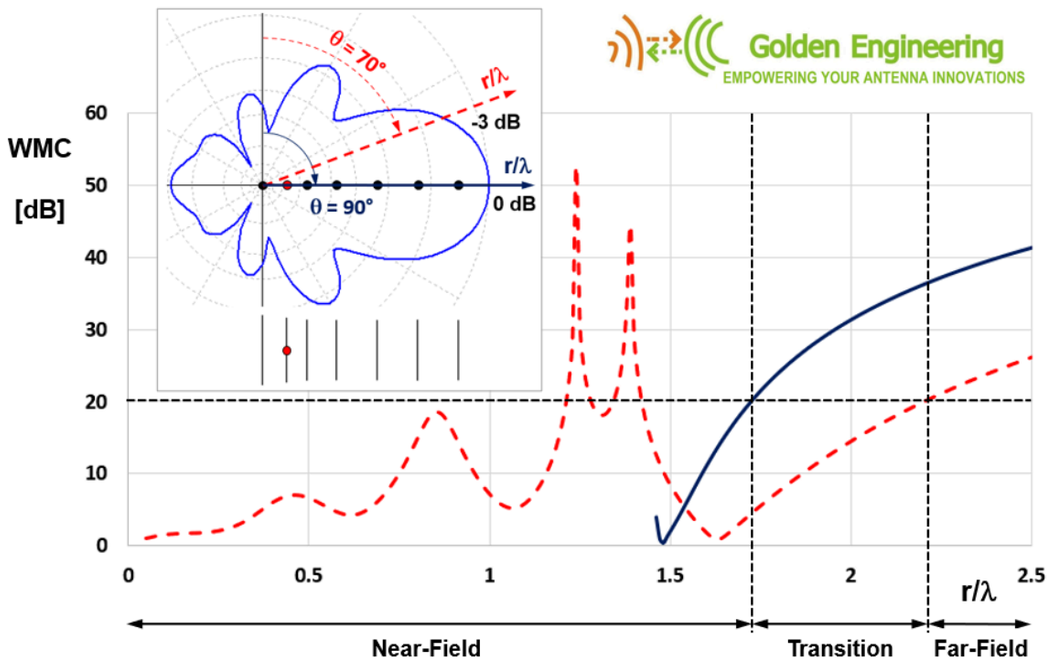

In this article, we explore **absolute wave impedance** and the **wave matching coefficient (WMC)** as practical tools for defining the near-far field boundary of antennas of any size or complexity relative to the wavelength. By utilizing these measures, we gain a better understanding of wave propagation as a function of distance from the source antenna, employing a decibel scale that enables clearer visualization of significant changes in wave impedance. As a general guideline, a **WMC value of 20 dB** proves to be an appropriate threshold for distinguishing between the **near and far field zones**. Through examples involving both elementary and large-scale antennas relative to the wavelength, we observe that the 20 dB boundary is consistently located at a distance of $\lambda/3$ for elementary antennas, while it takes on an irregular and non-spherical shape for antennas of comparable size or greater than the wavelength.

Introduction

The determination of the far-field region of an antenna has been a topic extensively discussed in books and texts on antennas for nearly a century. However, it continues to spark debates even today. Identifying the regions surrounding an antenna is crucial for various applications, such as near-field measurements in an anechoic chamber to predict the far-field radiation pattern or in electromagnetic compatibility (EMC) to optimize shielding in the near-field region, minimizing interference.

Based on the observation of **elementary electric or magnetic dipole fields**, three distinct regions can be identified in terms of the distance, r, from the dipole:

1. The **reactive near-field region**, where terms proportional to $1/r^3$ predominate.
2. A **transition region or Fresnel zone**, where terms proportional to $1/r^2$ predominate.
3. The **far-field region or Fraunhofer zone**, where terms proportional to $1/r$ predominate.

There is also a two-region model where the reactive near-field and the Fresnel zone are considered as part of the same near-field region. When antennas are more complex than elementary dipoles, it becomes nontrivial to identify the electromagnetic field zones. It is important to note that the definition of a boundary between the near-field and far-field regions is always **arbitrary** and depends on the acceptable **margin of error** in practice. There is no sharp edge or discontinuity between these regions; instead, the electromagnetic field initially behaves as a **quasi-static field** near the radiation source and gradually transforms into a **Transverse Electromagnetic (TEM) wave** with a spherical wavefront as the distance increases.

The Traditional Boundary Between Near Field and Far Field

In most textbooks, we can find that the far-field region begins at a distance from the antenna given by $2D^2/\lambda$, where D is the maximum dimension of the antenna and λ is the wavelength. This boundary between regions works reasonably well for cases of electrically large antennas, where $D \gg \lambda$. However, there are many exceptions to this rule, such as in the case of parabolic antennas where this boundary must be extended twofold. For electrically small antennas, where $D \ll \lambda$, the boundary between regions is located at $\lambda/(2\pi)$ regardless of the antenna size.

These calculations are based on placing the observation point of the field far enough away so that **the antenna remains within a sphere**, which, as it expands, approaches a **spherical wavefront in the far-field zone**. This allows us to develop the phase of the Green's function of the problem in a Taylor series with respect to distance and retain the first terms. Depending on the number of terms retained, the different field zones will be delimited. For an antenna that is large compared to the wavelength, if we move away to enclose it within a sphere, we may have already moved too far and find ourselves in the far-field region, missing the details of what

happens in the near field and where a boundary between both zones could be defined. Hence, these analytical formulas fail in many cases.

Note:

The traditional boundary between the near and far field regions can be calculated using this online tool: **RF Calculators**, which implements standard textbook formulas.

Definitions of Wave Impedance

Instead of using a single formula for all cases, which introduces a high level of uncertainty, a more convenient criterion for separating the near-field and far-field regions is to calculate the so-called **wave impedance**, which is calculated as the ratio of the electric and magnetic fields. Since fields are vectors, we can compute the ratio between their components. For example, when a wave is **vertically polarized**, at the wavefront, we consider the vertical component of the electric field, E_v, and the horizontal component of the magnetic field, H_h, omitting components in the direction of propagation (which rapidly diminish with distance from the emission source). We define the wave impedance as $Z_w = E_v/H_h$. This ratio involves two complex quantities with real and imaginary parts, so the wave impedance has both magnitude and phase. By decomposing the wave at the wavefront into its **right-handed** circular polarization components, E_R and H_R, and **left-handed** circular polarization components, E_L and H_L, we can define two complex wave impedances: **a right-handed impedance**, $Z_R = E_R/H_R$, and **a left-handed impedance**, $Z_L = E_L/H_L$.

Regardless of the chosen definition of wave impedance, it will have the following properties:

- Z_w is a function of the **distance** from the antenna measured in wavelengths, r/λ, and the **observation direction,** given by two angles, θ (zenith) and ϕ (azimuth), when using spherical coordinates.
- In any chosen direction (θ, ϕ), as the distance increases ($r \gg D$ and $r \gg \lambda$), Z_w tends to **377 Ω** in free space.

Therefore, in the far-field region, the wave impedance approaches the **intrinsic impedance of the medium,** which is 377 Ω for free space. For an ideal lossless and isotropic medium, the intrinsic impedance is given by $Z_i = \sqrt{\mu/\epsilon}$, where μ is the magnetic permeability and ϵ is the dielectric constant. For vacuum, this value is approximately rounded to 377 Ω, often approximated as 120π Ω for convenience, with three significant digits.

Absolute Wave Impedance

The problem with defining wave impedance in terms of components of the $\mathbf{E}$ and $\mathbf{H}$ vector fields is that we have more than one definition, as we have just seen, and these definitions depend on the chosen coordinate system or frame of reference. A

figure that allows us to identify the field regions should satisfy the following conditions:

1. It should be calculated based on **observables**, i.e., quantities that can be **measured in practice**.
2. It should be **independent of the frame of reference**, i.e., invariant under a coordinate transformation.
3. It should be obtainable for **any polarization of the field**, even when it is unpolarized, as is the case when uncorrelated fields with random phases are summed.

A simple figure that meets these three requirements is what we will call the **absolute wave impedance**, which is given by the ratio of the root mean square (rms) values of the $\mathbf{E}(\mathbf{r})$ and $\mathbf{H}(\mathbf{r})$ vector fields,

$$Z_w(\mathbf{r}) = \frac{E_{rms}(\mathbf{r})}{H_{rms}(\mathbf{r})} \quad \text{at each point } \mathbf{r} \text{ in space} \qquad (1)$$

These are observables that are independent of the coordinate system. For example, when transforming from Cartesian to spherical coordinates, we have:

$$E_{rms} = |\mathbf{E}| = \sqrt{|E_x|^2 + |E_y|^2 + |E_z|^2} = \sqrt{|E_r|^2 + |E_\theta|^2 + |E_\phi|^2} \qquad (2)$$

where E_x, E_y, E_z are complex components in Cartesian coordinates and E_r, E_θ, E_ϕ are complex components in spherical coordinates (if working with peak values, they should be divided by $\sqrt{2}$ to obtain rms values). The modulus of the vector $\mathbf{E}$ is given by the square root of the dot product of $\mathbf{E}$ with its complex conjugate $\mathbf{E}^*$, expressed as $|\mathbf{E}| = \sqrt{\mathbf{E} \cdot \mathbf{E}^*}$. The same applies to the rms value of the magnetic field, H_{rms} $= |\mathbf{H}| = \sqrt{\mathbf{H} \cdot \mathbf{H}^*}$.

Thus, equation (2) indicates that the rms value of a vector field remains invariant when transforming between Cartesian and spherical coordinates. More generally, the rms values of the $\mathbf{E}$ and $\mathbf{H}$ fields **are invariant under any coordinate transformation**. Therefore, $Z_w(\mathbf{r})$ is defined at every point $\mathbf{r}$ in space outside the antenna surface because it is a quantity that can be calculated at any point $\mathbf{r}$ based on the measured fields, $E_{rms}(\mathbf{r})$ and $H_{rms}(\mathbf{r})$. Since this definition disregards the phase, it is also useful for unpolarized waves. Disregarding the phase of the wave impedance is not an issue since we will need to compare it with a real value, equal to 377 Ω (with zero phase), to determine if we are in the far-field zone.

Wave Matching Coefficient

Analogous to the definition of “return loss” used for transmission lines, if 377 Ω were the characteristic impedance of a line, we can define a coefficient in **decibels** that measures how well the wave impedance is “matched” to the intrinsic impedance of the medium. We will call this coefficient the **Wave Matching Coefficient (WMC)**, given by

$$\mathrm{WMC} = -20 \log_{10} \left| \frac{Z_w - 377}{Z_w + 377} \right| \quad [\mathrm{dB}] \qquad (3)$$

where $Z_w = E_{rms}/H_{rms}$ is the **absolute wave impedance**. We will not use the term "return loss" because in the propagation mechanism we are considering, there is no loss or wave returning by reflection to the source that originated it.

As Z_w approaches 377 Ω, the WMC always increases. In a transmission line, a return loss of 20 dB implies that 99% of the power is transmitted and 1% is reflected. Although we don't have a reflection mechanism here, we could adopt the same tolerance and consider the limit of **WMC = 20 dB** as the **boundary between the near-field and far-field regions**. If this limit proves to be too strict or too lenient for a particular practical application, we are free to choose another boundary according to the acceptable tolerance. From an engineering standpoint, we would recommend placing the boundary between the near-field and far-field regions above WMC = 10 dB. In the examples we will consider next, we will use the 20 dB boundary.

Examples with a 20 dB Boundary

Figure 1(a) shows the absolute wave impedance as a function of distance for an **elementary electric dipole** and an **elementary magnetic dipole**, while **Figure 1(b)** shows the corresponding WMC. The direction along which the distance r/λ varies is perpendicular to the axis of the dipoles, where the far-field reaches its maximum value. In both cases, the 20 dB boundary is practically at r/λ = 0.33 ≈ 1/3. Additionally, we could divide the near-field region into two parts, one below the maximum at r/λ = 0.1 and one above.

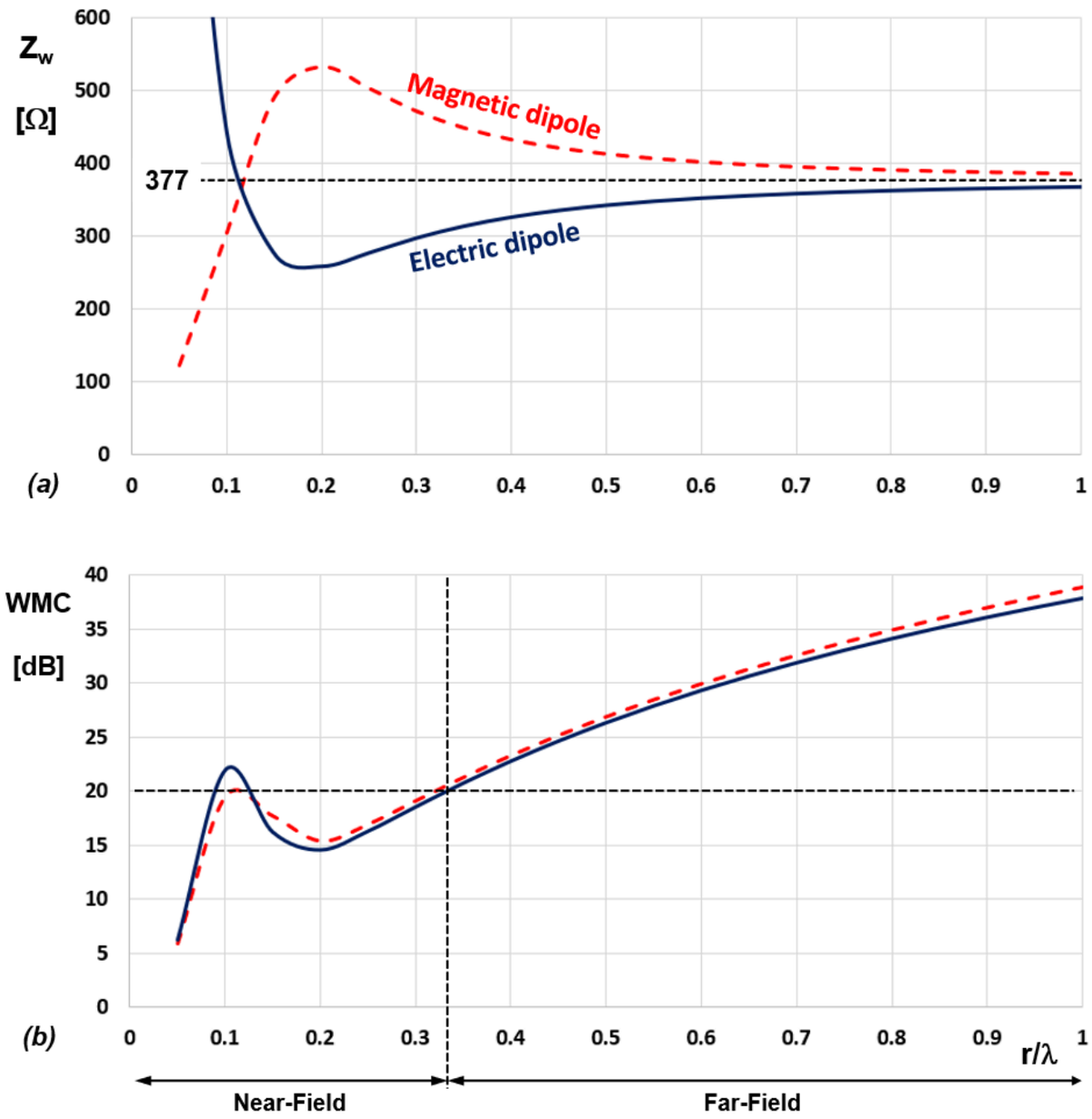

Fig. 1: (a) Absolute wave impedance for elementary electric and magnetic dipoles as a function of distance along the direction of maximum radiation. (b) The corresponding WMC and the separation between the near-field and far-field zones at a threshold of 20 dB.

Figure 2(a) displays the absolute wave impedance for an **elementary electric dipole** along a direction at 45° from its axis, where the **power density drops 3 dB** compared to its maximum value, as well as the curve obtained in the previous **Fig. 1(a)** along the direction at 90° from the dipole's axis. **Figure 2(b)** shows the corresponding WMC. In this way, we observe the wave impedance and WMC for the directions that define the radiation maximum and the **beamwidth** of an elementary dipole.

We can observe that the boundary between the near-field and far-field regions moves away from the dipole when observed from a direction other than that of maximum radiation, and a **transition zone opens** around $r/\lambda = 1/3$.

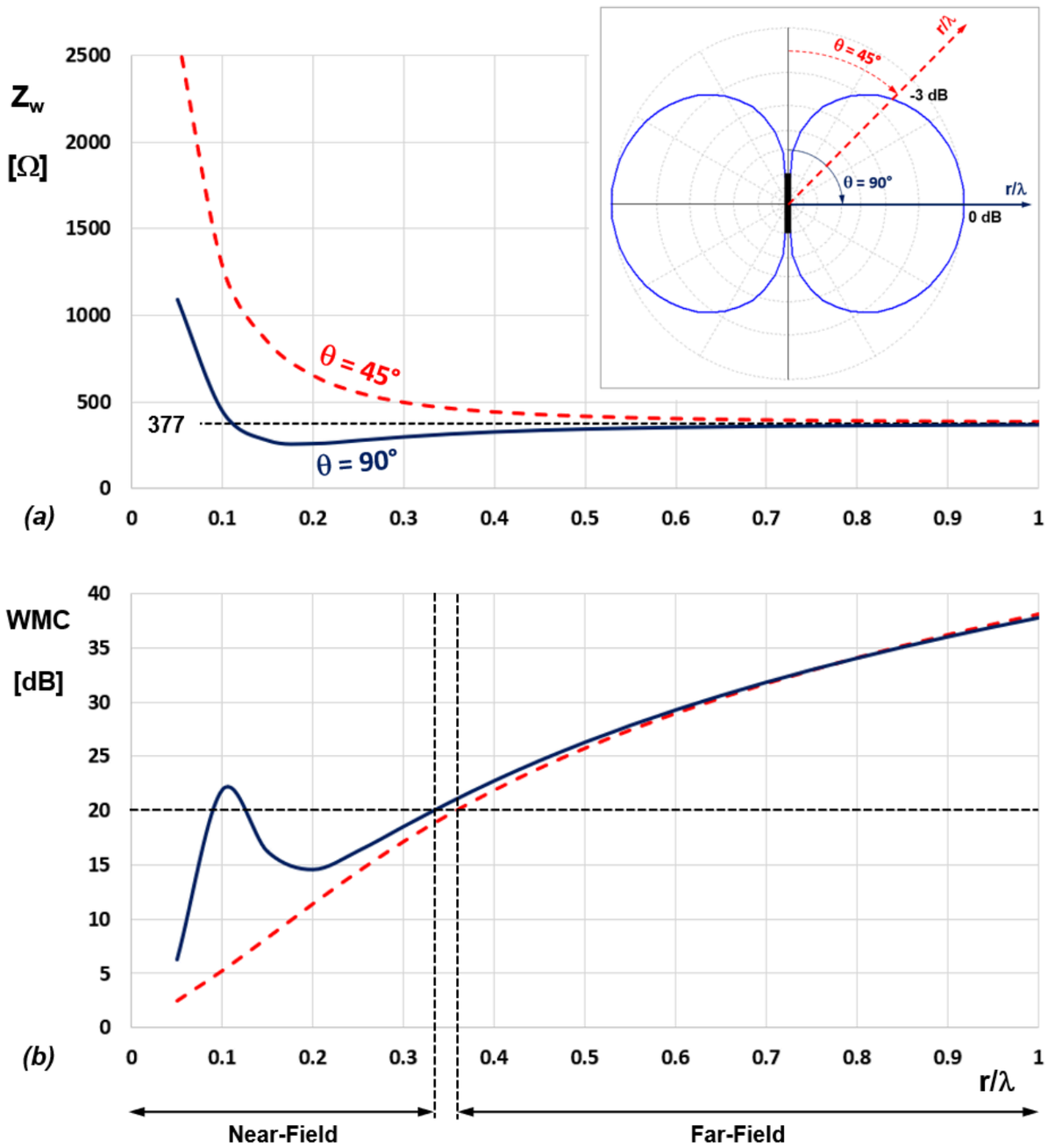

Fig. 2: (a) Absolute wave impedance for an elementary electric dipole as a function of distance along the direction of maximum radiation and the direction where the power density drops by 3 dB. (b) The corresponding WMC and the separation between the near-field and far-field zones at a threshold of 20 dB. A transition zone is opened.

As an example of an antenna with a size of multiple wavelengths, **Fig. 3** presents the results for a **7-element Yagi-Uda antenna**, optimized to provide maximum front-to-back ratio. **Figure 3(a)** shows the absolute wave impedance in the direction of maximum radiation, perpendicular to the antenna elements, and in the direction where the maximum power density drops by half (-3 dB) and defines the edge of the beamwidth. **Figure 3(b)** shows the corresponding WMC curves.

In this case, the **20 dB boundary also shifts to a greater distance** when the observation direction is different from the direction of maximum radiation, similar to the elementary dipole. Additionally, the **transition zone** between the near-field and far-field zones is approximately half a wavelength.

We can see that the wave impedance can reach very high values, so **representing the WMC provides a more convenient decibel scale for comparing large and small values.**

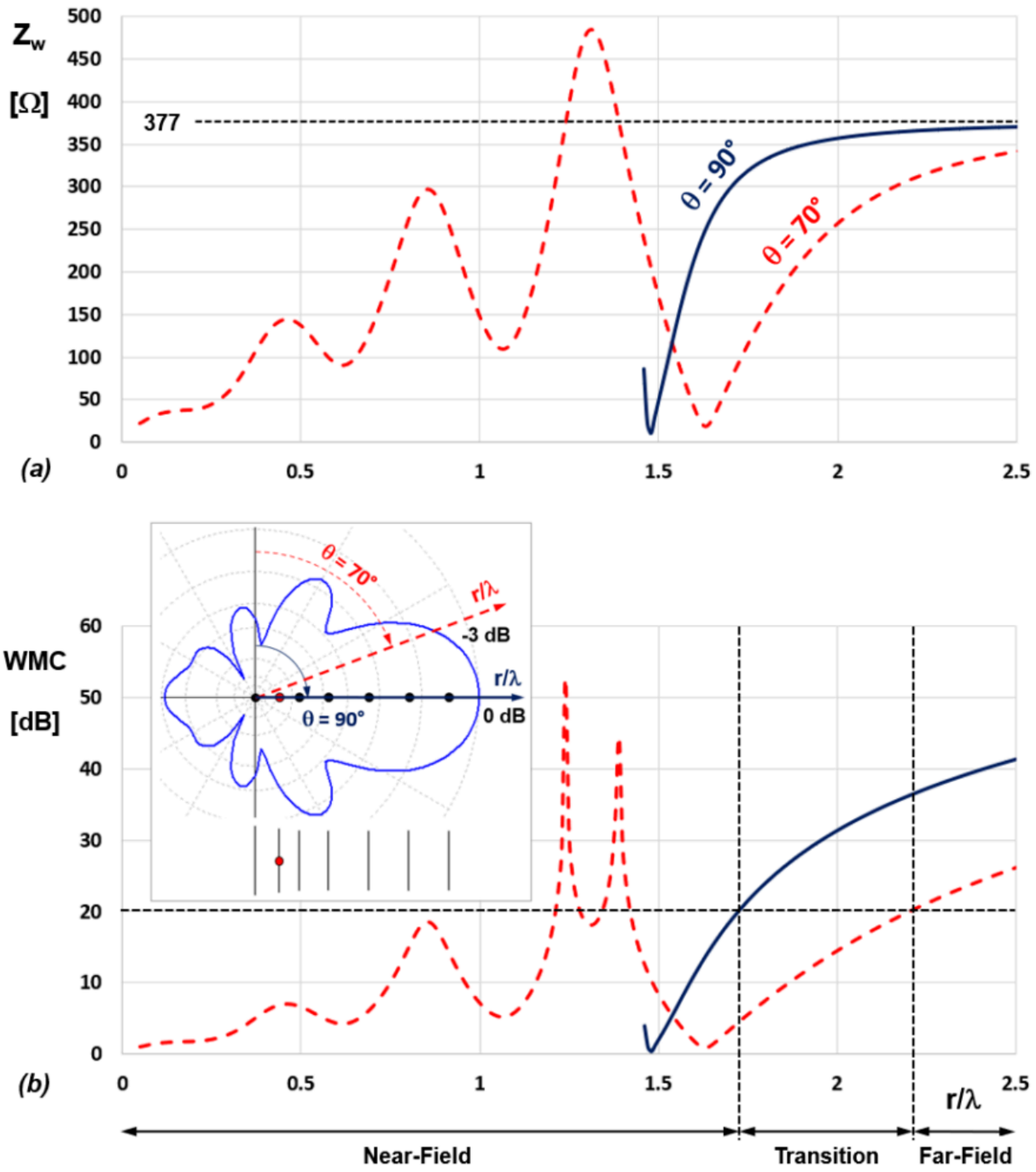

Fig. 3: (a) Absolute wave impedance for a 7-element Yagi-Uda antenna as a function of distance along the direction of maximum radiation and the direction where the power density drops by 3 dB. (b) The corresponding WMC and the separation between the near-field and far-field zones at a threshold of 20 dB. A transition zone of approximately half a wavelength is opened.

Another interesting example of a long-wavelength antenna is the **axial mode helical antenna**. **Figure 4** shows the results for a left-handed helical antenna with a diameter of 0.3λ, a pitch of 0.22λ, and 10 turns, resulting in a total length of 2.2λ from end to end. The helix reflector, which is necessary for it to operate in axial mode (with maximum radiation along the helix axis), has a diameter of 0.95λ.

Figure 4(a) shows the wave impedance along the axis of the helix, from the base, passing through the **interior of the helix** until it exits. It also shows the wave impedance along a direction corresponding to the -3 dB beamwidth edge. **Figure 4(b)** shows the corresponding WMC results. Here, too, a displacement of the boundary between the near-field and far-field regions can be observed. We can see that as we traverse the interior of the helix along its axis, **the boundary between the near and far-field zones begins at r/λ = 2.3**, which is just a distance of 0.1λ above the

top of the helix located at 2.2λ. This is logical since **the interior of the helix behaves like a waveguide**.

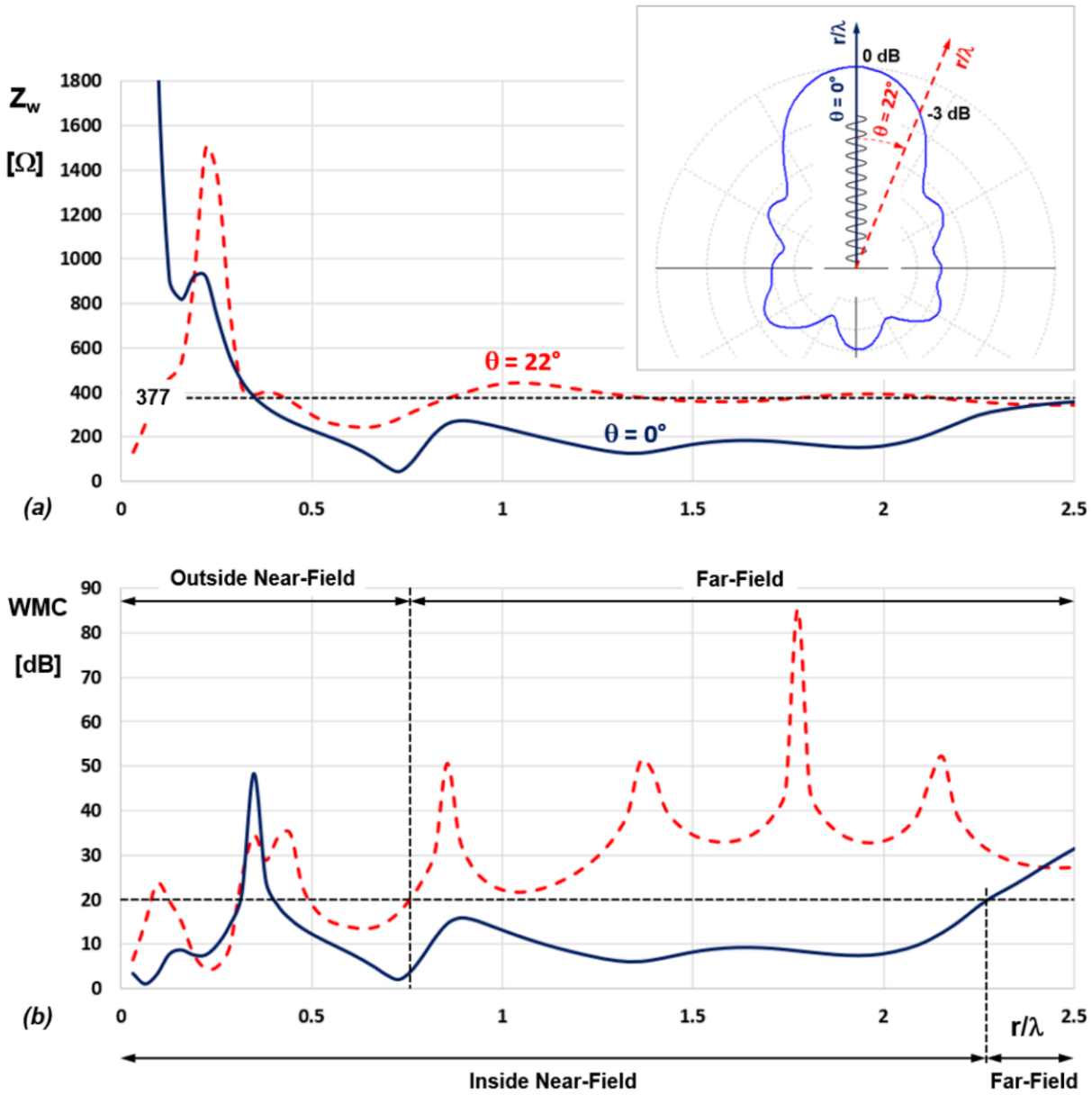

Fig. 4: (a) Absolute wave impedance for a helical antenna in axial mode as a function of distance along the helix axis, passing through its interior, and the direction where the power density drops by 3 dB. (b) The corresponding WMC and the separation between the near-field and far-field zones at a threshold of 20 dB. The near-field zones inside and outside the helix are indicated.

Figure 4(b) also reveals that the WMC outside the helix exhibits nearly periodic peaks due to oscillations in the absolute wave impedance around 377 Ω. While the magnitude of the wave impedance may approach 377 Ω in the near-field region, its phase will not be close to zero. **To define the boundary where the far field begins, the WMC must exceed 20 dB and remain above this threshold**. However, as this example illustrates, the WMC may oscillate instead of increasing monotonically.

From the examined examples, we conclude that **the three-dimensional boundary between the near and far-field regions is neither spherical nor regular** for antennas comparable to or larger than the wavelength. The absolute wave impedance, particularly the WMC, helps identify where the far-field region begins in each direction. **The farthest boundary from this analysis can then be used as the radius of a limiting sphere, marking the start of the far-field region in all directions.**

How to Obtain Wave Impedance and WMC in AN-SOF

The **AN-SOF Antenna Simulator** enables users to calculate the near field at a defined set of spatial points as a function of frequency. The near field calculations yield the electric ($\mathbf{E}$) and magnetic ($\mathbf{H}$) vector fields, which can be presented in **Cartesian, cylindrical, or spherical coordinates**.

Setting Up the Near Field Calculation

Before performing the near field computation, follow these steps:

1. Navigate to the **Setup tab** and select the **Near-Field panel**.
2. Choose the desired coordinate system and configure the grid of points where the near field will be evaluated (refer to **Fig. 5**).
3. Ensure the operating frequency or frequencies are set in the **Frequency panel**.

Once the setup is complete, execute the near field calculation by selecting **Run** > **Run Currents and Near-Field (F12)**.

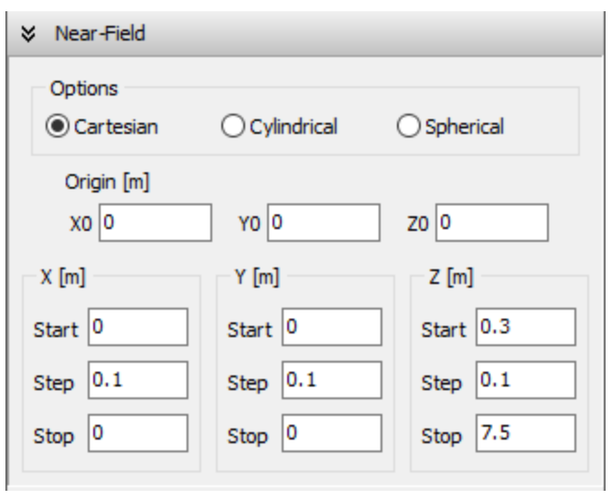

Fig. 5: The Near-Field panel, where the points for near field calculation can be configured.

Accessing the Results

After the calculation is complete, go to the **Results menu** to access the following options:

1. **List Power Density Pattern**:
    - Select a fixed frequency to view results.
    - The tabulated data will include the following at the specified spatial points:
        - Power density (S in W/m^2)
        - Absolute wave impedance (Z_w in Ohms)
        - Wave Matching Coefficient (WMC in dB)
    - See **Fig. 6** for an example.
2. **List Power Density Spectrum**:
    - Select a fixed point in space to view results.

- The tabulated data will include the following as a function of frequency:
  - Power density (S in W/m^2)
  - Absolute wave impedance (Z_w in Ohms)
  - Wave Matching Coefficient (WMC in dB)
- See **Fig. 7** for an example.

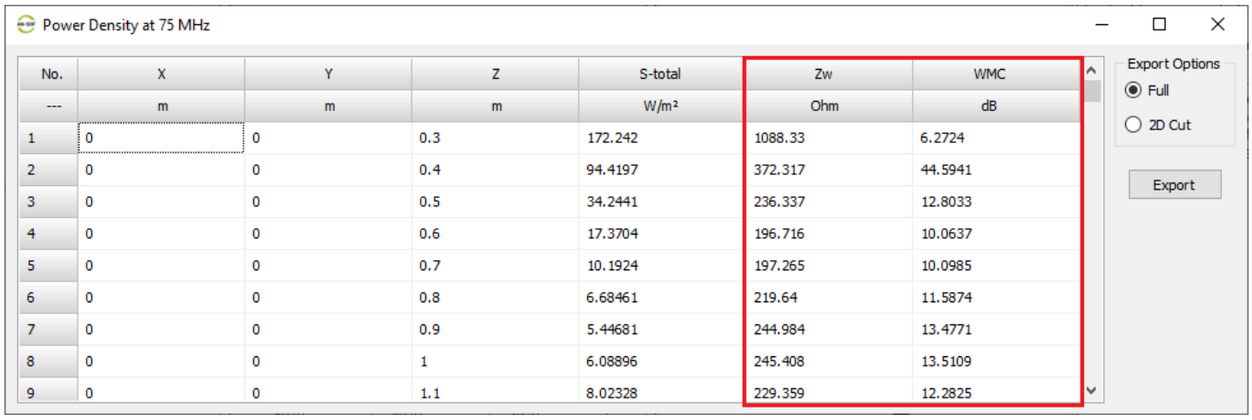

No.	X	Y	Z	S-total	Zw	WMC
---	m	m	m	W/m²	Ohm	dB
1	0	0	0.3	172.242	1088.33	6.2724
2	0	0	0.4	94.4197	372.317	44.5941
3	0	0	0.5	34.2441	236.337	12.8033
4	0	0	0.6	17.3704	196.716	10.0637
5	0	0	0.7	10.1924	197.265	10.0985
6	0	0	0.8	6.68461	219.64	11.5874
7	0	0	0.9	5.44681	244.984	13.4771
8	0	0	1	6.08896	245.408	13.5109
9	0	0	1.1	8.02328	229.359	12.2825

***Fig. 6**: Table displaying the power density, absolute wave impedance, and WMC at each specified spatial point for a selected frequency.*

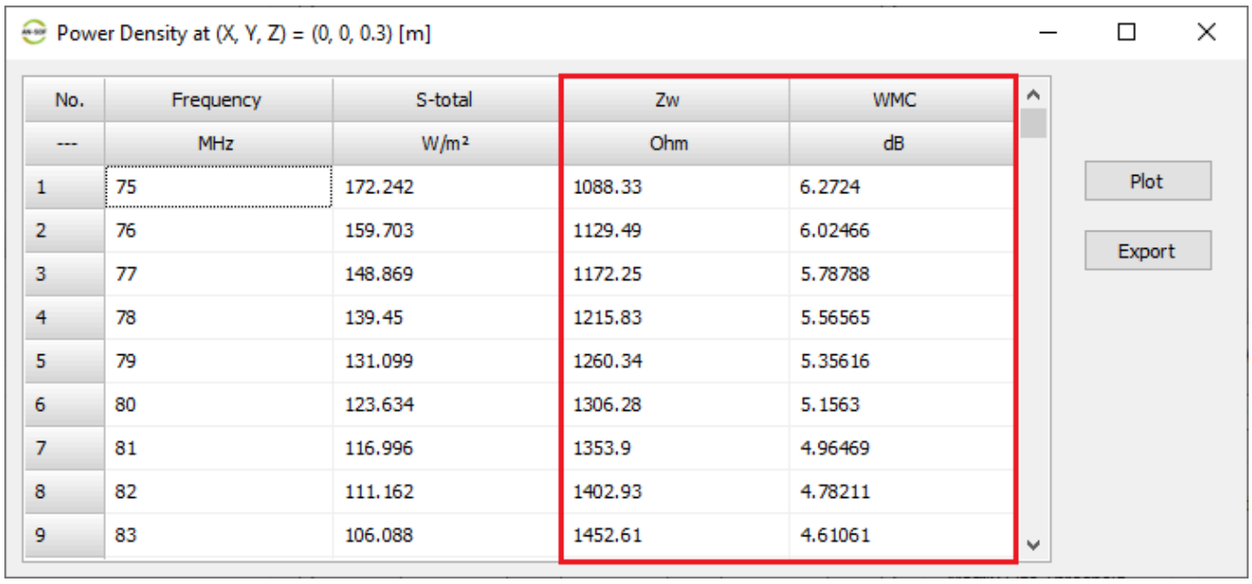

No.	Frequency	S-total	Zw	WMC
---	MHz	W/m²	Ohm	dB
1	75	172.242	1088.33	6.2724
2	76	159.703	1129.49	6.02466
3	77	148.869	1172.25	5.78788
4	78	139.45	1215.83	5.56565
5	79	131.099	1260.34	5.35616
6	80	123.634	1306.28	5.1563
7	81	116.996	1353.9	4.96469
8	82	111.162	1402.93	4.78211
9	83	106.088	1452.61	4.61061

***Fig. 7**: Table showing the power density, absolute wave impedance, and WMC as functions of frequency at a selected spatial point.*

Exporting and Analyzing the Data

Both the **Power Density Pattern** and **Power Density Spectrum** tables can be exported as CSV (Comma-Separated Values) files by clicking the **Export** button next to the respective table. The exported data, including Z_w and WMC, can be further analyzed or plotted using spreadsheet tools such as **Microsoft Excel®** or **Google Sheets®**.

Conclusions

In this article, we introduced the concepts of **absolute wave impedance** and the **Wave Matching Coefficient (WMC)** as practical tools for defining the boundary between the near and far-field regions of an antenna. The WMC, in particular, offers improved visualization of wave propagation as a function of distance from the

source antenna, using a decibel scale to highlight significant variations in wave impedance. As a general guideline, **a WMC value of 20 dB serves as an effective threshold for distinguishing between the near and far-field zones.**

Through examples involving elementary antennas and antennas of significant size relative to the wavelength, we observed that the 20 dB boundary lies at a distance of λ/3 for elementary antennas. However, for antennas comparable to or larger than the wavelength, the boundary takes on an irregular, non-spherical shape. In such cases, **the radius of a spherical boundary** separating the near-field and far-field regions is determined by **the maximum distance observed in all angular directions where the WMC reaches the 20 dB threshold**.

Further Reading

The traditional separation between field regions is explained in detail in section "4.4 Region Separation" of the renowned book *"Antenna Theory, Analysis and Design"* by Constantine A. Balanis, 4th edition, 2016, John Wiley & Sons. For a compelling analysis utilizing wave impedance, refer to *"Near Field or Far Field?"* by Charles Capps, EDN, Design Feature, Aug. 16, 2001, pp. 95-102. A comprehensive examination can also be found in the paper *"Where Does the Far Field of an Antenna Start?"* by M. Abdallah, T. Sarkar, M. Salazar-Palma, and V. Monebhurrun, published in IEEE Antennas & Propagation, Vol. 58, Issue 5, Oct. 2016, pp. 115-124.

See Also:

- **Evaluating EMF Compliance – Part 1: A Guide to Far-Field RF Exposure Assessments**
- **Evaluating EMF Compliance – Part 2: Using Near-Field Calculations to Determine Exclusion Zones**
- **Learning Antennas Through Simulation: 1.7 Thin Dipoles of Arbitrary Length**

Technical Keywords: Wave Matching Coefficient (WMC), Absolute Wave Impedance, Near-Field/Far-Field Boundary, Transition Zone, Wave Propagation, 20 dB Threshold, Field Region Separation, Antenna Impedance Matching, Non-spherical Boundaries, Electromagnetic Wave Theory.

About the Author

Tony Golden

RF ENGINEER & PHYSICS PH.D. With 25+ years in Computational Electromagnetics, I'm a passionate researcher focused on antenna modeling and design. As Founder of Golden Engineering LLC, I develop accessible, high-performance simulation tools that help RF engineers optimize their designs, educators teach complex concepts, and hobbyists bring antenna projects to life.

Have a question?